Hybrid beamforming using massive antenna arrays for fixed sensor networks

Jamal Beiranvand

Thèse de Doctorat

Université de Limoges

Université de Limoges
ED 653 : Sciences et Ingénierie – XLIM
Faculté des Sciences et Techniques – Institut de Recherche XLIM

Thèse pour obtenir le grade de
Docteur de l'Université de Limoges
Réseaux ubiquitaires adaptatif hauts débits, Systèmes & Réseaux Intelligents

Présentée et soutenue par
Jamal BEIRANVAND
Le 30 juin 2023

FORMATION DE FAISCEAUX HYBRIDE PAR L'UTILISATION MASSIVE D'ANTENNES POUR LES RÉSEAUX DE CAPTEURS FIXES

Thèse dirigée par Vahid MEGHDADI et Cyrille MENUDIER

JURY :

Président du jury
M. Cyril DECROZE, Professeur – XLIM – Université de Limoges

Rapporteurs
M. Didier LE RUYET, Professeur – Universités Conservatoire National des Arts et Métiers
M. Guillaume FERRE, Professeur – Universités ENSEIRB-MATMECA

Examinateurs
M. Vahid MEGHDADI, Professeur – XLIM – Université de Limoges
M. Cyrille MENUDIER, Professeur – XLIM – Université de Limoges
M. Bartolo SCANAVINO, Docteur – Chief Technology Officer- Firecell

Invités
M. Jean-Pierre CANCES, Professeur – XLIM – Université de Limoges

To my beloved family,

This thesis is dedicated to you with deep love and gratitude for your unwavering support and encouragement throughout my academic journey, during the three years I spent studying abroad. Despite the distance, your belief in me has been a constant source of motivation, and your sacrifices have made it possible for me to pursue my dreams. I am immensely grateful for your love, guidance, and patience, which helped me overcome the challenges of living in a foreign country and achieving my academic goals. I hope this work brings honor to our family and is a reflection of the values and principles you instilled in me. Thank you for being my inspiration, my strength, and my reason to strive for excellence.

“Success is not final, failure is not fatal: it is the courage to continue that counts”

Winston Churchill

Acknowledgements

I would like to express my deepest appreciation and gratitude to my primary supervisor, Professor **Vahid Meghdadi**, for his invaluable guidance and generous assistance throughout my PhD journey. Without his technical support and unwavering help, completing this thesis would not have been possible. I am grateful for his patience and immense effort in refining and perfecting my academic papers, which greatly improved the quality of my work.

I would like to extend my sincere appreciation and gratitude to my co-supervisors, **Cyrille Menudier**, as well as Professors **Hamid Meghdadi** and **Jean Pierre Cances**, for their invaluable guidance and direction.

I would like to express my heartfelt gratitude to Professor **Long Bao Le** for giving me the opportunity to visit his laboratory at Énergie Matériaux Télécommunications Research Centre, INRS, Quebec University. His collaboration and open-mindedness allowed me to have an invaluable and productive experience, which greatly enriched my research.

I would like to express my sincere gratitude to **Minh Dat Nguyen** for his invaluable support and collaboration during my time at INRS. His assistance was instrumental in the completion of our joint paper, and his insights greatly improved the quality of our work. His dedication and expertise were invaluable to me, and I am deeply grateful for his friendship and guidance.

I am deeply grateful to **my friends at Limoges** for making my three-year experience unforgettable. Their unwavering support, guidance, and companionship were invaluable to me, and I am eternally thankful for their friendship.

Lastly, I would like to express my profound gratitude to **my parents** for their unconditional love and continuous support throughout my life. Their unwavering belief in me has been a great source of motivation, and I am immensely grateful for their love and guidance.

Droits d'auteurs

List of Contents

List of Figures

List of Tables

List of Abbreviations

5G – Fifth Generation Mobile Radio.

ABF – Analog Beamforming.
ADC – Analog-to-Digital Converter.
AltMin – Alternating Minimization.

BS – Base Station.

CSI – Channel State Information.

DAC – Digital-to-Analog Converter.
dB – decibel.
DBF – Digital Beamforming.
DNN – Deep Neural Network.
DoF – Degree of Freedom.
DPS – Double Phase Shifter.

EB – Exabyte.
EE – Energy Efficiency.

FC – Fully-Connected.
FCA – Fully-Connected Antenna.
FP – Fractional Programming.
FPS – Fixed Phase Shifter.
FWA – Fixed Wireless Access.

GB – Gigabyte.
GC – Group Connected.
GHz – Gigahertz.

HBF – Hybrid Beamforming.

IFFT – Inverse Fast Fourier Transforms.

MHz – Megahertz.
MIMO – Multiple-Input and Multiple-Output.
MISO – Multiple-Input and Single-Output.
ML – Maximum Likelihood.
MMSE – Minimum Mean Squared Error.
mmWave – Millimeter-Wave.
MRC – Maximum-Ratio Combining.
MRT – Maximum-Ratio Transmission.
MSE – Mean Square Error.
MU-MC – Multi-User Multi-Carrier.
MU-MIMO – Multi-User MIMO.
MU-MISO – Multi-User MISO.
MU-SC – Multi-User Single-Carrier.

OFDM – Orthogonal Frequency Division Multiplexing.
OMP – Orthogonal Matching Pursuit.
OSA – Overlapped Sub-Array.

PC – Partially-Connected.
PFC – Partially/Fully-Connected.
PS – Phase Shifter.

QPS – Quantized Phase Shifter.

RF – Radio Frequency.

SCA – Singly-Connected Antenna.
SE – Spectral Efficiency.
SNR – Signal-to-Noise Power Ratio.
SPS – Single Phase Shifter.
SU-MC – Single-User Multi-Carrier.
SU-MIMO – Single-User MIMO.
SU-SC – Single-User Single-Carrier.
SVD – Singular Value Decomposition.
SZSS – Subset of Zero-Summation Set.

UESA – Unequal Sub-Array.
UPA – Uniform Planar Array.

ZF – Zero Forcing.
ZSS – Zero-Summation Set.

Table 1: Symbols with a Specific Meaning

Symbol	Definition
f_c	Carrier frequency
λ_c	Wavelength of the carrier frequency
N_{t}	Number of antennas at the transmitter
N_{r}	Number of antennas at receiver
N_{RF}	Number of RF chains
N_{s}	Number of streams
N_{cl}	Number of scattering clusters
N_{ray}	Number of path in each cluster
N_{ps}	Number of FPSs
$\mathbf{I}_N$	Identity matrix of the size $N \times N$
$\mathbf{H}$	Channel matrix
$\mathbf{F}_{\mathrm{RF}}$	Analog precoder matrix at the transmitter of the size $N_{\mathrm{t}} \times N_{\mathrm{RF}}$
$\mathbf{F}_{\mathrm{BB}}$	Digital precoder matrix at the transmitter of the size $N_{\mathrm{RF}} \times N_{\mathrm{s}}$
$\mathbf{F}_{\mathrm{opt}}$	Optimal precoder matrix at the transmitter of the size $N_{\mathrm{t}} \times N_{\mathrm{s}}$
$\mathbf{W}_{\mathrm{RF}}$	Analog combiner matrix at the receiver of the size $N_{\mathrm{r}} \times N_{\mathrm{RF}}$
$\mathbf{W}_{\mathrm{BB}}$	Digital combiner matrix at the receiver of the size $N_{\mathrm{RF}} \times N_{\mathrm{s}}$
$\mathbf{W}_{\mathrm{opt}}$	Optimal combiner matrix at the receiver of the size $N_{\mathrm{r}} \times N_{\mathrm{s}}$
$\mathcal{F}$	The feasible set of the analog precoder matrices
$\mathcal{F}_{N_{\mathrm{ps}}}$	The feasible set generated by N_{ps} FPSs
$\mathcal{F}^b_{N_{\mathrm{ps}}}$	The basic feasible set generated by N_{ps} FPSs
$\mathcal{W}$	The feasible set of the analog combiner matrices
$\mathbb{R}$	The set of real numbers
$\mathbb{C}$	The set of complex numbers
$\mathbb{N}$	The set of natural numbers
$\mathbf{a}_t$	The transmit array response vector of the size $N_{\mathrm{t}} \times 1$
$\mathbf{a}_r$	The receiver array response vector of the size $N_{\mathrm{r}} \times 1$
$\phi^t_{i\ell}$	Azimuth angle of departure of the ℓth ray in the ith cluster
$\phi^r_{i\ell}$	Azimuth angle of arrival of the ℓth ray in the ith cluster
$\overline{\phi^t_i}$	Mean of ℓ azimuth angles in the ith cluster of departure
$\overline{\phi^r_i}$	Mean of ℓ azimuth angles in the ith cluster of arrival
$\theta^t_{i\ell}$	Elevation angles of departure of ℓth ray in the ith cluster
$\theta^r_{i\ell}$	Elevation angles of arrival of the ℓth ray in the ith cluster
$\overline{\theta^t_i}$	Mean of ℓ elevation angles in the ith cluster of departure
$\overline{\theta^r_i}$	Mean of ℓ elevation angles in the ith cluster of arrival

Table 2: Mathematical Notation and Operators

Operator	Definition
$\jmath$	$\sqrt{-1}$
$(\cdot)^*$	Complex conjugate
$(\cdot)^{\mathrm{T}}$	Transpose
$(\cdot)^{\mathrm{H}}$	Conjugate transpose
$(\mathbf{X})^{-1}$	The inverse of the square matrix $\mathbf{X}$
$\lvert x\rvert$	The absolute value of the scalar x
$\lvert\mathbf{X}\rvert$	The determinant of the square matrix $\mathbf{X}$
$\lvert\mathcal{F}\rvert$	The cardinal numbers of the set $\mathcal{F}$
$\lVert\mathbf{x}\rVert$	The Euclidean norm of the vector/matrix $\mathbf{x}$
$\lVert\mathbf{x}\rVert_{\mathrm{F}}^2$	The Frobenius norm of the vector/matrix $\mathbf{x}$
$\mathrm{Tr}\{\mathbf{X}\}$	The trace of the square matrix $\mathbf{X}$
$\mathfrak{Re}\{x\}$	The real part of a complex variable x
$\mathbb{E}\{x\}$	The expected value of the random variable x
$\mathrm{var}\{x\}$	The variance value of the random variable x
$\mathcal{CN}\left(0,\sigma^2\right)$	Complex normal distribution with zero mean and variance σ^2
$\mathcal{L}\left(\mu,b\right)$	Laplace distribution with μ and b parameres
$\mathcal{U}\left(a,b\right)$	Uniform distribution in range a and b
$\mathcal{O}\left(.\right)$	The run time grows with the input size.
$\lfloor . \rfloor$	The floor function
$\lceil . \rceil$	The ceiling function
$\left[N\right]$	A set including $\{1,2,\ldots,N\}$
$\mathrm{vec}\left(\mathbf{X}\right)$	Stacks the matrix $\mathbf{X}$ as a column vector
$\mathrm{Blckdg}\left(\mathbf{X_1}\ldots,\mathbf{X_N}\right)$	Returns the block diagonal matrix created by aligning the input matrices $\mathbf{X_1}\ldots,\mathbf{X_N}$ along the diagonal
$\mathrm{mod}\left(a,b\right)$	The modulus function

1 Introduction

Sommaire

1.1 Motivation

In the past decade, mobile technology has had a significant and unexpected impact on both society and businesses. Looking ahead, it is more valuable to contemplate the lessons learned during this time and utilize them in shaping the future. Although the previous ten years were marked by significant changes, they may pale in comparison to what is anticipated to happen in the coming years. Data traffic (both mobile and fixed) has grown exponentially due to the dramatic growth of smartphones, tablets, laptops, and many other wireless data-consuming devices. At the end of 2022, it is anticipated that there will be one billion Fifth Generation Mobile Radio (5G) subscriptions, and the market will see an influx of smart 5G devices with advanced capabilities throughout 2023 [1]. Looking ahead to 2028, it is predicted that 5G subscriptions will surpass five billion, and there will be approximately 300 million Fixed Wireless Access (FWA) connections, with 5G accounting for almost 80% of FWA connections. Figure 1.1 shows the demand for mobile data traffic, total global mobile data traffic reached around 115 Exabyte (EB) per month at the end of 2022 and is estimated to grow by a factor of around 4.4 to reach 453 EB per month in 2028. The monthly global average usage per smartphone reached 15 Gigabyte (GB) at the end of 2022 and is forecast to reach 46 GB by the end of 2028.

Wireless throughput is a measure of the rate of data transfer in a wireless communication system, expressed in bits per second (bps) as:

$$\text{Throughput} = \text{Bandwidth (Hz)} \times \text{Spectral efficiency (bits/s/Hz)}. \tag{1.1}$$

It refers to the amount of data that can be transmitted over a wireless network in one second. To increase wireless throughput, it is necessary to use new technologies that can increase the available bandwidth or improve spectral efficiency, or both. Two key technologies that have been leveraged in the development of 5G networks to meet its stringent requirements are Millimeter-Wave (mmWave) communication and massive

Multiple-Input and Multiple-Output (MIMO). The following sections aim to provide an elaborate explication of the fundamental concepts behind mmWave communication and massive MIMO.

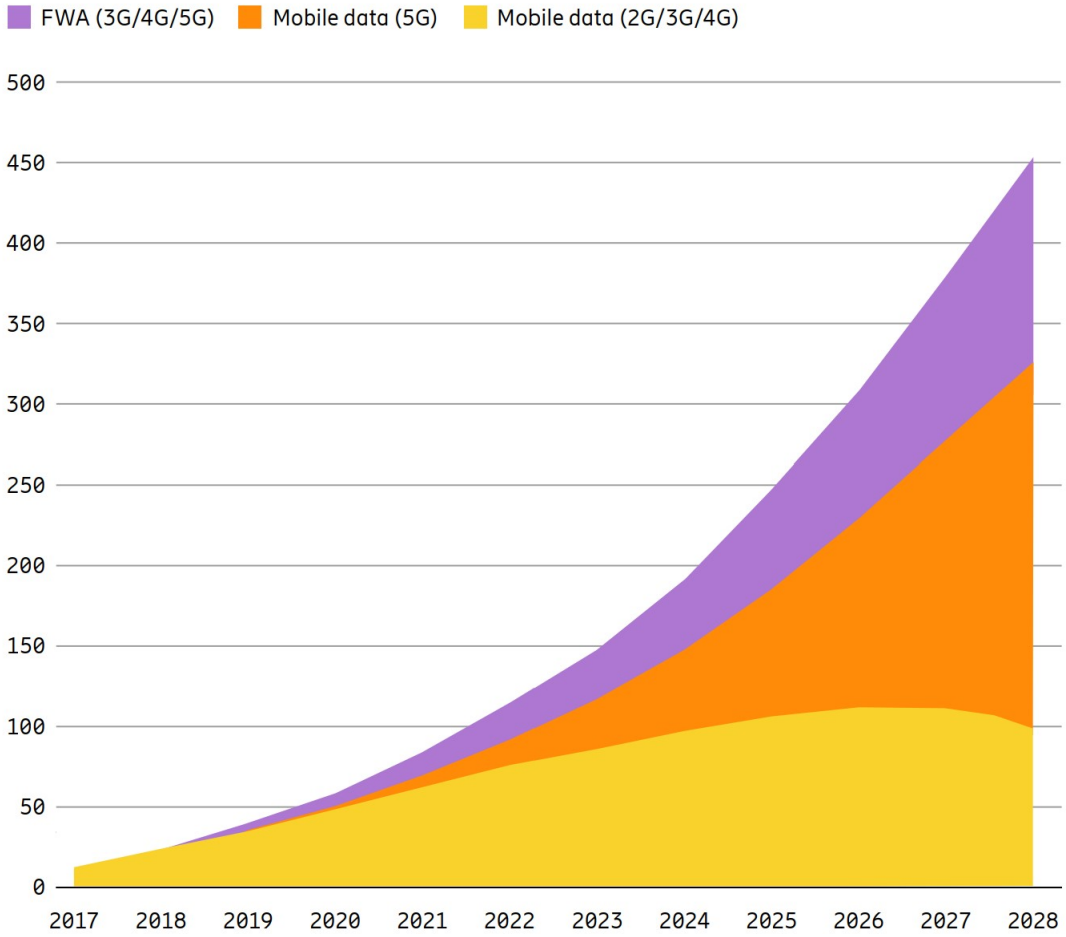

Figure 1.1: Global mobile network data traffic (EB per month) [Source file].

1.2 mmWave Communications

The pursuit of achieving higher data rates, lower latency, and energy efficiency has long been a fundamental objective in the advancement of wireless communication technologies. To accommodate the rapidly growing demand for wireless services, it becomes necessary to utilize wider spectrum bands. Until recently, the vast majority of wireless systems have been confined to a narrow band spectrum within the 300 Megahertz (MHz) to 5 Gigahertz (GHz) frequency range, as noted in [2]. However, the scarcity of available bandwidth within this frequency range, as well as challenges

associated with enhancing physical layer techniques to achieve greater efficiency, has prompted researchers to focus on exploring the utilization of frequency spectrum beyond 6 GHz for commercial communication networks. Large free bandwidths in mmWave band and developments in mmWave-hardware devices encourage the wireless industry to design mmWave systems to meet further data traffic demands.

The utilization of high-frequency bands enables the implementation of systems with a greater number of antenna elements in smaller form factors due to the smaller wavelengths. However, the mmWave frequency bands also present challenging propagation conditions such as severe path-loss, significant atmospheric and rain absorption, limited diffraction around obstacles, and reduced penetration through objects.

The primary factor contributing to transmission loss of mmWave is free space loss. A widespread misconception among wireless engineers is that higher frequencies experience greater propagation loss than lower frequencies due to the frequency-dependent nature of free-space propagation loss. This misconception stems from the common practice in radio engineering textbooks of calculating path loss between two isotropic antennas or $\lambda/2$ dipoles at a specific frequency. The effective aperture area of these antennas increases with wavelength (and decreases with carrier frequency), resulting in a larger gain for antennas with larger aperture areas that capture more energy from passing radio waves. However, shorter wavelengths allow for more antennas to be packed into the same area, and therefore, shorter wavelengths (higher frequencies) with the same antenna aperture areas should not inherently experience greater free space loss than longer wavelengths (lower frequencies) [3]. Moreover, a large number of antennas facilitate beamforming with high gains for both transmitters and receivers. For instance, if the antenna areas are kept constant, a beam at 80 GHz will exhibit approximately 30 decibel (dB) more gain (with a narrower beam) than a beam at 2.4 GHz [2].

Therefore, it is imperative to design mmWave systems with large array antennas, and to utilize spatial signal-processing techniques, such as beamforming, to mitigate the path-loss and other undesirable channel characteristics. Thus, it is crucial for mmWave systems to implement an efficient beamforming strategy that can effectively concentrate the beams in the intended direction, thereby significantly enhancing the received signal

strength.

1.3 Massive MIMO Systems

Massive MIMO, a wireless communication technology that utilizes a large number of antennas, was introduced in the early 2010s [4]. In this context, the term "massive" refers to having numerous antennas, and the central idea behind this technology is to employ large arrays of antennas to transmit narrow beams and increase the received signal power.

Leveraging multiple antennas in the transmitter and/or receiver offers greater spatial degrees of freedom in the beamforming design [5], [6]. This enables the attainment of multiplexing gain, which involves the transmission of multiple parallel data streams over multiple antennas simultaneously to significantly enhance communication capacity. The pursuit of spatial multiplexing gain has been observed in Multi-User MIMO (MU-MIMO) systems, where a multitude of users are simultaneously served by a Base Station (BS) equipped with multiple antennas. In such MU-MIMO setups, the spatial multiplexing gain can be realized even when each user has only one antenna. Moreover, diversity gain can be achieved by transmitting redundant data streams to enhance communication reliability. Additionally, antenna gain can be attained by improving the Signal-to-Noise Power Ratio (SNR) at the receiver and mitigating co-channel interference in multi-user systems.

The use of large antenna arrays presents a challenge for conventional signal processing techniques, such as Maximum Likelihood (ML) detection, due to their prohibitive complexity. However, recent studies have demonstrated that the limitations of ill-behaved channels, which cause a significant reduction in performance, are no longer a concern when the number of BS antennas grows significantly large [4], [6]. As a result, even simple linear signal processing techniques, such as Maximum-Ratio Combining (MRC) and Zero Forcing (ZF), can achieve nearly optimal performance by exploiting the favorable propagation characteristics. Thus, the massive MIMO system has garnered significant attention in the research community in the last decade [6]–[8].

1.4 Beamforming for mmWave Massive MIMO Systems

Beamforming is a signal processing technique used to enhance the directional properties of an antenna array [9]. This technique improves the signal-to-noise ratio of a received signal and increases the array gain in a particular direction. By weighting the signals from the individual elements of an array, beamforming allows the array to focus its energy in a desired direction and reject signals from other directions.

Radiating the radio signal on a narrow beam helps to overcome the effects of ill-behaved propagation associated with mmWave channels. Nonetheless, achieving this requires the capability to exert independent control over the weight of each element in the antenna array. This poses a challenge since it requires a dedicated RF chain for each such element, which is not feasible in massive MIMO systems due to power, cost, and space limitations. It is notable that there is always a trade-off between performance and complexity [5].

Beamforming techniques have been studied and classified extensively in the literature based on different aspects. One of the classification schemes is based on the system architecture performing beamforming. According to this scheme, beamforming techniques can be divided into three categories: Analog Beamforming (ABF), Digital Beamforming (DBF), and Hybrid Beamforming (HBF) [10]. ABF uses low-cost Phase Shifters (PSs) to perform beamforming in the RF domain, while DBF provides more precise and faster results by performing beamforming at the baseband. However, DBF adds more complexity and cost to the system, making it less suitable for massive MIMO. HBF, on the other hand, combines ABF and DBF, by performing beamforming in both baseband and the RF domain to make it an appropriate technique for massive MIMO systems. These three categories of beamforming techniques and their characteristics are further discussed in the following subsections.

1.4.1 Analog Beamforming

ABF, the simplest spatial filter, was introduced 50 years ago. ABF is a technique used to control the transmitted signal phase through low-cost PSs, as depicted in Figure 1.2a. Typically, analog or RF beamforming is implemented using PSs where all the antenna

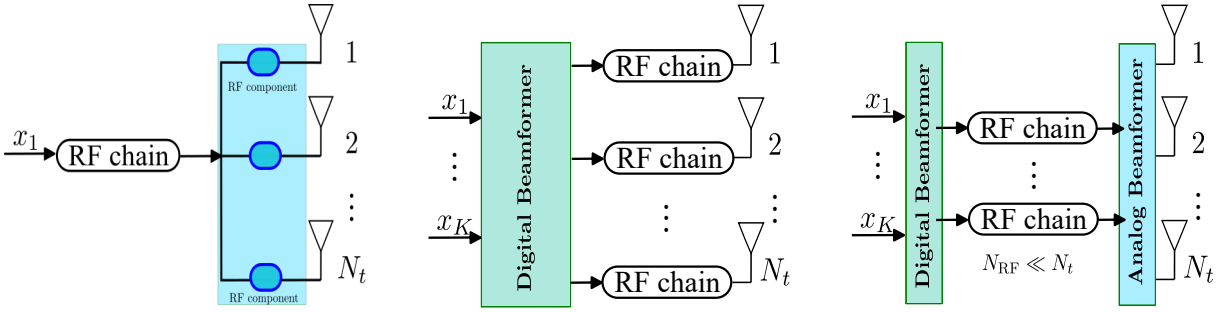

(a) Analog beamforming **(b)** Digital beamforming **(c)** Hybrid beamforming

Figure 1.2: System Architecture for analog, digital and hybrid beamforming [Source file].

elements share a single RF chain, and the beamforming matrix weights are constrained by the PSs' constant amplitude. The ABF has been extensively studied in the literature and explored in mmWave MIMO systems [11]–[15]. Although ABF has been found to have lower complexity compared to DBF, it suffers from insufficient antenna gain and only moderate performance.

1.4.2 Digital Beamforming

In comparison to the ABF approach, the DBF technique utilizes a digital signal processor to perform beamforming, thereby providing a greater Degree of Freedom (DoF). This results in greater flexibility in implementing effective beamforming algorithms which control over amplitude and phase of the signals. Figure 1.2b illustrates that for each antenna, this structure requires dedicated filters, Digital-to-Analog Converter (DAC) or Analog-to-Digital Converter (ADC), and amplifiers. These series of components that connect the antennas to the baseband is called RF chain. Nonetheless, using a large number of RF chains would result in a complex architecture with high power consumption due to the complexity and power consumption of its mixed-signal circuits. Additionally, due to the large number of antenna elements in massive MIMO, DBF can be expensive to implement. Therefore, the fully DBF approach is not practical for realizing massive MIMO systems at mmWave frequencies.

1.4.3 Hybrid Beamforming

The HBF architecture has been proposed as a solution to achieve an optimal trade-off between hardware complexity and performance. It combines the advantages of

analog and DBF, enabling efficient utilization of the available RF spectrum. As shown in Figure 1.2c, this technique divides the beamforming into two parts, namely, the analog and digital parts. The analog part is performed via PSs, while the digital part is performed at processors to provide fine-grained control over the phase and amplitude of the baseband signals. The HBF architecture reduces the number of RF chains required to support massive MIMO, making it more energy-efficient and cost-effective.

In the HBF architecture, a network of PSs connects a small number of RF chains to a large number of antennas. HBF has been recognized as a promising solution for mmWave massive MIMO systems due to its energy and cost-efficiency. The effectiveness of HBF depends on several factors, such as the number of antennas, the number of RF chains, the channel characteristics, and the beamforming algorithm used. Therefore, a thorough understanding of these factors is essential to design an optimal HBF system. It motivates the study of HBF architectures in this thesis.

1.5 Outline and Contributions

The objective of this thesis is to investigate the use of HBF in mmWave massive MIMO systems as a mean of balancing system performance and hardware complexity. The thesis is structured as follows:

Chapter 2 provides a comprehensive overview of HBF and its implementation in wireless communication systems. It covers the fundamental concepts and principles underlying HBF, such as the design problem, implementation challenges, and optimization constraints. The chapter also presents a survey of the current state of research in this area, highlighting different system architectures. The chapter starts by describing the general HBF design problem to obtain the analog and digital matrices. It then delves into the constraints on the analog precoder coefficients raised from different hardware implementations, and mapping strategies in the analog network. The effect of the connections on the analog precoder matrix shape and optimization problems is also discussed. Finally, the chapter provides a categorization of different system architectures and their state of the art.

Chapter 3 addresses the computational complexity issue faced in the design of HBF systems using fixed PSs and switches. The chapter proposes a low-complexity algorithm to efficiently design HBF systems by significantly reducing the search space. The algorithm decomposes the problem into independent and tractable sub-problems, leading to a search space that grows linearly with the number of antennas instead of exponentially. The approach further reduces the complexity by identifying the basic set and superimposed points in the search space. The algorithm presented in this chapter serves as a foundation for future research.

Chapter 4 focuses on addressing the challenge of determining the optimal number of PSs required to generate analog precoder coefficients with negligible error. The chapter presents an analytical formula to calculate the number of distinct coefficients that can be generated using practical values of the PSs. The analytical formula highlights the dependence of system performance on the number of distinct coefficients that can be generated, rather than the number of PSs used. The chapter provides important insights into how to optimize the hardware design of RF paths to achieve high performance with minimal hardware complexity.

Chapter 5 studies the impact of the number of RF paths in mapping strategies on hardware complexity. The chapter proposes a novel mapping strategy that provides a range of distinct levels of complexity and performance trade-off, with each level having a specific number of RF paths. Additionally, a dynamic version of the mapping strategy is developed to enhance performance. The chapter also presents innovative methodologies for obtaining the analog precoder matrix based on the zero-forcing approach and the use of a DNN to reduce the computational complexity of obtaining the precoding matrix in the dynamic strategy.

Chapter 6 focuses on the design of HBF for mmWave wideband channels. Particularly, this chapter considers a multiuser MISO-OFDM system that serves users over all subcarriers. It formulates an optimization problem to maximize the sum rate while satisfying a per subcarrier power constraint. The proposed method for achieving this objective is an iterative solution that builds on the results presented in previous chapters and employs "Lagrangian dual transform" and "quadratic transform" techniques.

Chapter 7 reflects on the research objectives, methods, and results presented in the previous chapters to evaluate the research's overall success in achieving goals. It outlines potential areas of research that may build upon the study's findings and proposes possible methodologies and approaches that could be used to explore these areas.

2

An Overview of Hybrid Beamforming Fundamentals

Sommaire

THE overarching goal of this chapter is to provide a thorough understanding of the fundamental concepts and principles underlying HBF in wireless communication systems. This includes a detailed exploration of the design problem, implementation challenges, and optimization constraints. In addition, the chapter offers an overview of the latest research in this area, highlighting the diverse system architectures that have been designed.

To begin, the chapter outlines the general design problem of obtaining digital and analog matrices for HBF. The various constraints that are imposed on the analog precoder coefficients for different hardware implementations are then explored in depth. The chapter also includes a comprehensive discussion of the connections between RF chain-antenna pairs, which play a crucial role in determining the system architecture, such as Fully-Connected (FC) and Partially-Connected (PC). The impact of these connections on the shape of the analog precoder matrix is also explained, along with the imposition of zero entries, which leads to different optimization problems.

Finally, the chapter provides an up-to-date review of the current state of the art, categorizing different system architectures that have been proposed in recent research. Overall, this chapter offers a deep dive into the key concepts and principles that underpin HBF, providing readers with a comprehensive understanding of this field.

2.1 Introduction

The deployment of mmWave MIMO systems faces significant signal processing challenges due to practical constraints. High costs and power consumption associated with mmWave RF chains prevent the industry from dedicating an RF chain for each MIMO antenna element, a practice commonly employed in microwave systems.

To address these issues, HBF has been proposed as a promising solution. HBF is a two-part precoding approach that combines analog and digital beamforming as shown in Figure 2.1. By doing so, HBF reduces the required number of RF chains in the order of the number of data streams. Consequently, mmWave signal processing relies on RF processing, which is subject to limitations imposed by RF components such as PSs and switches [16]–[18].

Optimizing system performance while adhering to hardware constraints is a significant challenge in the design of HBF. These constraints include the use of a reduced number of RF chains and a high-dimensional PS-based analog beamformer. Notably, HBF problems are inherently nonconvex and depend heavily on the hardware architecture, unlike digital beamforming problems, which are typically convex and have access to powerful tools associated with convex optimization [19]. Additionally, hardware complexity remains a concern in HBF, despite being significantly reduced compared to fully digital beamforming, particularly when considering the power consumption and cost of mmWave devices [20].

The design of HBF involves crucial issues that require careful consideration, including:

1. **Hardware complexity**, which can be minimized by reducing the number of hardware components required, resulting in lower costs and reduced power consumption. The analog network plays a crucial role in determining the system's hardware complexity. The analog network's complexity can be viewed in terms of two factors: the number of RF paths and the RF components deployed within these paths. The former is determined by the mapping strategy, which governs the interconnections between RF chains and antenna pairs, while the latter depends on the hardware implementation of the analog precoder coefficients within the RF paths.

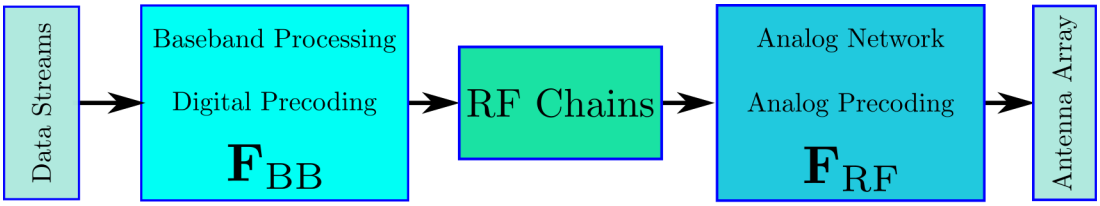

Figure 2.1: Conceptual block diagram of hybrid beamforming [Source file].

2. **Computational complexity**, which is closely related to the algorithm's complexity in obtaining both beamforming matrices. This computational complexity is closely related to the hardware complexity of the system, as the hardware implementation limits the choice of analog coefficients to a feasible set, thereby imposing constraints on the precoding design problem.

3. **Spectral efficiency**, a key performance indicator that should be comparable to that of fully digital beamforming. Spectral Efficiency (SE) is closely related to both hardware and computational complexity.

2.2 Hybrid Beamforming System Model

In this section, we describe the structure of the HBF system in the context of a MIMO transceiver. The block diagram of the MIMO system employing HBF at the transceiver is shown in Figure 2.2. First, the N_{s} data streams are combined at baseband using a digital precoder, $\mathbf{F}_{\mathrm{BB}}$, to generate N_{RF} signals. These N_{RF} signals are then up-converted to the carrier frequency through N_{RF} RF chains. The analog precoder, $\mathbf{F}_{\mathrm{RF}}$, which constructs N_{t} signals to transmit, is then applied in the RF domain. HBF significantly reduces hardware complexity compared to fully DBF because the number of RF chains is much smaller than the number of antennas, i.e., $N_{\mathrm{RF}} \ll N_{\mathrm{t}}$. The received signal at the user's side can be expressed as:

$$\mathbf{y} = \mathbf{H}\mathbf{F}_{\mathrm{RF}}\mathbf{F}_{\mathrm{BB}}\mathbf{x} + \mathbf{n} \tag{2.1}$$

where $\mathbf{y}$ is the $N_r \times 1$ received vector. The precoder design problem can be stated as maximizing mutual information achieved by Gaussian signalling over the mmWave

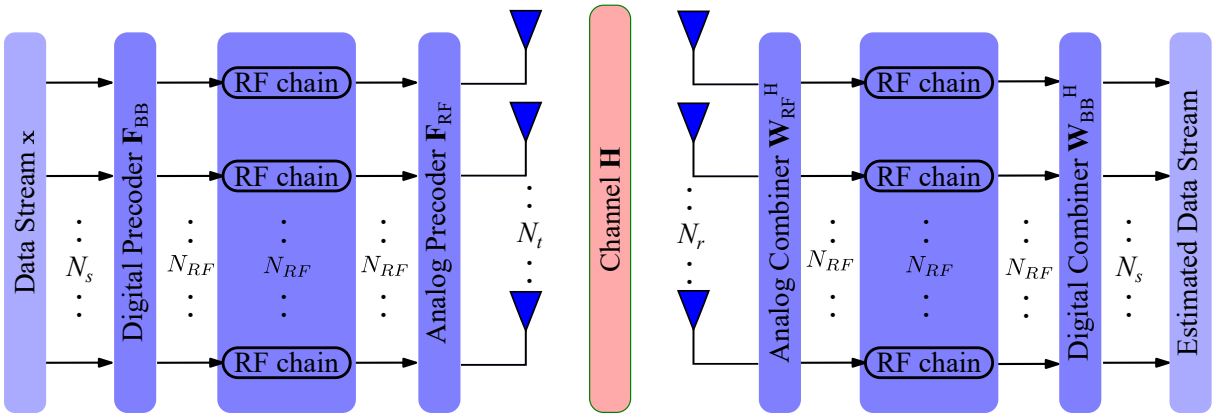

Figure 2.2: Hybrid beamforming architecture for a MIMO system [Source file]

channel:

$$
\begin{aligned}
(\mathbf{F}_{\mathrm{RF}}, \mathbf{F}_{\mathrm{BB}}) &= \underset{\mathbf{F}_{\mathrm{RF}}, \mathbf{F}_{\mathrm{BB}}}{\operatorname{argmax}} \quad \mathcal{I}(\mathbf{x}; \mathbf{y}) \\
\text{s.t.} \quad & \|\mathbf{F}_{\mathrm{RF}} \mathbf{F}_{\mathrm{BB}}\|_{\mathrm{F}}^2 = P \\
& \mathbf{F}_{\mathrm{RF}}(i, \ell) \in \mathcal{F}, \quad \forall i, \ell
\end{aligned}
\tag{2.2}
$$

where P denotes the power constraint at the transmitter, and $\mathcal{F}$ is the feasible set for each element of the analog matrix $\mathbf{F}_{\mathrm{RF}}$.

2.3 Analog Network Structure

Analog precoding is executed within the analog network through the use of RF components, namely PSs and switches. Each RF path connecting an RF chain to an antenna element in the analog network corresponds to an entry in the analog precoder. A thorough comprehension of the constraints imposed on the analog precoder necessitates an examination of the analog network structure, which can be characterized by two fundamental factors: the mapping strategy and the hardware implementation. The mapping strategy pertains to how the signals are distributed from the RF chains to antenna elements, while the hardware implementation refers to the physical components employed to implement the analog network.

Analog precoding is implemented within the analog network, and the constraints on $\mathbf{F}_{\mathrm{RF}}$ arise from within the analog network. Analog precoder coefficients are primarily

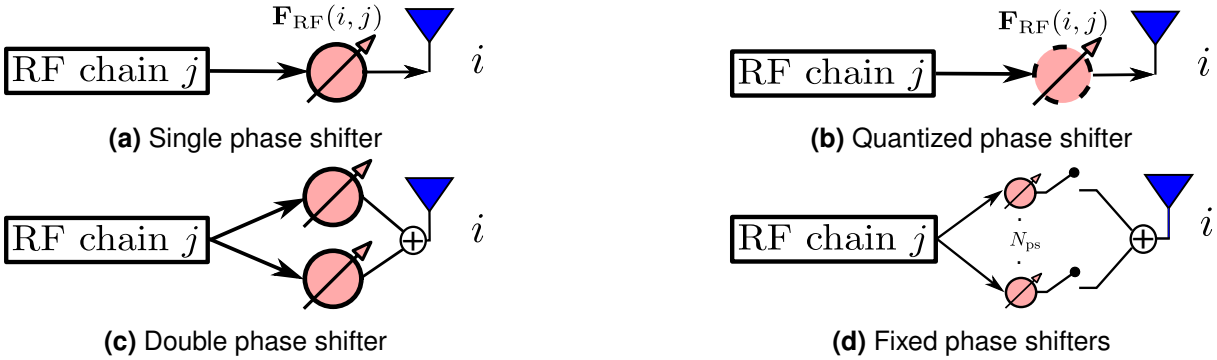

(a) Single phase shifter

(b) Quantized phase shifter

(c) Double phase shifter

(d) Fixed phase shifters

Figure 2.3: Hardware implementations of analog precoding coefficients [Source file]

influenced by two factors: mapping strategy and hardware implementation.

- *Mapping strategy*: This factor determines the RF paths connecting the RF chains to the antenna elements. Each RF path represents a non-zero entry in the analog precoding matrix $\mathbf{F}_{\mathrm{RF}}$, regardless of the RF components. The analog beamforming matrix associated with each mapping strategy has a special structure that affects the beamformer design. Therefore, the mapping strategy has a significant impact on both performance and complexity. More RF paths result in improved performance at the expense of increased complexity. Some architectures that address this issue are discussed in the following sections.

- *Hardware implementation*: This factor specifies the hardware components used in the RF paths and how they will be employed. The hardware implementation determines the constraints on the signal processing in RF paths, i.e., imposing non-zero entries in $\mathbf{F}_{\mathrm{RF}}$. Different hardware implementations are described in the following sections.

Overall, both mapping strategy and hardware implementation play critical roles in the design of analog precoders. Their impact on system performance and complexity should be carefully considered in the beamformer design process.

2.3.1 The Hardware Implementation

The present subsection provides a detailed discussion of the Hardware Implementation, which encompasses the hardware components used in the RF paths and how they are

employed. Figure 2.3 illustrates four distinct Hardware Implementations that enable signal transmission between the RF chain j and antenna i using various techniques, including a Single Phase Shifter (SPS), a Quantized Phase Shifter (QPS), Double Phase Shifters (DPSs), or Fixed Phase Shifters (FPSs) with switches. Each Hardware Implementation modifies the received signal from the RF chain in specific ways, thereby constraining the values of the corresponding entry of the analog precoding. Therefore, the analog precoding coefficients are chosen from a feasible set which significantly impacts the precoding design problem.

1. **Single continuous phase shifters**

   Figure 2.3a illustrates the interconnection between RF chain j and antenna i via a continuous phase shifter. The implementation of infinite-resolution PSs allows for precise control of the signal phase transmitted from the RF chain to the antenna. Assuming a PS with zero insertion loss, a constant modulus constraint is imposed on the corresponding analog precoder coefficients, $|\mathbf{F}_{\mathrm{RF}}(i,j)| = 1$. As a result of the constant modulus constraint on the analog precoder coefficients, the feasible set encompasses all points located on the unit circle, $e^{\jmath\theta} \in \mathcal{F} \quad \forall\theta \in [0,\ 2\pi)$. As such, the analog precoder's elements can be modelled as follows:

   $$\mathbf{F}_{\mathrm{RF}}(i,j) = e^{\jmath\theta} \qquad \theta \in [0,\ 2\pi) \tag{2.3}$$

   where θ denotes the phase variation. It should be noted that the cost and energy consumption of a PS is relatively expensive for commercial applications [21]. For instance, even low-resolution PSs can cost up to a hundred dollars, making it prohibitively expensive and energy-intensive to deploy a large number of such devices.

2. **Quantized phase shifters**

   The design of hybrid structures with finite-resolution PSs is deemed more practical than infinite-resolution PSs in systems with large antenna arrays. This is due to the fact that the number of PSs required in a hybrid structure scales proportionally with the number of antennas. As shown in Figure 2.3b, the interconnection between an RF chain-antenna pair is established via a QPS. In contrast to infinite-

resolution PSs, finite-resolution PSs generate a limited number of phase angles, thereby imposing an additional constraint on the analog precoder coefficients. Consequently, the analog precoder coefficients are chosen from the feasible set, $\mathbf{F}_{\mathrm{RF}}(i,j) \in \mathcal{F}$, which consists of discrete points located on the unit circle. This feasible set is defined as:

$$\mathcal{F} = \left\{0, e^{\jmath 2\pi \frac{1}{N_{ps}}}, \ldots, e^{\jmath 2\pi \frac{N_{ps}-1}{N_{ps}}}\right\}, \tag{2.4}$$

where N_{ps} is the number of possible phase angles which is $N_{ps} = 2^b$, and b is the bit-resolution of PSs.

The deploying of QPSs transforms the precoding design problem into a combinatorial optimization problem, which can have exponential complexity when an exhaustive search is performed. This is due to the combinatorial nature of optimization over analog beamformers, which makes the design of analog beamformers more challenging. Although theoretically it is possible to perform an exhaustive search over all feasible choices since the set of feasible analog beamformers is finite, the number of feasible analog beamformers increases exponentially with the number of antennas and the resolution of the PSs. For instance, if the transmitter is equipped with ten RF chains and one hundred antennas, and then the search space with two-bit PSs is equal to $2^{100\times10\times4}$.

3. **Double Phase Shifter**

The implementation of an analog precoder coefficient can be realized through the utilization of DPSs, as depicted in Figure 2.3c. This approach involves the modification of the RF signal by passing it through two PSs, and subsequently summing their outputs to perform the desired coefficient. Therefore, the coefficient can be expressed as:

$$\mathbf{F}_{\mathrm{RF}}(i,j) = e^{\jmath\theta_1} + e^{\jmath\theta_2} \qquad \theta_1, \theta_2 \in [0,\ 2\pi) \tag{2.5}$$

where θ_1 and θ_2 are two phase shifts. It is evident that any point within the circular region with radius 2 can be equivalently represented as the sum of two complex

exponentials, as given below:

$$\begin{aligned} x &= re^{\jmath\phi} \qquad 0 \leq r \leq 2, \quad \phi \in [0,\, 2\pi) \\ &= e^{\jmath\left(\cos^{-1}\left(\frac{r}{2}\right)+\phi\right)} + e^{-\jmath\left(\cos^{-1}\left(\frac{r}{2}\right)-\phi\right)} \end{aligned} \tag{2.6}$$

Thus, the feasible set encompasses all the points residing inside the aforementioned circular region. Consequently, the new constraint for the analog precoder matrix is that $|\mathbf{F}_{\mathrm{RF}}(i,j)| \leq 2$, implying that the signal's amplitude can be controlled by a factor of less than two. This results in a convex constraint, thereby simplifying the design of the precoder. However, it comes at the cost of doubling the number of PSs required for implementing the precoder.

4. **FPSs & Switch**

The deployment of FPSs with switches to interconnect RF chains to antennas is demonstrated in Figure 2.3d. The process begins with the RF chain's output signal, which is passed through N_{ps} FPSs, thereby producing N_{ps} signals with diverse phases. Subsequently, the N_{ps} signals are routed via N_{ps} dedicated switches before combining at the antenna's side. The precoding coefficient can be expressed as:

$$\mathbf{F}_{\mathrm{RF}}(i,j) = \sum_{n=1}^{N_{\mathrm{ps}}} s_n e^{\jmath\theta_n} \qquad \theta_n = e^{\jmath 2\pi n/N_{\mathrm{ps}}}, \qquad s_n \in \{0,1\} \tag{2.7}$$

where θ_n and s_n are the phase shift and switch state corresponding to the nth FPS. Although N_{ps} switches are required to generate the analog precoding gain between each RF chain-antenna pair, it is important to note that adaptive switches are significantly easier to implement than adaptive PSs due to their binary on-off states [22], [23]. By utilizing the adaptive switch network, the analog precoder can provide various precoding gains for different RF chain-antenna pairs. In this thesis, we will investigate the FPS implementation and demonstrate that it is limited to select analog precoding coefficients within a feasible set, i.e., $\mathbf{F}_{\mathrm{RF}}(i,j) \in \mathcal{F}$. Nevertheless, we will show that the FPS implementation's performance remains satisfactory even with a relatively small value of N_{ps}.

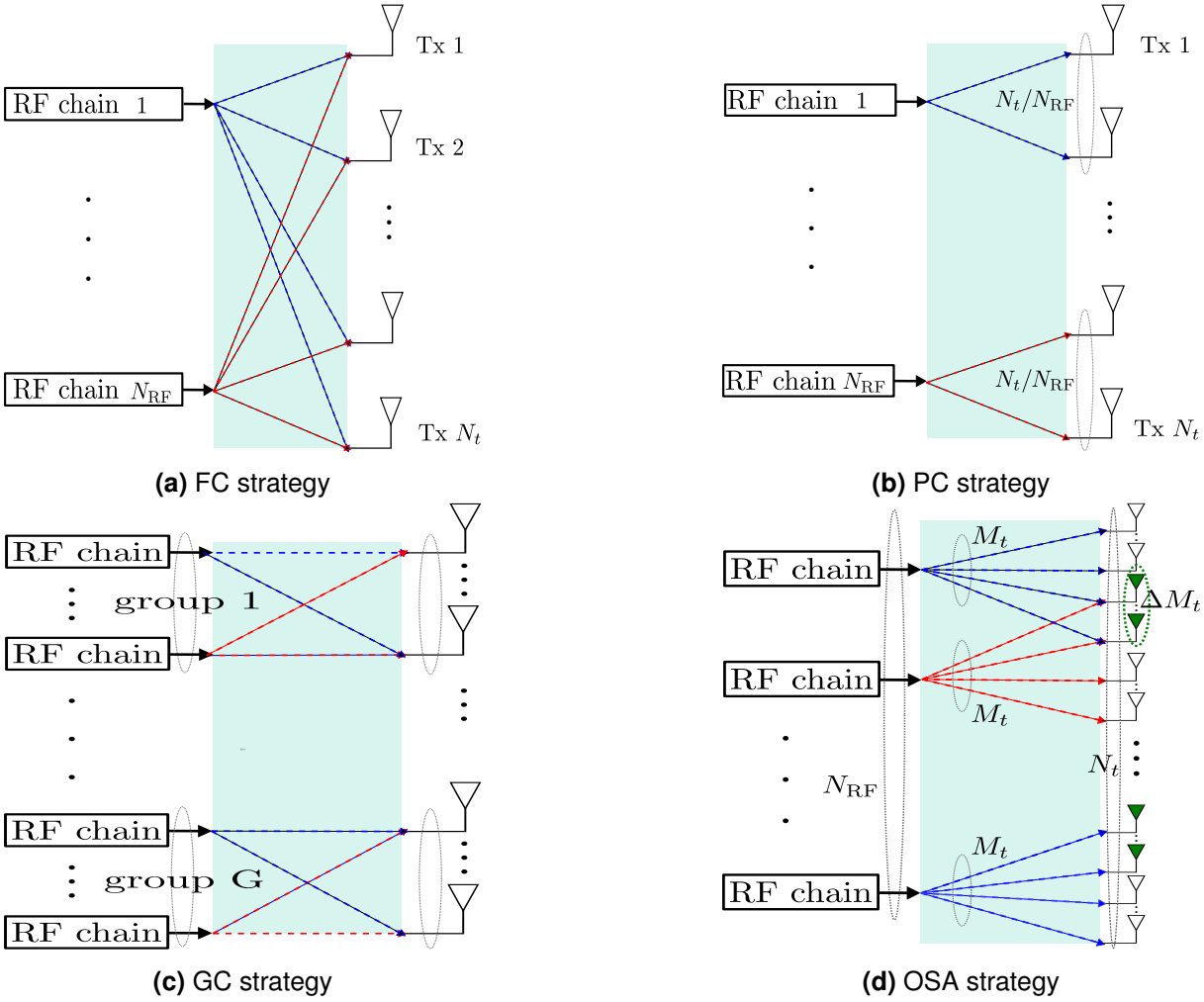

Figure 2.4: Mapping strategies [Source file]

2.3.2 The Mapping Strategy

The mapping strategy applied in the analog network of HBF systems affects both the performance and complexity of the system. The mapping strategy specifies the RF paths between RF chains and antenna elements, and the number of RF paths illustrates the complexity of the analog network, regardless of the RF components within RF paths. Each RF path contributes a non-zero entry to the analog precoding matrix $\mathbf{F}_{\mathrm{RF}}$, whereas the absence of a connection between an RF chain and an antenna element results in a zero entry. The maximum and minimum numbers of RF paths are obtained when all antennas are connected to every RF chain and when each antenna is connected to a single RF chain, respectively. This leads to a total of $\left(N_{\mathrm{RF}}-1\right)N_{\mathrm{t}}$ possible configurations

for the analog network, each with a unique number of RF paths. However, not all of these configurations are equally efficient for solving the precoding design problem. In general, mapping strategies with more RF paths tend to yield better performance but also increase system complexity. To balance this trade-off, several mapping strategies have been proposed, and among them, some of the most commonly used are described below.

1. **Fully-connected**

   As shown in Figure 2.4a, the FC strategy connects all the RF chains to all the antennas through $N_{\mathrm{RF}}N_{\mathrm{t}}$ RF paths. Despite requiring the most complex architecture, this mapping strategy provides full beamforming gain which allowing the achievement of optimal performance. The analog precoder matrix associated with this mapping approach contains no zero entries, making it an attractive option for precoding design. However, hardware implementation constraints are the primary challenge to addressing the precoding design problem when using the FC strategy.

2. **Partially-connected**

   The PC or sub-connected strategy links each of the N_{RF} RF chains to a distinct sub-array of size $N_{\mathrm{t}}/N_{\mathrm{RF}}$, as illustrated in Figure 2.4b. In comparison with the FC architecture, the PC structure has a lower hardware complexity of N_{t} RF paths, at the cost of a lower beamforming gain of $1/N_{\mathrm{RF}}$. This configuration introduces an additional constraint on the analog beamforming matrix, forcing $N_{\mathrm{t}} - N_{\mathrm{t}}/N_{\mathrm{RF}}$ entries to zero value in each column. Typically, the non-zero entries create a diagonal matrix as follows:

$$\mathbf{F}_{\mathrm{RF}} = \begin{bmatrix} \mathbf{f}_1 & \mathbf{0} & \dots & \mathbf{0} \\ \mathbf{0} & \mathbf{f}_2 & & \mathbf{0} \\ \vdots & \vdots & \ddots & \vdots \\ \mathbf{0} & \mathbf{0} & \dots & \mathbf{f}_{N_{\mathrm{RF}}} \end{bmatrix}_{N_t \times N_{\mathrm{RF}}} \tag{2.8}$$

   where $\mathbf{f}_j \in \mathbb{C}^{N_{\mathrm{t}}/N_{\mathrm{RF}} \times 1}$ represents the vector of coefficients associated with the jth RF chain.

3. **Group connected (or Hybridly connected)**

The Group Connected (GC) strategy, as depicted in Figure 2.4c, entails dividing RF chains and antennas into G disjoint groups, with the FC strategy being employed for intra-group connections. The key distinction between this strategy and above mentioned ones is that the number of groups in the GC strategy can range from 1, equivalent to the FC strategy, to N_{RF}, equivalent to the PC strategy. This results in a total of N_{RF} feasible configurations for the analog network, with each configuration featuring a distinct number of RF paths chosen from the set $\{N_{\mathrm{t}}, 2N_{\mathrm{t}}, \ldots, N_{\mathrm{RF}}N_{\mathrm{t}}\}$. Consequently, the analog precoding matrix displays a block diagonal pattern, with each block representing one RF chain-antenna group, expressed as:

$$\mathbf{F}_{\mathrm{RF}} = \begin{bmatrix} \mathbf{F}_1 & \mathbf{0} & \ldots & \mathbf{0} \\ \mathbf{0} & \mathbf{F}_2 & & \mathbf{0} \\ \vdots & \vdots & \ddots & \vdots \\ \mathbf{0} & \mathbf{0} & \ldots & \mathbf{F}_G \end{bmatrix}, \tag{2.9}$$

where $\mathbf{F}_g \in \mathbb{C}^{\frac{N_{\mathrm{t}}}{G} \times \frac{N_{\mathrm{RF}}}{G}}$ represents the submatrix of the analog precoding which corresponds to the g-th group. The GC strategy encompasses both FC and PC mapping strategies as special configurations:

- In the case where $G = 1$, all RF chains and antennas belong to the same group, resulting in a FC mapping strategy.
- When $G = N_{\mathrm{RF}}$, there is only one RF chain connected to $N_{\mathrm{t}}/N_{\mathrm{RF}}$ antennas within each group, and the mapping strategy is identical to that of the PC mapping.

4. **Overlapped subarray**

The Overlapped Sub-Array (OSA) mapping strategy connects each RF chain to a sub-array, similar to the PC strategy, but with the added capability of permitting overlap between sub-arrays. This results in some antennas in the overlap region being linked to more than one RF chain. As illustrated in Figure 2.4d, each RF chain is linked to a subarray of size $M_{\mathrm{t}} = N_{\mathrm{t}} - (N_{\mathrm{RF}} - 1)\Delta M_{\mathrm{t}}$, where ΔM_{t} denotes the number of overlapping elements. Therefore, $N_{\mathrm{t}}/N_{\mathrm{RF}} + 1$ distinct configurations can be created, each with a unique number of overlapping elements ΔM_{t}. The

pattern of the analog precoding matrix $\mathbf{F}_{\mathrm{RF}}$ can be expressed as:

$$\mathbf{F}_{\mathrm{RF}} = \begin{bmatrix} \mathbf{f}_1(1) & \mathbf{0} & \dots & \mathbf{0} \\ \vdots & \mathbf{f}_2(1) & \dots & \mathbf{0} \\ \mathbf{f}_1(M_{\mathrm{t}}) & \vdots & & \mathbf{0} \\ \mathbf{0} & \mathbf{f}_2(M_{\mathrm{t}}) & \ddots & \mathbf{0} \\ \mathbf{0} & \mathbf{0} & \dots & \mathbf{f}_{N_{\mathrm{RF}}}(1) \\ \mathbf{0} & \mathbf{0} & \dots & \vdots \\ \mathbf{0} & \mathbf{0} & \dots & \mathbf{f}_{N_{\mathrm{RF}}}(M_{\mathrm{t}}) \end{bmatrix} \tag{2.10}$$

where $\mathbf{f}_n(i), i = 1, \dots, M_{\mathrm{t}}, n = 1, \dots, N_{\mathrm{RF}}$ are non-zero coefficients in the precoding matrix $\mathbf{F}_{\mathrm{RF}}$. Indeed, the FC and PS strategies are two special cases of the OSA mapping strategy, with $\Delta M_{\mathrm{t}} = 0$ and $\Delta M_{\mathrm{t}} = N_{\mathrm{t}}/N_{\mathrm{RF}}$, respectively.

5. **Dynamic strategies**

   The above-mentioned mapping strategies rely on fixed RF paths between specific RF chain-antenna pairs. On the other hand, several adaptive architectures have been proposed which incorporate RF switches to enable the modification of RF paths. Dynamic architectures are primarily motivated by two objectives: Energy Efficiency (EE) and SE. Higher EE can be achieved by *deactivating* specific RF paths (e.g., a PS, an element/subarray of antenna array), resulting in reduced energy consumption. On the other hand, SE can be enhanced by *adjusting* the RF paths according to the Channel State Information (CSI). It is important to note that implementing a dynamic architecture comes at the cost of increased hardware and computational complexity, stemming from the additional switches required.

2.4 Related Works

In this section of the thesis, we present a comprehensive overview of the relevant literature pertaining to the research topic. We organize numerous research studies conducted on HBF based on the system architectures considered, which are aimed at developing solutions for various scenarios, such as Single-User Single-Carrier (SU-SC), Single-User Multi-Carrier (SU-MC) [24]–[26], Multi-User Single-Carrier (MU-SC) [10],

[27]–[29], and Multi-User Multi-Carrier (MU-MC) scenarios [29], [30]. Furthermore, we recommend that readers refer to several surveys published in recent years that have gathered a wealth of information and perspectives from researchers in the field [5], [17], [18], [31]–[33].

2.4.1 Early Research Works

The concept of HBF originated in the early 2000s, when it was proposed as a soft antenna selection approach to serve as an alternative to conventional antenna selection, which provides limited array gains and performs poorly in correlated channels [34]. That idea replaces simple RF switches with PSs that enable processing in the RF domain. Nearly a decade later, with the introduction of mmWave massive MIMO as a potential candidate for 5G systems, HBF has regained attention as a means of reducing the high cost and power consumption of mmWave RF hardware. This renewed interest has attracted significant attention from both academia and industry. [35]–[40].

The authors of [35] presented relatively simple analytical solutions for analog receiver processing using quantized phase control and ADCs. However, their work made assumptions about idealized fading distributions, such as correlated Rayleigh fading, which are not suitable for mmWave massive MIMO systems. In [36], Robert W. Heath and his colleagues conducted a preliminary investigation of HBF, which was based on the characteristics of mmWave channels, including limited scattering at high frequencies and antenna correlation in large arrays. They formulated the precoding problem as a sparsity-constrained least squares problem and solved it using basis pursuit. To develop the algorithmic precoding, they employed the concept of Orthogonal Matching Pursuit (OMP), which approximates the optimal unconstrained precoder as a linear combination of beam steering vectors that can be implemented in RF hardware [39]. The OMP algorithm was specifically designed for cases where partial channel knowledge is available on both sides of the communication link [37]. El et al. [38] introduced the PC architecture for the first time and presented a straightforward algorithmic approach for single-user MIMO systems. Kim et al. [40] developed algorithms that aim to optimize the received signal strength or the aggregate rate across diverse subcarriers for a single-stream MIMO-OFDM scenario in this architecture.

2.4.2 Works on the FC Mapping Strategy

The FC mapping strategy has received significant attention in the research community, and numerous optimization algorithms have been proposed to compute digital and analog beamformers for different hardware implementations, e.g., single phase shifter (FC-SPS) [24], [25], [27], [39], quantized phase shifter (FC-QPS) [41]–[43], double phase shifter (FC-DPS) [30], [44], and fixed phase shifter (FC-FPS) [45]–[49]. Among these techniques, the OMP algorithm stands out as one of the most important and widely-used algorithms [39].

The Alternating Minimization (AltMin) principle had been adopted to design hybrid precoding algorithms for FC-SPS architecture [25]. The authors propose a manifold optimization approach based on AltMin (MO-AltMin). Despite the fact that this algorithm directly obtains precoder matrices under unit modulus constraints, it suffers from high computational complexity for a large number of antennas. The authors exploited the orthogonal property of the digital precoder to decouple the design problem of the hybrid precoder into two subproblems, and then alternately optimized the digital and analog precoders. In [41], hybrid precoders are designed to maximize the SE for massive MIMO systems by considering the FC architecture. When infinite-resolution PS is used, they demonstrated that the number of RF chains needed to achieve digital beamforming performance should be twice the number of data streams, i.e., $N_{\mathrm{RF}} = 2 \times N_{\mathrm{s}}$. In case $N_{\mathrm{s}} \leq N_{\mathrm{RF}} \leq 2N_{\mathrm{s}}$, they propose an element-wise algorithm that iteratively updates the analog beamforming coefficients and then computes the digital beamforming matrix utilizing the water-filling method. Further, the algorithm has been modified for systems with FC-QPS architecture [42]. Du et al. (2018) investigated the performance of the FC-QPS hybrid precoding system under a practical hardware network model that accounts for dissipation [50]. The study examined the impact of quantized analog and digital precoding, analyzing parameters such as feedback bits, signal power, and the number of antennas on system performance. The research revealed that increasing signal power can compensate for the degradation in system performance caused by quantized analog precoding. In [44], Bogale et al. (2016) investigated the number of required RF chains and PSs in the FC-DPS architecture to achieve the same performance as fully DBF through the proposed HBF technique. The authors determined that the performance of

fully DBF can be achieved by utilizing RF chains that are equal in number to the rank of the combined digital precoder matrices of all subcarriers. Additionally, the number of PSs required was found to be $2N_{\mathrm{RF}}(N_{\mathrm{t}} - N_{\mathrm{RF}} + 1)$. In [30], Yu and colleagues (2019) demonstrated that in multiuser single carrier scenarios, the design of a hybrid precoder can be formulated as a low-rank matrix approximation problem, which can be solved analytically using a closed-form solution. However, in the case of multicarrier scenarios, they observed that the hybrid precoder may introduce residual interuser interference due to its approximation of the fully digital precoder. To address this issue, they proposed a solution that involves cascading an additional block diagonalization precoder at the baseband stage. This approach effectively cancels out the interuser interference. In [45], Yu et al. (2018) introduced the FC-FPS architecture for analog networks, which has been demonstrated to require only a limited number of PSs with fixed and quantized phases. The authors further developed an effective alternating minimization algorithm that leverages closed-form solutions in each iteration to determine the hybrid precoders and the states of switches.

2.4.3 Works on the PC Mapping Strategy

In the existing literature, some researches focus on enhancing the performance of PC architecture [38], [51]–[56]. As proposed by [38], the PC architecture features a one-to-one mapping between each RF chain and a distinct subset of $N_{\mathrm{t}}/N_{\mathrm{RF}}$ antennas, as illustrated in Figure 2.4b. Several recent studies have proposed novel techniques and optimization approaches to improve the efficiency and design of PC architectures. For instance, Gao et al. (2016) introduced a hybrid precoding technique that utilizes successive interference cancellation to decompose the optimization problem into simpler sub-problems, thereby reducing the complexity of the algorithm [51]. Similarly, Park et al. (2017) proposed a hybrid precoding design for mmWave MIMO-OFDM systems, which not only derived solutions for both fully and PC hybrid architectures but also explored the use of adaptively adjusted antenna subarrays [52]. In [53], He et al. (2016) presented a two-layer optimization method to maximize system EE. The first layer optimized the analog precoder and combiner using the alternating-direction optimization method, which adjusted the PS through an analytical structure. The second layer optimized the digital precoder and combiner based on an effective MIMO channel coefficient.

Likewise, Li et al. (2017) proposed a HBF design approach for multiple-user MIMO systems, where the analog combiner for each user is based on their channel's Singular Value Decomposition (SVD), and the analog precoder is obtained through channel conjugate transposition, maximizing the effective channel gain [54]. In [55], Zhu (2016) proposed an adaptive PS scheme that jointly designed the connection network and PSs to improve the performance of PC architectures. In [57], the authors extended the implementation of DPS to the PC structure for multiuser Orthogonal Frequency Division Multiplexing (OFDM) systems. They identified the hybrid precoding problem as an eigenvalue problem with a closed-form solution. The literature has introduced a variety of adaptive PS schemes, such as those discussed in [55], [58]. Nevertheless, the majority of sub-connected architectures allocate the same number of antennas to each sub-array [38], [51], [52], [55]. Nguyen et al. (2019) introduced the Unequal Sub-Array (UESA) architecture, which is a specific type of PS design that enables the allocation of different numbers of antennas to sub-antenna arrays, thereby improving the flexibility of PS systems. These studies collectively contribute to advancing the design and optimization of PC architectures for various wireless communication systems [56].

2.4.4 Works on the Other Architectures

Based on current research, it is evident that there is no single HBF structure that can optimally balance the trade-off between performance and complexity. Thus, various research efforts have been made to propose fixed and dynamic structures, followed by solving the corresponding precoder design problem [38], [56], [59], [60]. These include the PC, UESA, hybridly connected, and OSA architectures. The PC structure, introduced by El et al. (2013), connects each RF chain to a distinct subarray of the same size [38]. On the other hand, the UESA architecture, presented by Nguyen et al. (2019), allows for the allocation of variable numbers of antennas to sub-antenna arrays, which provides greater flexibility in PS systems [56]. Zhang et al. (2017) introduced the hybridly connected structure, which comprises multiple sub-arrays, with each sub-array connecting to multiple RF chains [59]. Subsequently, each RF chain is connected to all of the corresponding antennas that belong to the respective sub-array. Moreover, Song et al. (2017) proposed the OSA structure, which permits the subarrays to overlap, allowing certain antennas in the overlapping region to connect with multiple RF chains.

The OSA architecture is adaptable to FC and non-OSA configurations [60].

Adaptive architectures have also been proposed to achieve significant performance enhancement by adding RF switches to adjust the RF-paths or enable/disable RF components [22], [57], [61]–[65]. For instance, Mendez et al. (2016) proposed four hybrid architectures based on switching networks as an alternative solution to reduce the complexity and power consumption of PS-based structures [22]. The proposed architectures are: (1) replacing each PS with a switch in the FC architecture, (2) replacing each variable PS with a switch in the PC architecture, (3) selecting N antennas from the antenna array, and (4) selecting one antenna from each subset in the PC architecture. In [57], Yu et al. (2017) proposed an extension of the implementation of DPS to the adaptive PC structure in multiuser OFDM systems. To achieve improved spectral efficiency, the authors proposed two effective algorithms: the greedy algorithm and the modified K-means algorithm. These algorithms were designed to dynamically optimize the RF chain-antenna mapping. Payami (2016) proposed a PS selection scheme for FC structure that employs a dedicated switch for each PS to disable unnecessary shifters [61]. The scheme aims to enhance the EE of the beamformer by reducing excess power consumption and improving spectral efficiency. Guo et al. (2019) proposed an adaptive OSA structure that utilizes a connection network to adjust the states of the PSs, with a heuristic hybrid pre-coding scheme presented to optimize the EE of the system [62]. Yan et al. (2020) introduced a dynamic PC structure for the precoding matrix in which the interconnections between RF chains and subarrays are dynamically adjusted by means of a network of switches [63]. The authors developed two types of algorithms: element-by-element and vectorization-based algorithms. In [64] Xue et al. (2020) proposed a joint optimization approach for hybrid precoding and connection-state matrix to maximize EE. Li et al. (2020) presented a dynamic PC architecture that employs low-resolution PSs and switch networks to connect each RF chain to non-overlapping antenna subarrays [65]. The hybrid precoder and combiner are jointly designed to maximize the average spectral efficiency of the mmWave MIMO-OFDM system.

3

Hybrid Beamforming Matrices Calculation: A New Approach

Sommaire

THE main objective of this chapter is to address the issue of computational complexity in HBF systems that employ FPSs and switches in their analog networks. The complexity associated with switch state selection is a critical component in obtaining the digital and analog beamforming matrices simultaneously, which requires a significant computational effort.

To tackle this challenge, the chapter presents a detailed analysis of the HBF problem in such a system and establishes that the analog precoder matrix is dependent on the switch matrix. However, obtaining the optimal switch state requires an exhaustive search, which becomes computationally infeasible due to the exponential increase in the number of possibilities of switch states with the number of antennas and data streams.

To overcome this computational complexity, the chapter proposes a low-complexity algorithm that decomposes the main problem into sub-problems, leading to a reduction in complexity to linear complexity with the number of antennas and data streams. This approach makes the optimal solution achievable by searching through a much smaller feasible set.

Further investigation into the feasible set leads to two crucial observations: the points in the set are periodic with a phase difference of $360/N_{\mathrm{ps}}$, and some points are superimposed. By exploiting these two properties, the chapter shows that the size of the feasible set can be significantly reduced. Specifically, the optimal solution can be found by searching through less than 1% of the search space if the number of phase levels

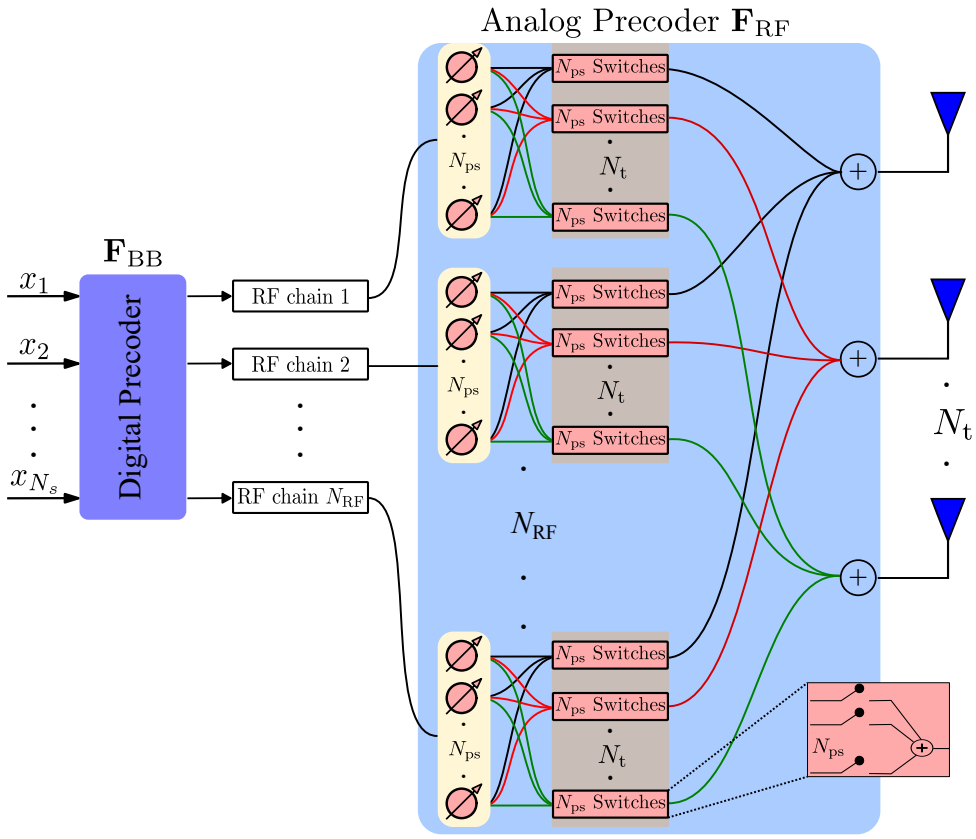

Figure 3.1: Transmitter structure [Source file]

exceeds 14.

Finally, the proposed algorithm is evaluated in the context of a multi-user massive MIMO system, demonstrating that it can implement precoders designed for fully digital architecture.

3.1 System Model

In this section, a Single-User MIMO (SU-MIMO) system is examined, with a transmitter architecture illustrated in Figure 3.1. This architecture has been proposed as a hardware-efficient structure for performing HBF [45]. Specifically, the transmitter is capable of transmitting N_{s} streams simultaneously to the intended user by employing N_{t} antennas for data transmission, while the user employs N_{r} antennas for reception. Both the transmitter and receiver utilize the minimum number of RF chains, which, in this case, is $N_{\mathrm{RF}} = N_{\mathrm{s}}$, for transferring data streams from the baseband to RF and vice versa. Under

this assumption, the received signal at the user's end can be expressed as follows:

$$\mathbf{y} = \sqrt{\rho}\mathbf{H}\mathbf{F}_{\mathrm{RF}}\mathbf{F}_{\mathrm{BB}}\mathbf{x} + \mathbf{n}, \tag{3.1}$$

where $\mathbf{y}$ is the $N_{\mathrm{r}} \times 1$ received vector, $\mathbf{x} \in \mathbb{C}^{N_{\mathrm{s}} \times 1}$ denotes the data stream vector such that $\mathbb{E}\{\mathbf{x}\mathbf{x}^{\mathrm{H}}\} = \mathbf{I}_{N_{\mathrm{s}}}$, $\mathbf{H} \in \mathbb{C}^{N_{\mathrm{r}} \times N_{\mathrm{t}}}$ is the channel matrix with $\mathbb{E}\{\|\mathbf{H}\|_{\mathrm{F}}^2\} = N_{\mathrm{t}}N_{\mathrm{r}}$, ρ represents the average received power, and $\mathbf{n} \in \mathbb{C}^{N_{\mathrm{r}} \times 1}$ is the vector of independent and identically distributed (i.i.d.) complex Gaussian noise that follows $\mathcal{CN}(0, \sigma_{\mathrm{n}}^2)$ such that $\mathbb{E}\{\mathbf{n}\mathbf{n}^{\mathrm{H}}\} = \sigma_{\mathrm{n}}^2\mathbf{I}_{N_{\mathrm{r}}}$. The $\mathbf{F}_{\mathrm{RF}} \in \mathbb{C}^{N_{\mathrm{t}} \times N_{\mathrm{s}}}$ and $\mathbf{F}_{\mathrm{BB}} \in \mathbb{C}^{N_{\mathrm{s}} \times N_{\mathrm{s}}}$ are respectively analog and digital precoder matrices that are used in the transmitter to apply HBF. The system architecture depicted in Figure 3.1 employs N_{ps} FPSs in front of each RF chain to generate signals with distinct phases, which are then passed into switch networks. The coefficients of analog beamforming are subsequently constructed by selecting appropriate switch states behind the antennas. The resulting analog precoding matrix, denoted as $\mathbf{F}_{\mathrm{RF}}$, can be expressed as:

$$\mathbf{F}_{\mathrm{RF}} = \mathbf{S}\mathbf{C}, \tag{3.2}$$

where the switch matrix $\mathbf{S}$ is an $N_{\mathrm{t}} \times N_{\mathrm{ps}}N_{\mathrm{s}}$ binary matrix defined as:

$$\mathbf{S} \triangleq \begin{bmatrix} \mathbf{s}_{11} & \mathbf{s}_{12} & \dots & \mathbf{s}_{1N_{\mathrm{s}}} \\ \vdots & & \ddots & \vdots \\ \mathbf{s}_{N_{\mathrm{t}}1} & \mathbf{s}_{N_{\mathrm{t}}2} & \dots & \mathbf{s}_{N_{\mathrm{t}}N_{\mathrm{s}}} \end{bmatrix}, \tag{3.3}$$

where $\mathbf{s}_{ij}$ is a binary horizontal vector of size N_{ps} representing the switch network's states that connect the jth RF chain to the ith antenna. The phase shift operation carried out by the FPSs is represented by the matrix $\mathbf{C} \in \mathbb{C}^{N_{\mathrm{ps}}N_{\mathrm{s}} \times N_{\mathrm{s}}}$, which is given by a block diagonal matrix:

$$\mathbf{C} \triangleq \begin{bmatrix} \mathbf{c} & \mathbf{0} & \dots & \mathbf{0} \\ \mathbf{0} & \mathbf{c} & & \mathbf{0} \\ \vdots & \vdots & \ddots & \vdots \\ \mathbf{0} & \mathbf{0} & \dots & \mathbf{c} \end{bmatrix}, \tag{3.4}$$

where $\mathbf{c} = \left[1, e^{\jmath 2\pi \frac{1}{N_{\mathrm{ps}}}}, \ldots, e^{\jmath 2\pi \frac{N_{\mathrm{ps}}-1}{N_{\mathrm{ps}}}}\right]^{\mathrm{T}}$ is the phase shift vector. The entries of $\mathbf{c}$ lie on the unit circle in the complex plane, with an equal phase difference of $e^{\jmath \frac{2\pi}{N_{\mathrm{ps}}}}$ between adjacent entries. At the receiver's end, a HBF scheme is also employed to process the received vector $\mathbf{y}$:

$$\widetilde{\mathbf{y}} = \mathbf{W}_{\mathrm{BB}}^{\mathrm{H}} \mathbf{W}_{\mathrm{RF}}^{\mathrm{H}} \mathbf{y}, \tag{3.5}$$

where $\mathbf{W}_{\mathrm{RF}}$ is the $N_{\mathrm{r}} \times N_{\mathrm{s}}$ analog combining matrix and $\mathbf{W}_{\mathrm{BB}}$ is the $N_{\mathrm{s}} \times N_{\mathrm{s}}$ digital combining matrix. Based on this assumption, the spectral efficiency achieved when Gaussian symbols are transmitted over the mmWave channel can be expressed as:

$$R = \log_2\left(\left|\mathbf{I}_{N_{\mathrm{s}}} + \frac{\rho}{\sigma_{\mathrm{n}}^2} \mathbf{R}_{\mathrm{n}}^{-1} \mathbf{W}_{\mathrm{BB}}^{\mathrm{H}} \mathbf{W}_{\mathrm{RF}}^{\mathrm{H}} \mathbf{H} \mathbf{F}_{\mathrm{RF}} \mathbf{F}_{\mathrm{BB}} \times \mathbf{F}_{\mathrm{BB}}^{\mathrm{H}} \mathbf{F}_{\mathrm{RF}}^{\mathrm{H}} \mathbf{H}^{\mathrm{H}} \mathbf{W}_{\mathrm{RF}} \mathbf{W}_{\mathrm{BB}}\right|\right), \tag{3.6}$$

where $\mathbf{R}_{\mathrm{n}} = \mathbf{W}_{\mathrm{BB}}^{\mathrm{H}} \mathbf{W}_{\mathrm{RF}}^{\mathrm{H}} \mathbf{W}_{\mathrm{RF}} \mathbf{W}_{\mathrm{BB}}$, and $|.|$ is the determinant operator.

3.2 Problem Formulation

To design HBF that maximizes the spectral efficiency, the following optimization problem needs to be solved:

$$\underset{\mathbf{W}_{\mathrm{BB}}, \mathbf{W}_{\mathrm{RF}}, \mathbf{F}_{\mathrm{RF}}, \mathbf{F}_{\mathrm{BB}}}{\text{maximize}} \quad \log_2\left(\left|\mathbf{I}_{N_{\mathrm{s}}} + \frac{\rho}{\sigma_{\mathrm{n}}^2} \mathbf{R}_{\mathrm{n}}^{-1} \mathbf{W}_{\mathrm{BB}}^{\mathrm{H}} \mathbf{W}_{\mathrm{RF}}^{\mathrm{H}} \mathbf{H} \mathbf{F}_{\mathrm{RF}} \mathbf{F}_{\mathrm{BB}} \times \mathbf{F}_{\mathrm{BB}}^{\mathrm{H}} \mathbf{F}_{\mathrm{RF}}^{\mathrm{H}} \mathbf{H}^{\mathrm{H}} \mathbf{W}_{\mathrm{RF}} \mathbf{W}_{\mathrm{BB}}\right|\right) \tag{3.7a}$$

$$\text{s.t.} \quad \|\mathbf{F}_{\mathrm{RF}} \mathbf{F}_{\mathrm{BB}}\|_{\mathrm{F}}^2 = 1 \tag{3.7b}$$

$$\mathbf{F}_{\mathrm{RF}}(i, \ell) \in \mathcal{F}, \quad \forall i, \ell \tag{3.7c}$$

$$\mathbf{W}_{\mathrm{RF}}(i, \ell) \in \mathcal{W}, \quad \forall i, \ell. \tag{3.7d}$$

The condition $\|\mathbf{F}_{\mathrm{RF}} \mathbf{F}_{\mathrm{BB}}\|_{\mathrm{F}}^2 = 1$ is imposed to ensure that the beamforming operation does not change the total power. Here, $\mathcal{F}$ and $\mathcal{W}$ denote the feasible sets for each element of the analog matrices at the transmitter and receiver, respectively.

The problem of maximizing spectral efficiency in (3.7) requires joint optimization over the hybrid precoders and combiners, which is often intractable due to the non-convex constraints on $\mathbf{F}_{\mathrm{RF}}$ and $\mathbf{W}_{\mathrm{RF}}$ [66]. To address this issue, the joint transmitter-receiver

optimization problem can be decoupled into separate precoder (transmitter-side) and combiner (receiver-side) problems, as proposed in [39]. In this work, we focus on the design of the hybrid precoders $\mathbf{F}_{\mathrm{RF}}\mathbf{F}_{\mathrm{BB}}$ such that the mutual information achieved by Gaussian signalling over the mmWave channel is maximized:

$$\mathcal{I}\left(\mathbf{x};\mathbf{y}\right)=\log_2\left(\left|\mathbf{I}_{N_{\mathrm{r}}}+\frac{\rho}{\sigma_{\mathrm{n}}^2}\mathbf{H}\mathbf{F}_{\mathrm{RF}}\mathbf{F}_{\mathrm{BB}}\mathbf{F}_{\mathrm{BB}}^{\mathrm{H}}\mathbf{F}_{\mathrm{RF}}^{\mathrm{H}}\mathbf{H}^{\mathrm{H}}\right|\right). \tag{3.8}$$

The precoder optimization problem can be stated as

$$\begin{aligned}\left(\mathbf{F}_{\mathrm{RF}}^{\mathrm{opt}},\mathbf{F}_{\mathrm{BB}}^{\mathrm{opt}}\right) &= \underset{\mathbf{F}_{\mathrm{RF}},\mathbf{F}_{\mathrm{BB}}}{\operatorname{argmax}} \quad \mathcal{I}\left(\mathbf{x};\mathbf{y}\right) && \text{(3.9a)}\\ \text{s.t.} \quad & \left\|\mathbf{F}_{\mathrm{RF}}\mathbf{F}_{\mathrm{BB}}\right\|_{\mathrm{F}}^2=1 && \text{(3.9b)}\\ & \mathbf{F}_{\mathrm{RF}}\left(i,\ell\right)\in\mathcal{F}, \quad \forall i,\ell && \text{(3.9c)}\end{aligned}$$

In the presence of the non-convex feasibility constraint $\mathbf{F}_{\mathrm{RF}}(i,\ell)\in\mathcal{F}, \quad \forall i,\ell$, a general solution for (3.9) does not exist. To obtain a near-optimal precoder, the problem can be approximated as [39]

$$\begin{aligned}\left(\mathbf{F}_{\mathrm{RF}}^{\mathrm{opt}},\mathbf{F}_{\mathrm{BB}}^{\mathrm{opt}}\right) &= \underset{\mathbf{F}_{\mathrm{RF}},\mathbf{F}_{\mathrm{BB}}}{\operatorname{argmin}} \quad \left\|\mathbf{F}_{\mathrm{opt}}-\mathbf{F}_{\mathrm{RF}}\mathbf{F}_{\mathrm{BB}}\right\|_{\mathrm{F}}^2 && \text{(3.10a)}\\ \text{s.t.} \quad & \left\|\mathbf{F}_{\mathrm{RF}}\mathbf{F}_{\mathrm{BB}}\right\|_{\mathrm{F}}^2=1 && \text{(3.10b)}\\ & \mathbf{F}_{\mathrm{RF}}\left(i,\ell\right)\in\mathcal{F}, \quad \forall i,\ell && \text{(3.10c)}\end{aligned}$$

Here, $\mathbf{F}_{\mathrm{opt}}$ is the optimal fully-digital precoder, which is formed by the first N_{s} columns of the unitary matrix $\mathbf{V}$ derived from the ordered SVD of the channel matrix, i.e., $\mathbf{H}=\mathbf{U}\boldsymbol{\Sigma}\mathbf{V}^{\mathrm{H}}$. By substituting (3.2) into (3.10), the precoder design problem can be rewritten as:

$$\begin{aligned}\left(\mathbf{S}^{\mathrm{opt}},\mathbf{F}_{\mathrm{BB}}^{\mathrm{opt}}\right) &= \underset{\mathbf{S},\mathbf{F}_{\mathrm{BB}}}{\operatorname{argmin}} \quad \left\|\mathbf{F}_{\mathrm{opt}}-\mathbf{S}\mathbf{C}\mathbf{F}_{\mathrm{BB}}\right\|_{\mathrm{F}}^2 && \text{(3.11a)}\\ \text{s.t.} \quad & \left\|\mathbf{S}\mathbf{C}\mathbf{F}_{\mathrm{BB}}\right\|_{\mathrm{F}}^2=1 && \text{(3.11b)}\\ & \mathbf{S}\left(i,\ell\right)\in\left\{0,1\right\}, \quad \forall i,\ell. && \text{(3.11c)}\end{aligned}$$

To focus on the properties of the analog part, let us assume that $\mathbf{F}_{\mathrm{BB}}=\mathbf{I}_{N_{\mathrm{s}}}$ for the moment. This assumption reduces the optimization problem to equation (3.12), where

the only matrix to be optimized is the binary matrix $\mathbf{S}$. Note that the simulation results will evaluate the degradation in performance of the sub-optimal approach with respect to optimal digital beamforming.

$$\mathbf{S} = \underset{\mathbf{S}}{\operatorname{argmin}} \quad \left\|\mathbf{F}_{\text{optn}} - \mathbf{SC}\right\|_{\text{F}}^{2} \tag{3.12a}$$

$$\text{s.t.} \quad \mathbf{S}\left(i,\ell\right) \in \{0,1\}, \quad \forall i,\ell, \tag{3.12b}$$

where $\mathbf{F}_{\text{optn}}$ is the normalized version of $\mathbf{F}_{\text{opt}}$ with respect to the maximum possible amplitude of $\mathbf{SC}$, which is explained in more detail in equation (3.20). Note that the power constraint in (3.11) is temporarily removed and will be satisfied with $\mathbf{F}_{\text{BB}}$ in subsection 3.3.2. The problem (3.12) is an NP-hard integer programming problem, as stated in [67], and the optimal solution is obtained through exhaustive search. However, the exhaustive search on the switch matrix $\mathbf{S}$ is infeasible as it includes $N - e = 2^{N_{\text{t}}N_{\text{s}}N_{\text{ps}}}$ different states, which is too large for practical massive MIMO systems. It is worth noting that $\mathbf{s}_{ij}$ only depends on $\mathbf{F}_{\text{optn}}(i,j)$ due to the zero-elements in the matrix $\mathbf{C}$. As a result, the problem (3.12) can be decomposed into $N_{\text{t}}N_{\text{s}}$ independent sub-problems as:

$$\mathbf{s}_{ij} = \underset{\mathbf{s}_{ij}}{\operatorname{argmin}} \quad \left|\mathbf{F}_{\text{optn}}(i,j) - \mathbf{s}_{ij}\mathbf{c}\right|^{2} \tag{3.13a}$$

$$\text{s.t.} \quad \mathbf{s}_{ij}(\ell) \in \{0,1\}, \quad \forall \ell. \tag{3.13b}$$

Since the size of $\mathbf{s}_{ij}$ is independent of the number of antennas and RF chains, the exhaustive search is tractable even in a massive MIMO system. In other words, the number of feasible solutions is a function of only the number of PSs N_{ps}. Specifically, the size of the feasible set $\mathcal{F}$ is $2^{N_{\text{ps}}}$. This means that the number of candidate solutions grows linearly with the number of PSs, which is a much more manageable problem than the original $N_e = 2^{N_{\text{t}}N_{\text{s}}N_{\text{ps}}}$ candidate solutions in the original problem. To illustrate this point, Figure 3.2 shows the feasible set for $N_{\text{ps}} = 18$, which has a size of $2^{18} = 262144$. The feasible set will be investigated in more detail in the next section.

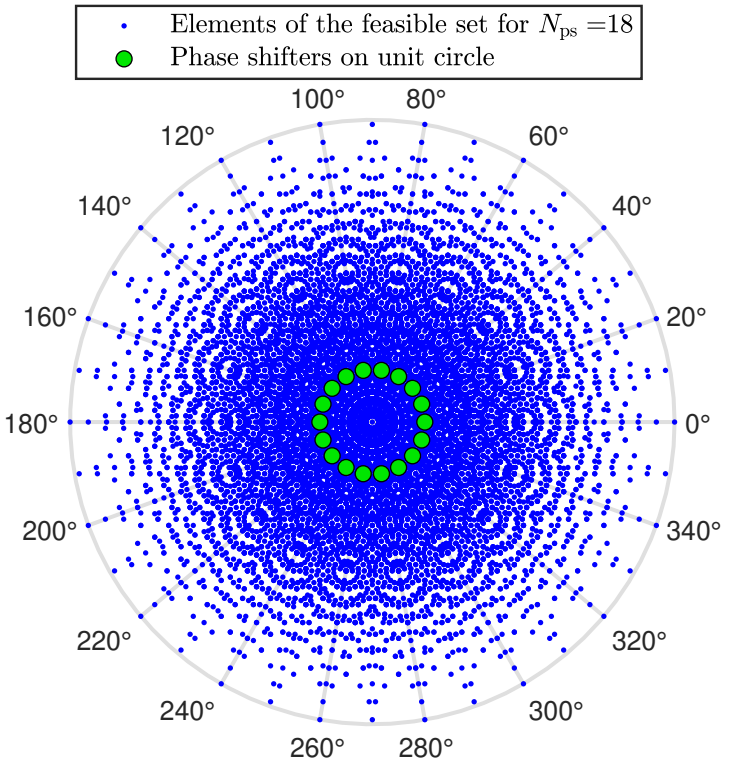

Figure 3.2: The feasible set $\mathcal{F}_{18}$ [MATLAB code], [Source file].

3.3 Hybrid Precoder Design

3.3.1 Feasible Set Analysis

Considering the cases where the numbers of active switches are even, the sum of the outputs of active PSs will determine a point in $\mathcal{F}_{N_{\rm ps}}$ with magnitude α and angle θ as follows:

$$\begin{aligned}\alpha e^{\jmath\theta} &= \sum_{i=1}^{\widetilde{N}_p} \left(e^{\jmath \frac{2\pi}{N_{\rm ps}} k_i} + e^{\jmath \frac{2\pi}{N_{\rm ps}} n_i} \right) \\ &= \sum_{i=1}^{\widetilde{N}_p} 2\cos\left(\frac{\pi}{N_{\rm ps}} (n_i - k_i) \right) e^{\jmath \frac{\pi}{N_{\rm ps}} (n_i + k_i)}, \end{aligned} \tag{3.14}$$

where $\widetilde{N}_p$ is the number of pairs of active switches. The number of active PSs is limited by the fact that any two switches at a distance of $N_{\rm ps}/2$ must not be active simultaneously, because each phase shifter is counterbalanced by another phase shifter with a phase difference of π. Therefore, the maximum number of active PSs is $N_{\rm ps}/2$. When $N_{\rm ps}/2$

active PSs are adjacent to each other, the outcome is a point with the maximum possible amplitude $\eta_{N_{\rm ps}}$ as (which is proven in section A.2):

$$\eta_{N_{\rm ps}} = \begin{cases} 2\sum_{n=1}^{\lceil N_{\rm ps}/4 \rceil} \cos\left(\frac{2n-1}{N_{\rm ps}}\pi\right) & \lceil \frac{N_{\rm ps}}{2} \rceil = \text{ even} \\ \sum_{n=-\lfloor N_{\rm ps}/4 \rfloor}^{\lfloor N_{\rm ps}/4 \rfloor} \cos\left(\frac{2n}{N_{\rm ps}}\pi\right) & \lceil \frac{N_{\rm ps}}{2} \rceil = \text{ odd} \end{cases}. \tag{3.15}$$

By using the principle mentioned above, after selecting the first phase shifter, the next selection is done within a set of size $N_{\rm ps}-2$. Therefore, the number of points for n selections can be expressed as:

$$\frac{1}{n!}\prod_{m=0}^{n-1}(N_{\rm ps}-2m). \tag{3.16}$$

Since $0 \leq n \leq N_{\rm ps}/2$, the number of points in $\mathcal{F}_{N_{\rm ps}}$ will be given by:

$$\left|\mathcal{F}_{N_{\rm ps}}\right| \leq 1 + \sum_{n=1}^{\frac{N_{\rm ps}}{2}} \frac{1}{n!}\prod_{m=0}^{n-1}(N_{\rm ps}-2m). \tag{3.17}$$

Interestingly, it can be verified that the expression for the size of the feasible set given in (3.17) is equal to:

$$\left|\mathcal{F}_{N_{\rm ps}}\right| \leq 3^{\frac{N_{\rm ps}}{2}}. \tag{3.18}$$

The above derivation shows that the size of the feasible set is significantly reduced compared to the initial search space of $2^{N_{\rm ps}}$. Specifically, the ratio of size reduction with respect to the initial search space is $(\frac{3}{4})^{\frac{N_{\rm ps}}{2}}$. Note that $\left|\mathcal{F}_{N_{\rm ps}}\right| = 3^{\frac{N_{\rm ps}}{2}}$ points are distinct when $N_{\rm ps}$ is a power of 2.

Periodic property

If $\alpha e^{j\theta}$ is a member of $\mathcal{F}_{N_{\rm ps}}$, then points $\alpha e^{j(\theta+k2\pi/N_{\rm ps})}$ for $k = 1, \ldots, N_{\rm ps}-1$ are also in $\mathcal{F}_{N_{\rm ps}}$, since it represents a circular shift of the active PSs. Therefore, the feasible set is created by $N_{\rm ps}$ periods of a basic sector as shown in Figure 3.3. The points in the basic

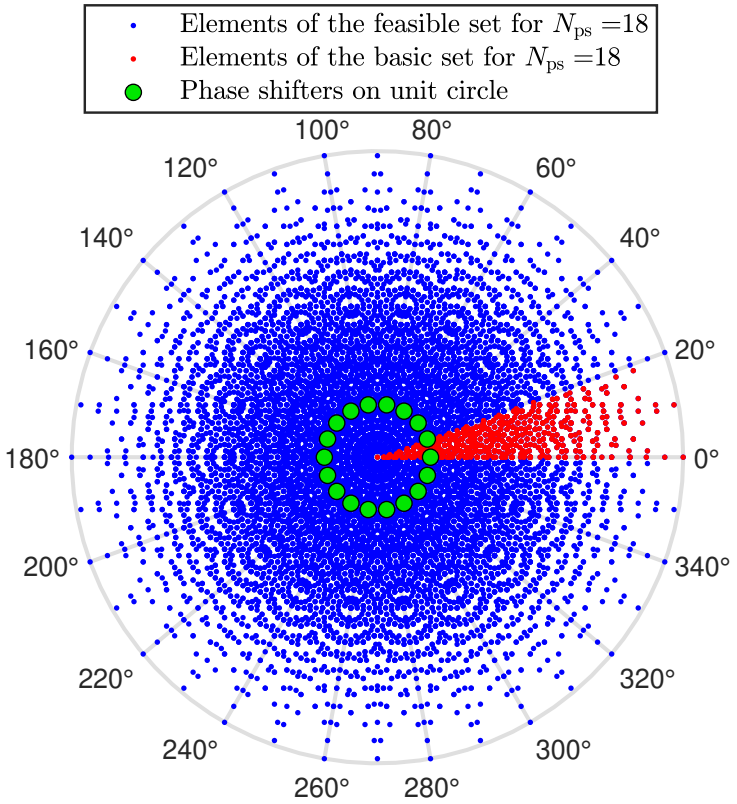

Figure 3.3: The basic set for $N_{\rm ps} = 18$ [MATLAB code], [Source file].

sector form a basic set with a size of:

$$\left|\mathcal{F}^{b}_{N_{\rm ps}}\right| \leq \left\lfloor \frac{3^{\frac{N_{\rm ps}}{2}} - 1}{N_{\rm ps}} \right\rfloor + 1. \tag{3.19}$$

Using the basic set, the size of the search space is reduced $N_{\rm ps}$ times without losing any points, resulting in a reduced search space of $\left(0.75\right)^{\frac{N_{\rm ps}}{2}}/N_{\rm ps}$ instead of the original $2^{N_{\rm ps}}$. Table 3.1 provides numerical values for the size of the search space required to solve the combinatorial optimization problem presented in (3.13). The table demonstrates that using the proposed basic set, the searching complexity is reduced to less than 1% for $N_{\rm ps} \geq 14$. As each point in the set corresponds to a unique combination of active switches, a lookup table can be constructed to contain the switch states for each point.

3.3.2 The Proposed Algorithm to Obtain Switch States

The previous sections have shown that the optimal solution to (3.13) is found by searching through the feasible set $\left|\mathcal{F}_{N_{\rm ps}}\right|$, which consists of $N_{\rm ps}$ shifted versions of the basic

Table 3.1: Comparison of the size of search space to obtain the optimal solution of (3.13).

N_{ps}	Complete set $\left\|\mathcal{S}_{N_{\mathrm{ps}}}\right\| = 2^{N_{\mathrm{ps}}}$	Feasible set $\left\|\mathcal{F}_{N_{\mathrm{ps}}}\right\| = 3^{\frac{N_{\mathrm{ps}}}{2}}$	Basic set $\left\|\mathcal{F}^{b}_{N_{\mathrm{ps}}}\right\| \leq \left\lfloor \frac{3^{\frac{N_{\mathrm{ps}}}{2}}-1}{N_{\mathrm{ps}}} \right\rfloor + 1$	Simplification $\left\|\mathcal{F}^{b}_{N_{\mathrm{ps}}}\right\| / \left\|\mathcal{S}_{N_{\mathrm{ps}}}\right\|$
2	4	3	2	50%
4	16	9	3	18.75%
6	64	27	5	7.81%
8	256	81	11	4.30%
10	1024	243	24	2.44%
12	4096	729	61	1.49%
14	16384	2187	157	0.96%
16	65536	6561	411	0.63%
18	262144	19683	1094	0.42%
20	1048576	59049	2953	0.28%

set. This section presents a low-complexity algorithm that uses the basic set, which only includes $\left|\mathcal{F}^{b}_{N_{\mathrm{ps}}}\right|$ points in a sector of the circle with a radius of $\eta_{N_{\mathrm{ps}}}$. The proposed algorithm uses a normalization step to distribute the elements of $\mathbf{F}_{\mathrm{opt}}$ to the feasible circle (see Figure 3.2). To perform this normalization, the largest element magnitude in $\mathbf{F}_{\mathrm{opt}}$, denoted as δ, is used to scale the coefficients of $\mathbf{F}_{\mathrm{opt}}$ as follows:

$$\mathbf{F}_{\mathrm{optn}} = \gamma \mathbf{F}_{\mathrm{opt}} \tag{3.20}$$

$$\gamma = \frac{\eta_{N_{\mathrm{ps}}}}{\delta} \tag{3.21}$$

Next, to transfer $\mathbf{F}_{\mathrm{optn}}$ into the basic set (see Figure 3.3), each of its elements is shifted repeatedly by $2\pi/N_{\mathrm{ps}}$ until it reaches the basic set. The resulting transfer matrix, denoted as $\mathbf{F}_{\mathrm{s}}$, is expressed as:

$$\mathbf{F}_{\mathrm{s}}(i,j) = \left|\mathbf{F}_{\mathrm{optn}}(i,j)\right| e^{\jmath\left(\measuredangle \mathbf{F}_{\mathrm{optn}}(i,j) - \frac{2\pi}{N_{\mathrm{ps}}}\mathbf{M}(i,j)\right)}. \tag{3.22}$$

where the element in ith row and jth column of matrix $\mathbf{M} \in \mathbb{Z}^{N_{\mathrm{t}} \times N_{\mathrm{s}}}$ represents the number of times $\mathbf{F}_{\mathrm{optn}}(i,j)$ is shifted to reach the basic set and is given by:

$$\mathbf{M}(i,j) = \left\lfloor \frac{\measuredangle \mathbf{F}_{\mathrm{optn}}(i,j)}{2\pi/N_{\mathrm{ps}}} \right\rfloor. \tag{3.23}$$

The mapping between $\mathbf{F}_{\mathrm{s}}$ and the basic set is achieved by finding the nearest element in the basic set to each element of $\mathbf{F}_{\mathrm{s}}$. This is done by calculating the Euclidean distance between each element of $\mathbf{F}_{\mathrm{s}}$ and all the members of the basic set, and selecting the element with the minimum distance as the nearest neighbor. The mapping process is expressed as:

$$\mathbf{F}_{\mathrm{s}} \longmapsto \mathbf{F}_{\mathrm{m}}, \tag{3.24}$$

where $\mathbf{F}_{\mathrm{m}}$ is the mapped version of $\mathbf{F}_{\mathrm{s}}$ into $\mathcal{F}^{b}_{N_{\mathrm{ps}}}$. Each element of $\mathbf{F}_{\mathrm{m}}$ corresponds to a specific state of the active switches:

$$\mathbf{F}_{\mathrm{m}}\big(i,j\big) = \widetilde{\mathbf{s}}_{ij}\mathbf{c}, \tag{3.25}$$

where $\widetilde{\mathbf{s}}_{ij}$ is extracted from the lookup table of $\mathcal{F}^{b}_{N_{\mathrm{ps}}}$. To turn $\mathbf{F}_{\mathrm{m}}\big(i,j\big)$ back to the original sector, i.e. $\mathbf{M}\big(i,j\big)$, one can simply perform $\mathbf{M}\big(i,j\big)$ circular shift to the $\mathbf{s}_{ij}$ vector as follows:

$$\mathbf{s}_{ij} = \widetilde{\mathbf{s}}_{ij} \gg \mathbf{M}(i,j), \tag{3.26}$$

where $\gg$ represents the circular right-shift operation. Thereupon, the element in ith row and jth column of the matrix $\mathbf{F}_{\mathrm{RF}}$ is obtained by:

$$\mathbf{F}_{\mathrm{RF}}\big(i,j\big) = \mathbf{s}_{ij}\mathbf{c}. \tag{3.27}$$

Once the $\mathbf{F}_{\mathrm{RF}}$ is calculated, the HBF problem in (3.11) is a classical optimization problem for the variable $\mathbf{F}_{\mathrm{BB}}$, that can be solved by pseudoinverse matrix as:

$$\widehat{\mathbf{F}}_{\mathrm{BB}} = \left(\mathbf{F}^{\mathrm{H}}_{\mathrm{RF}}\mathbf{F}_{\mathrm{RF}}\right)^{-1}\mathbf{F}^{\mathrm{H}}_{\mathrm{RF}}\mathbf{F}_{\mathrm{opt}}. \tag{3.28}$$

In order to satisfy the power constraint in (3.11), $\|\mathbf{F}_{\mathrm{RF}}\mathbf{F}_{\mathrm{BB}}\|^2_{\mathrm{F}} = 1$, we normalize $\mathbf{F}_{\mathrm{BB}}$ as:

$$\mathbf{F}_{\mathrm{BB}} = \frac{\widehat{\mathbf{F}}_{\mathrm{BB}}}{\left\|\mathbf{F}_{\mathrm{RF}}\widehat{\mathbf{F}}_{\mathrm{BB}}\right\|_{\mathrm{F}}}. \tag{3.29}$$

The proposed algorithm is summarized in Algorithm 1.

Algorithm 1 A Low-Complexity Algorithm for Hybrid Systems

Require: $\mathbf{F}_{\text{opt}}$;

Compute $\mathbf{F}_{\text{optn}} = \gamma \mathbf{F}_{\text{opt}}$;
Obtain the matrix $\mathbf{M}$ from (3.23);
Transfer $\mathbf{F}_{\text{optn}}$ into the basic sector and obtain $\mathbf{F}_{\text{s}}$ from (3.22);
For $i = 1, \ldots, N_{\text{t}}$;
  For $j = 1, \ldots, N_{\text{s}}$;
    Find the nearest point of the basic set to $\mathbf{F}_{\text{s}}(i,j)$, $\mathbf{F}_{\text{s}}(i,j) \longmapsto \mathbf{F}_{\text{m}}(i,j)$;
    Extract $\widetilde{\mathbf{s}}_{ij}$ corresponds $\mathbf{F}_{\text{m}}(i,j)$ from the code book of $\mathcal{F}^{b}_{N_{\text{ps}}}$;
    Compute $\mathbf{s}_{ij}$ by $\mathbf{M}(i,j)$ circular right-shifts of $\widetilde{\mathbf{s}}_{ij}$;
    Calculate $\mathbf{F}_{\text{RF}}(i,j) = \mathbf{s}_{ij}\mathbf{c}$;
  End for
End for
$\widehat{\mathbf{F}}_{\text{BB}} = \left(\mathbf{F}^{\text{H}}_{\text{RF}}\mathbf{F}_{\text{RF}}\right)^{-1}\mathbf{F}^{\text{H}}_{\text{RF}}\mathbf{F}_{\text{opt}}$;
$\mathbf{F}_{\text{BB}} = \dfrac{\widehat{\mathbf{F}}_{\text{BB}}}{\left\|\mathbf{F}_{\text{RF}}\widehat{\mathbf{F}}_{\text{BB}}\right\|_{\text{F}}}$.

3.3.3 Computational Complexity

The computational complexity of the proposed algorithm and the FPS-AltMin algorithm [45], which was proposed for the same architecture, can be compared. In the proposed algorithm, the computational complexity of the digital precoder mainly depends on the matrix inversion, which has an order of $\mathcal{O}(N_{\text{s}}^3)$. However, the overall complexity mostly depends on the analog precoder. In this algorithm, since the analog beamforming coefficients are obtained independently, the complexity grows linearly with the dimensions of the analog beamforming matrix, i.e., N_{t} and N_{s}. Moreover, to find the best switch states for each coefficient, $\left|\mathcal{F}^{b}_{N_{\text{ps}}}\right| \approx 3^{\frac{N_{\text{ps}}}{2}}/N_{\text{ps}}$ Euclidean distances need to be calculated. Therefore, the exhaustive search complexity of the proposed algorithm is $\mathcal{O}\left(N_{\text{s}}^3 + N_{\text{t}}N_{\text{s}}3^{\frac{N_{\text{ps}}}{2}}/N_{\text{ps}}\right)$.

On the other hand, the FPS-AltMin algorithm has a complexity of order $\mathcal{O}\Big(N_{\text{s}}^3 + N_{\text{t}}N_{\text{s}}N_{\text{ps}}\log\left(N_{\text{t}}N_{\text{s}}N_{\text{ps}}\right)\Big)$. The complexity of the digital parts is comparable in the two algorithms. However, in the analog part, due to the SVD calculations and sorting procedure, computational complexity increases non-linearly with the number of antennas and data streams. As shown in Figure 3.4, the complexity of the proposed algorithm

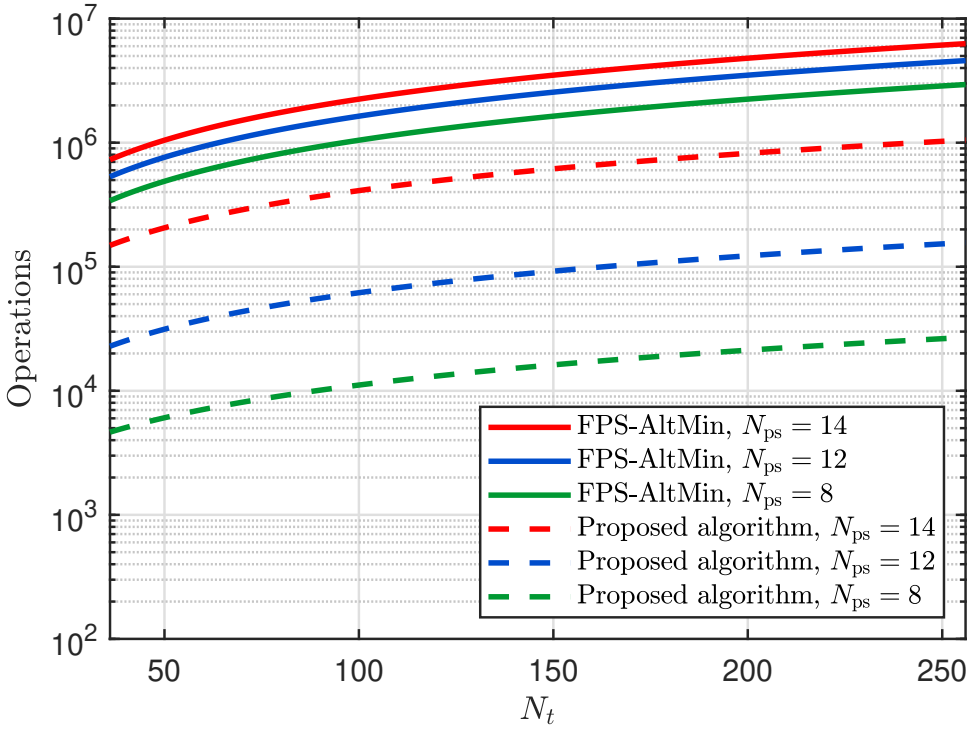

Figure 3.4: Computational complexity comparison of the proposed algorithm with FPS-AltMin algorithm (for 10 iterations [45]) for $N_{\rm s} = 10$ [MATLAB code], [Source file].

is considerably lower than the complexity of the FPS-AltMin algorithm for the practical number of PSs (see the simulation results).

3.4 MU-MISO System

In this section, we consider a scenario where a BS serves K active users in downlink transmission. The BS deploys $N_{\rm t}$ antennas to transmit $N_{\rm s} = K$ data streams to K single-antenna users at the same time-frequency resource. Furthermore, the BS employs CSI to perform HBF by the minimum number of RF chains, i.e., $N_{\rm RF} = N_{\rm s}$. Let $\mathbf{H} \in \mathbb{C}^{K \times N_{\rm t}}$ be the channel matrix between $N_{\rm t}$ antennas at the transmitter side and the K users. Therefore, the kth row of channel matrix, $\mathbf{h}_k$, represents the channel between BS and kth user. Under these assumptions, the vector $\mathbf{y}$ in (3.1) contains the received signals at users' side, so the kth user receives:

$$y_k = \sqrt{\rho}\mathbf{h}_k\mathbf{F}_{\rm RF}\mathbf{F}_{\rm BB}\mathbf{x} + n_k. \tag{3.30}$$

Therefore, the achievable rate for user k can be expressed as [68]:

$$R_k = \log_2\left(1 + \frac{\rho\left|\mathbf{h}_k\mathbf{F}_{\mathrm{RF}}\mathbf{f}_{\mathrm{BB}_k}\right|^2}{\rho\sum_{i=1,i\neq k}^{K}\left|\mathbf{h}_k\mathbf{F}_{\mathrm{RF}}\mathbf{f}_{\mathrm{BB}_i}\right|^2 + \sigma_{\mathrm{n}}^2}\right) \tag{3.31}$$

where $\mathbf{f}_{\mathrm{BB}_k}$ is the kth column of $\mathbf{F}_{\mathrm{BB}}$. The Multi-User MISO (MU-MISO) systems differ from the SU-MIMO systems in that in the MU-MISO, the receiving antennas are non-cooperative. It means that the users do not have the ability to remove receiving interference from each other. Thereby, the inter-user interference effect must be taken into account for precoder design at the BS. This additional condition leads to complicated algorithms with much higher convergence time. Since the proposed algorithm can implement any fully-digital beamforming matrix, it has the potential to overcome the obstacle. Hence, we consider the full-digital precoders Maximum-Ratio Transmission (MRT), ZF, and Minimum Mean Squared Error (MMSE) that have exhibited good performance with low computational complexity [6], as $\mathbf{F}_{\text{opt}}$:

$$\mathbf{F}_{\text{opt}} = \begin{cases} \mathbf{H}^{\mathrm{H}} & \text{MRT} \\ \mathbf{H}^{\mathrm{H}}\left(\mathbf{H}\mathbf{H}^{\mathrm{H}}\right)^{-1} & \text{ZF} \\ \mathbf{H}^{\mathrm{H}}\left(\mathbf{H}\mathbf{H}^{\mathrm{H}} + \frac{K}{\rho}\mathbf{I}_K\right)^{-1} & \text{MMSE.} \end{cases} \tag{3.32}$$

Then, we utilize the proposed algorithm to compute the HBF matrices. The next section indicates that the loss in the performance is negligible, regarding simulations.

3.5 Simulation Results

3.5.1 Performance of Proposed Algorithm for a SU-MIMO System

n this section, a SU-MIMO system is considered where the proposed algorithm is utilized for beamforming at both the transmit and receive sides. It is assumed that the transmitter and the receiver are equipped with a 12×12 Uniform Planar Array (UPA) and a 6×6 UPA, respectively, such that the distance between elements is half-wavelength. The number of RF chains is set to $N_{\mathrm{RF}} = N_{\mathrm{s}} = 5$ for both sides of the communication. The channel is assumed to have $N_{\mathrm{cl}} = 10$ clusters and $N_{\mathrm{ray}} = 5$ paths in each cluster. The spread angles in azimuth and elevation are assumed to be the same for the transmitter

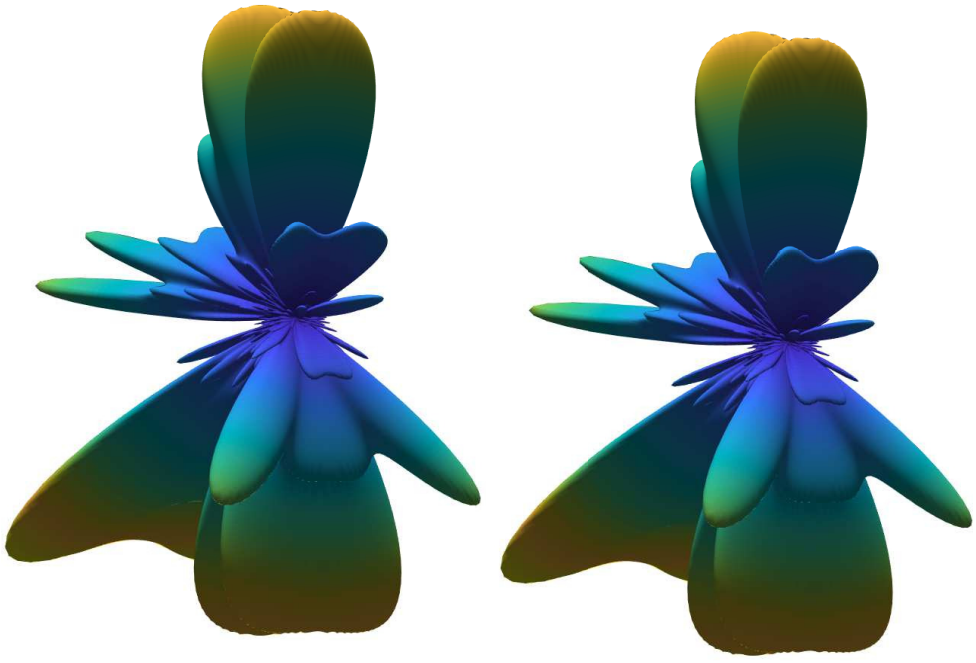

Figure 3.5: (a) Optimum beam pattern generated by $\mathbf{F}_{\text{opt}}$, (b) Beam pattern using proposed algorithm with $N_{\text{ps}} = 8$ [MATLAB code], [Source file].

and the receiver, with $\sigma_{\phi^t} = \sigma_{\phi^r} = \sigma_{\theta^t} = \sigma_{\theta^r} = 10^{\circ}$. The signal-to-noise ratio is expressed as $\text{SNR} = \frac{\rho}{\sigma_{\text{n}}^2}$.

The beam patterns at the transmitter side for $N_{\text{ps}} = 8$ are compared in Figure 3.5, which shows a particular channel realization. The benchmark beam pattern generated by fully digital beamforming is presented in Figure 3.5a, while Figure 3.5b illustrates the beam pattern generated by the proposed algorithm. The algorithm successfully produces the desired beam pattern using low-resolution PSs.

Figure 3.6 illustrates the spectral efficiency performance of various algorithms proposed for infinite-resolution PSs. To ensure a fair comparison, the analog beamformer coefficients of all algorithms were quantized to the nearest state of the PSs. Specifically, we constrained the phase shifter values to $\mathbf{F}_{\text{RF}}(i,j) \in \left\{1, e^{j2\pi\frac{1}{N_{\text{ps}}}}, \ldots, e^{j2\pi\frac{N_{\text{ps}}-1}{N_{\text{ps}}}}\right\} \quad \forall i,j$. The resulting figure clearly shows the impact of implementation constraints on the performance of each algorithm in terms of spectral efficiency. The resulting figure clearly shows the impact of implementation constraints on the performance of each algorithm in terms of spectral efficiency. The performance of the proposed algorithm for $N_{\text{ps}} = 8$

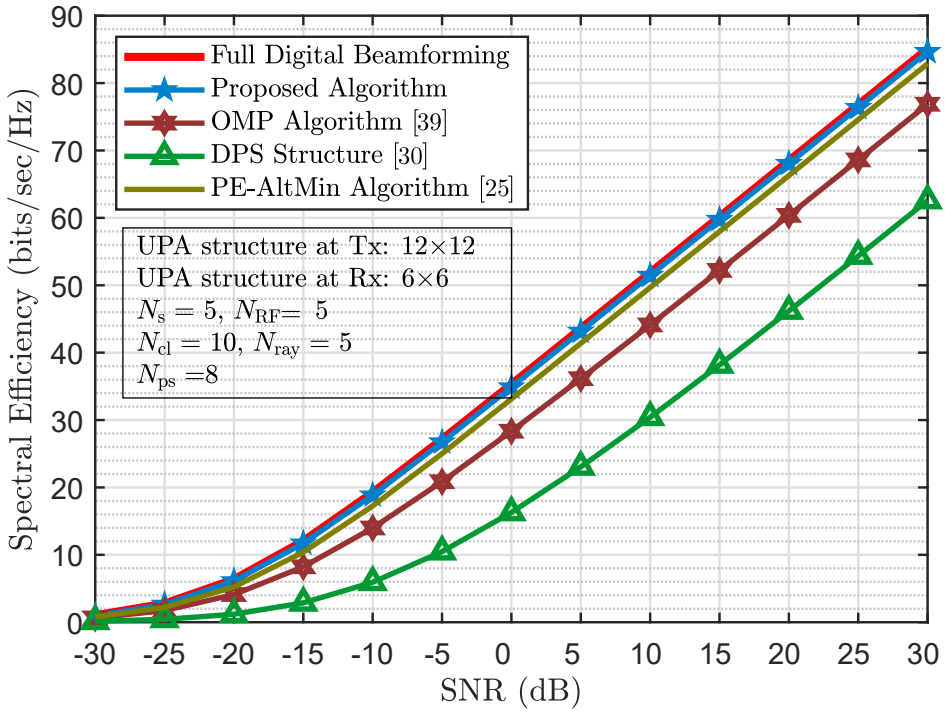

Figure 3.6: Performance comparison of proposed algorithm and existing ones for $N_{\text{ps}} = 8$ [MATLAB code], [Source file], [Source file].

is practically the same as for the full digital beamforming. Figure 3.7 compares the spectral efficiency of the proposed algorithm with FPS-AltMin [45] and HBF design in [41], both of which have been developed for non-continuous PSs. The output of the FPS-AltMin algorithm has been obtained after 10 iterations. The performance of these methods is comparable, as shown in the figure. However, the computational complexity of both methods is much higher than that of the proposed algorithm, while the hardware complexity of the HBF design in [41] is greater than the others. Furthermore, Figure 3.8 illustrates the performance of these algorithms as the number of PSs increases. It is evident from the figure that the proposed algorithm achieves optimal performance with only a few PSs, while the FPS-AltMin algorithm fails to do so even with more PSs. The proposed analog beamforming scheme yields surprising results as shown in Figure 3.9, where the optimal performance of full digital beamforming is achieved without requiring any digital precoder. The analog beamformer matrix $\mathbf{F}_{\text{RF}}$ is multiplied by a normalizing factor γ_0, resulting in an approximation of the optimal beamformer matrix as $\mathbf{F}_{\text{opt}} \approx \gamma_0 \mathbf{F}_{\text{RF}}$, where $\gamma_0 = \frac{1}{\|\mathbf{F}_{\text{RF}}\|_{\text{F}}}$. This is a significant finding, as it simplifies the beamforming process and eliminates the need for digital precoding. The overall

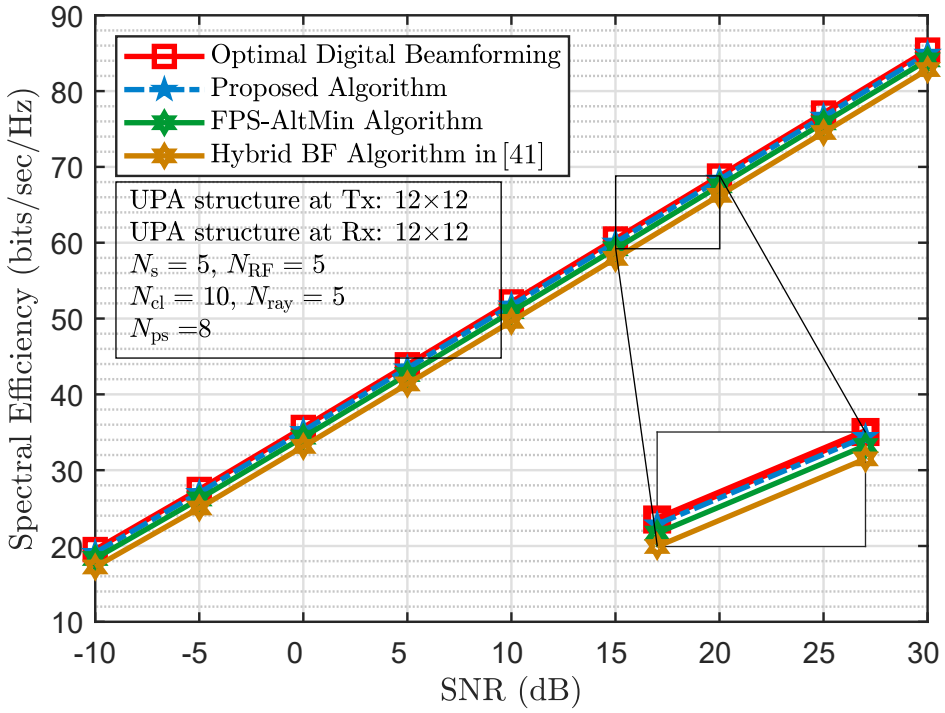

Figure 3.7: Performance comparison of the proposed algorithm with FPS-AltMin algorithm [45] and HBF design in [41] for $N_{\text{ps}} = 8$ [MATLAB code], [Source file].

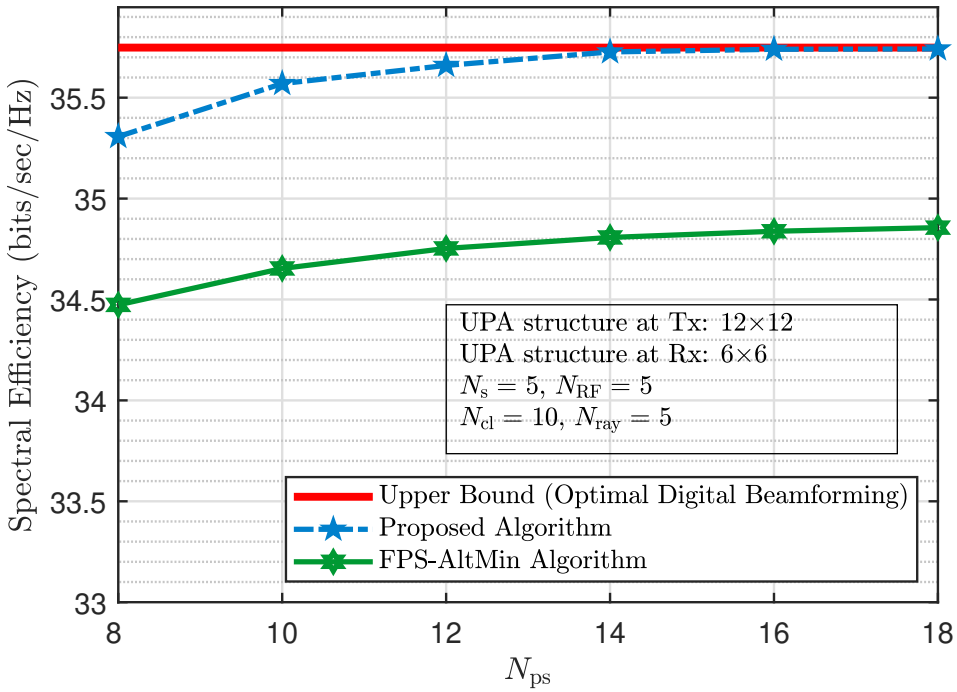

Figure 3.8: Performance comparison of the proposed algorithm with FPS-AltMin algorithm for different values of N_{ps} and $\text{SNR} = 0$ [MATLAB code], [Source file].

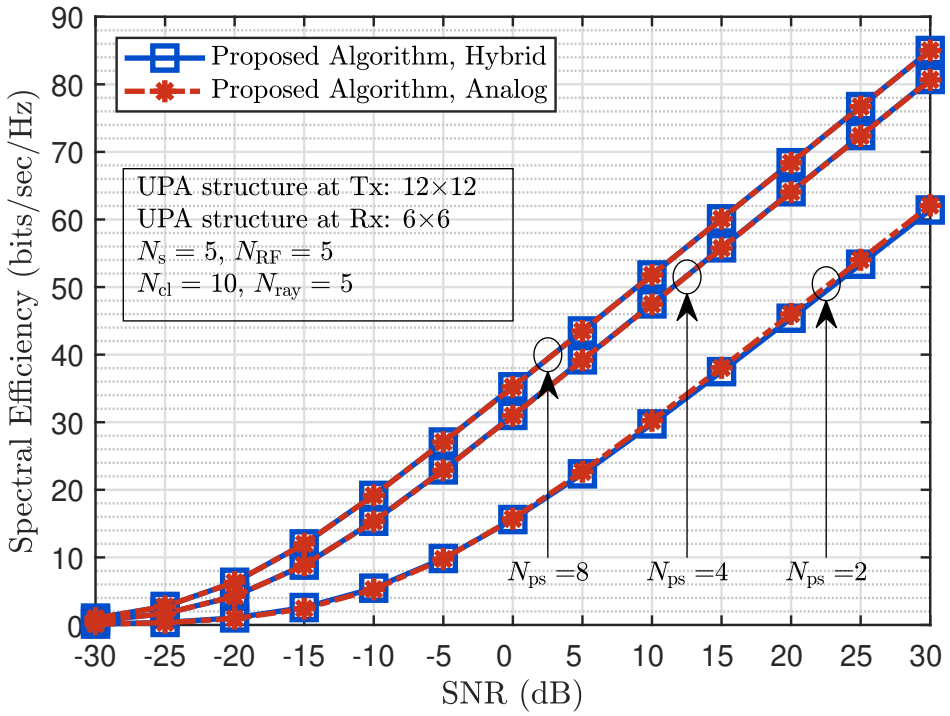

Figure 3.9: Performance of the proposed algorithm without digital beamforming for different values of N_{ps} [MATLAB code], [Source file].

computational complexity of the proposed algorithm grows linearly with the number of antennas and data streams, i.e., $\mathcal{O}\left(N_{\text{t}}N_{\text{s}}3^{\frac{N_{\text{ps}}}{2}}/N_{\text{ps}}\right)$, making it computationally efficient for large-scale antenna systems.

3.5.2 Performance of Proposed Algorithm in a MU-MISO System

To evaluate the performance of the proposed algorithm in a multi-user setting, we consider a scenario where a BS is equipped with a 12×12 UPA antenna and 20 RF chains to serve 20 users. We analyze the performance of the algorithm with three popular linear beamformers: MMSE, ZF, and MRT. As depicted in Figure 3.10, the proposed algorithm can implement all beamformers without any performance degradation.

3.6 Summary

In this chapter, a massive MIMO system that deploys FPSs for HBF was considered. The chapter proposed an efficient low-complexity algorithm to solve the problem, which

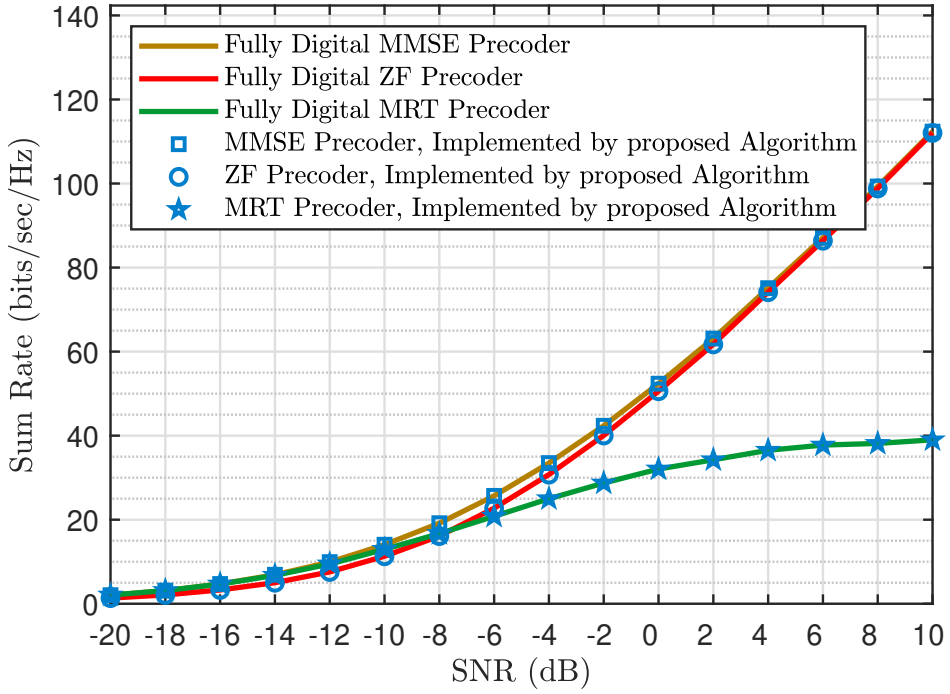

Figure 3.10: Sum rate achieved by different precoders in a 20-user MISO system [MATLAB code], [Source file].

decomposed the problem into independent and tractable sub-problems with a search space size of $2^{N_{\mathrm{ps}}}$. It was discovered, by analyzing the feasible set, that some points in the space were superposed, reducing the search space to $3^{\frac{N_{\mathrm{ps}}}{2}}$. Additionally, the investigation indicated that the feasible set includes the basic set, which was exploited to reduce the search space by a factor of N_{ps}.

The simulation results demonstrated the potential of the proposed algorithm to achieve fully digital performance even by applying a few FPSs for a SU-MIMO system. Moreover, for multiuser massive MISO systems, it achieved the performance of linear beamformers, MMSE, ZF, and MRT by computing corresponding hybrid beamformer matrices. The results also proved that the optimal performance could be achieved only by analog beamforming, whereupon the computational complexity grew linearly with the number of antennas and streams, i.e., $\mathcal{O}\left(N_{\mathrm{t}}N_{\mathrm{s}}3^{\frac{N_{\mathrm{ps}}}{2}}/N_{\mathrm{ps}}\right)$.

4

Hardware Implementation: Determining the Optimal Number of PSs

Sommaire

THE previous chapter proposed a method to mitigate the complexity of the combinatorial optimization problem that leads to the optimal states of the switch network. This chapter seeks to reduce hardware complexity through a comprehensive analysis of hardware implementation. Specifically, the chapter aims to investigate the trade-off between system performance and hardware complexity by examining the impact of the number of PSs in each RFs path.

Binary linear combinations of PSs are performed via switches in the RFs paths to generate different coefficients. By representing the generable coefficients as points in a scattering diagram, the density of the points provides an estimate of how closely it can approximate the optimized ideal coefficients. Increasing the number of PSs is expected to lead to an increase in the density of the scattering diagram, enabling the analog BF to approach the ideal DBF. However, as demonstrated in the previous chapter, the complete set of points includes redundancies, and the number of distinct points, or feasible set, is less than the number of points in the complete set. Therefore, the chapter aims to mathematically evaluate the size of the feasible set by identifying and eliminating redundant points.

Given that around 15 PSs can achieve near-optimal performance, this chapter focuses on values of N_{ps} slightly larger than 15. The analysis shows that the size of the feasible set is not strictly an increasing function of N_{ps}. This finding suggests that increasing the number of PSs can sometimes degrade the precision of the BF, which is contrary to

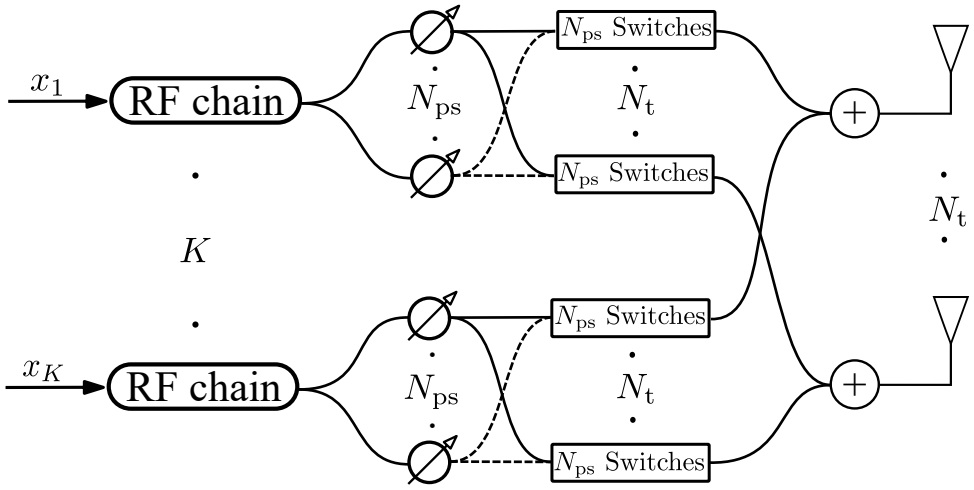

Figure 4.1: System Structure [Source file]

what one might expect. Interestingly, a prime number of PSs is shown to be the most efficient option, as it provides a larger feasible set than the next even number, $N_{\text{ps}}+1$. Therefore, the conventional choice of 2^n PSs is not optimal, and other options should be considered when designing switch networks.

4.1 System Model

We consider a downlink transmission, where a BS simultaneously transmits K streams to K single-antenna users. As shown in the Figure 4.1, the BS is equipped with an array of antennas of size N_{t} and employs N_{RF} RF chains, which can serve at most $K = N_{\text{RF}}$ users. As detailed in the previous chapter, we employ FPSs followed by a switch network to generate the complex coefficients of the analog BF. In our structure, we are not using digital precoder[1]. Let $\mathbf{H} \in \mathbb{C}^{K\times N_{\text{t}}}$ be the channel matrix between N_{t} BS antennas and K users. The received signal at users' side is given by:

$$\mathbf{y} = \sqrt{\rho\alpha}\mathbf{H}\mathbf{F}_{\text{RF}}\mathbf{x} + \mathbf{n}, \tag{4.1}$$

where $\mathbf{y}$ is the $K \times 1$ received signal vector, $\mathbf{x} \in \mathbb{C}^{K\times 1}$ denotes the data stream vector such that $\mathbb{E}\left\{\mathbf{x}\mathbf{x}^{\text{H}}\right\} = \mathbf{I}_K$, $\mathbf{n} \in \mathbb{C}^{K\times 1}$ is the vector of independent and identically distributed (i.i.d.) complex Gaussian noise with $\mathcal{CN}(0, \mathbf{I})$, ρ is the average signal to

[1]The system shown in Figure 4.1 can approximately achieve the performance of fully digital systems in flat fading channels [47]. For frequency selective channels, a DBF precoder is normally added.

noise ratio (SNR), α is a normalization constant chosen to satisfy the power constraint $\mathbb{E}\left\{\|\sqrt{\alpha}\mathbf{F}_{\mathrm{RF}}\|_{\mathrm{F}}^2\right\} = 1$, and $\mathbf{F}_{\mathrm{RF}} \in \mathbb{C}^{N_{\mathrm{t}} \times K}$ is the analog BF matrix whose entry in ith row and jth column, $\mathbf{F}_{\mathrm{RF}}(i,j)$, is given by [47]:

$$\mathbf{F}_{\mathrm{RF}}(i,j) = \mathbf{s}_{ij}\mathbf{c}. \tag{4.2}$$

In this expression, $\mathbf{c} = \left[1, e^{\jmath 2\pi \frac{1}{N_{\mathrm{ps}}}}, \ldots, e^{\jmath 2\pi \frac{N_{\mathrm{ps}}-1}{N_{\mathrm{ps}}}}\right]^{\mathrm{T}}$ is the phase shift vector (see Figure 4.1), and $\mathbf{s}_{ij}$ is a binary horizontal vector of size N_{ps}, representing the states of the switch network that connects the ith antenna to the jth RF chain. This structure has the potential to approach the optimal fully-digital beamformers by optimizing the switch states $\mathbf{s}_{ij}$ [47]. Since in this chapter, we are focused on the accurate generation of analog complex coefficient, we consider, without loss of generality, the ZF precoder $\mathbf{F}$ as a goal to implement:

$$\mathbf{F} = \mathbf{H}^{\mathrm{H}}\left(\mathbf{H}\mathbf{H}^{\mathrm{H}}\right)^{-1}. \tag{4.3}$$

The previous chapter showed that the switch states $\mathbf{s}_{ij}$ can be obtained as:

$$\begin{aligned} \mathbf{s}_{ij} = & \underset{\mathbf{s}_{ij}}{\operatorname{argmin}} \quad |\gamma\mathbf{F}(i,j) - \mathbf{s}_{ij}\mathbf{c}|^2 \\ & \text{s.t.} \quad \mathbf{s}_{ij}(v) \in \{0,1\}, \quad \forall v = 1, \ldots, N_{\mathrm{ps}}. \end{aligned} \tag{4.4}$$

where $\gamma = \frac{\eta_{N_{\mathrm{ps}}}}{\delta}$ is a scaling factor in which δ denotes the maximum modulus in $\mathbf{F}$, and $\eta_{N_{\mathrm{ps}}}$ is the maximum possible amplitude that can be generated by $\mathbf{s}_{ij}\mathbf{c}$, which is given by:

$$\eta_{N_{\mathrm{ps}}} = \begin{cases} 2\sum\limits_{n=1}^{\lceil N_{\mathrm{ps}}/4 \rceil} \cos\left(\dfrac{2n-1}{N_{\mathrm{ps}}}\pi\right) & \lceil \frac{N_{\mathrm{ps}}}{2} \rceil = \text{ even} \\ \sum\limits_{n=-\lfloor N_{\mathrm{ps}}/4 \rfloor}^{\lfloor N_{\mathrm{ps}}/4 \rfloor} \cos\left(\dfrac{2n}{N_{\mathrm{ps}}}\pi\right) & \lceil \frac{N_{\mathrm{ps}}}{2} \rceil = \text{ odd} \end{cases}. \tag{4.5}$$

The values of $\mathbf{s}_{ij}\mathbf{c}$, which are the constructed analog coefficients for the $2^{N_{\mathrm{ps}}}$ combinations of switches, generate a complete set $\mathcal{S}_{N_{\mathrm{ps}}}$ as:

$$\sum_{m \in \mathcal{A}_i} P_m \in \mathcal{S}_{N_{\mathrm{ps}}} \quad \forall i = 1, \ldots, 2^{N_{\mathrm{ps}}}, \tag{4.6}$$

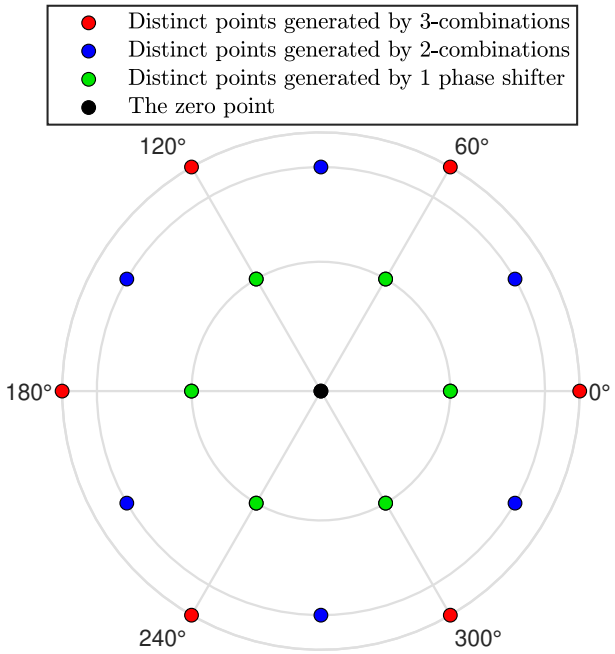

Figure 4.2: Scattering diagram of the feasible set for $N_{\text{ps}} = 6$ [MATLAB code], [Source file].

where $P_m = e^{\jmath \frac{2\pi}{N_{\text{ps}}}(m-1)}$, and $\mathcal{A}_i$ is the ith member of the power set $\Pi\big([N_{\text{ps}}]\big)$ (let $[N_{\text{ps}}] = \{n \in \mathbb{N} : n \leq N_{\text{ps}}\}$, i.e., the set of natural numbers $1, 2, \ldots, N_{\text{ps}}$). In the next section, the feasible set $\mathcal{F}_{N_{\text{ps}}}$ of the complete set $\mathcal{S}_{N_{\text{ps}}}$ is analyzed to clarify the details of hardware complexity and performance.

4.2 The Complete Set and Feasible Set

The complete set $\mathcal{S}_{N_{\text{ps}}}$ is composed of all the binary linear combinations of the PSs outputs. As some combinations generate repetitive points, the number of distinct points (feasible set) $|\mathcal{F}_{N_{\text{ps}}}|$ in the complete set $\mathcal{S}_{N_{\text{ps}}}$ is less than $|\mathcal{S}_{N_{\text{ps}}}|$. For example, Figure 4.2 demonstrates that the $|\mathcal{F}_6| = 19$ while $|\mathcal{S}_6| = 2^6$. To analytically discuss the size of the feasible set, some definitions are presented as follows;

- $\Pi_n\Big([N_{\text{ps}}]\Big)$: a subset of $\Pi\Big([N_{\text{ps}}]\Big)$ including members with cardinal n.
- $\Pi_{\geq n}\Big([N_{\text{ps}}]\Big)$: a subset of $\Pi\Big([N_{\text{ps}}]\Big)$ including all members with cardinal greater than or equal to n.
- $\Pi_{<n}\Big([N_{\text{ps}}]\Big)$: a subset of $\Pi\Big([N_{\text{ps}}]\Big)$ including all members with cardinal less than n.

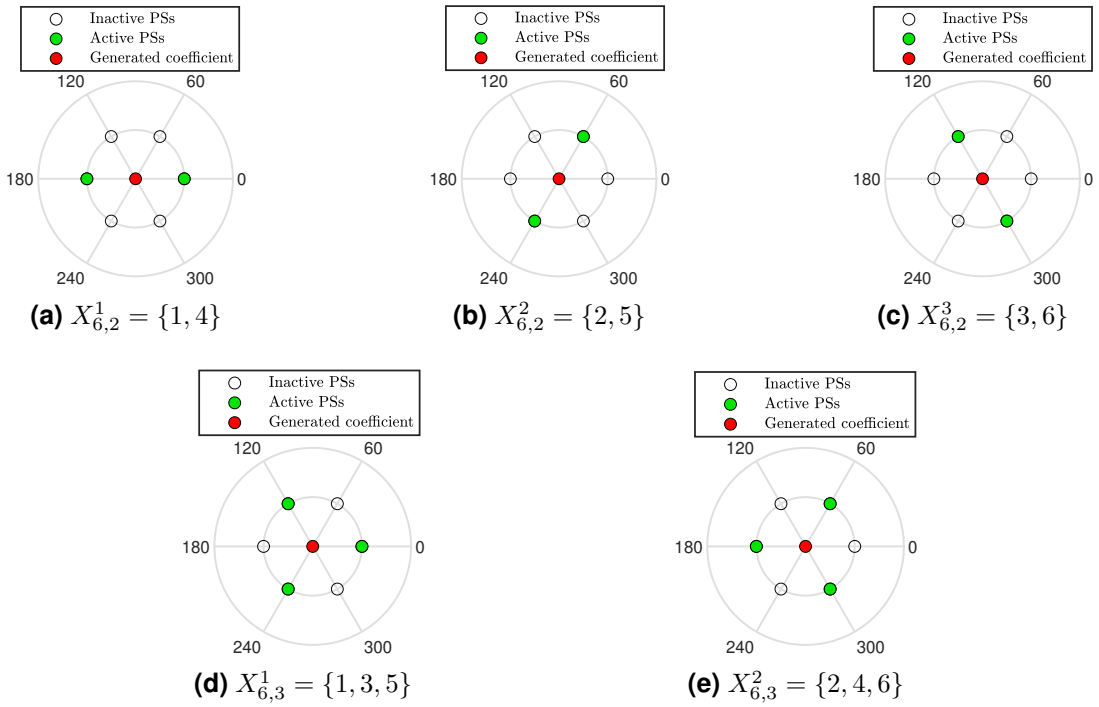

(a) $X^1_{6,2} = \{1, 4\}$ **(b)** $X^2_{6,2} = \{2, 5\}$ **(c)** $X^3_{6,2} = \{3, 6\}$

(d) $X^1_{6,3} = \{1, 3, 5\}$ **(e)** $X^2_{6,3} = \{2, 4, 6\}$

Figure 4.3: All the ZSSs generated by $N_{\text{ps}} = 6$ [MATLAB code], [Source file].

- Distinct points of $\Pi_n\Big([N_{\text{ps}}]\Big)$: the points of $\mathcal{S}_{N_{\text{ps}}}$ that cannot be generated by $\Pi_{<n}\Big([N_{\text{ps}}]\Big)$.
- $\mathcal{P}_{N_{\text{ps}}} = \{p_1, p_2, \ldots, p_T\}$: the set inducing sorted prime factors of N_{ps} without repetition, i.e., $p_1 < p_2 < \cdots < p_T$.

4.2.1 Zero-Summation Sets

Consider a set composed of p ($p \in \mathcal{P}_{N_{\text{ps}}}$) elements such as:

$$\mathcal{X}^i_{N_{\text{ps}},p} = \Big\{ tN_{\text{ps}}/p + i \in \mathbb{N} \;\Big|\; i \leq tN_{\text{ps}}/p + i \leq N_{\text{ps}} \Big\}. \tag{4.7}$$

It creates a zero member in $\mathcal{S}_{N_{\text{ps}}}$, i.e., $\mathcal{S}_{N_{\text{ps}}}\Big(\mathcal{X}_{N_{\text{ps}},p}\Big) = \sum_{m \in \mathcal{X}_{N_{\text{ps}},p}} P_m = 0$, so we call it Zero-Summation Set (ZSS). Figure 4.3 depicts different ZSSs for $N_{\text{ps}} = 6$. In order to determine the number of subsets including a ZSS, we define the following lemmas.

☐ **Lemma 1**: If $\mathcal{A}_j = \mathcal{A}_i \bigcup \mathcal{X}_{N_{\text{ps}},p}$, $\mathcal{A}_j$ generates a redundant point onto $\mathcal{S}_{N_{\text{ps}}}\Big(\mathcal{A}_i\Big)$ in

$\mathcal{S}_{N_{\rm ps}}$, since:

$$\begin{aligned}\mathcal{S}_{N_{\rm ps}}\Big(\mathcal{A}_j\Big) &= \sum_{m\in\mathcal{A}_i} P_m + \sum_{m\in\mathcal{X}_{N_{\rm ps},p}} P_m \\ &= \sum_{m\in\mathcal{A}_i} P_m \\ &= \mathcal{S}_{N_{\rm ps}}\Big(\mathcal{A}_i\Big) \end{aligned} \tag{4.8}$$

■

□ **Lemma 2**: For a given pair $\big(N_{\rm ps}, p\big)$, there are $N_{\rm ps}/p$ different ZSSs (see Figure 4.3) as:

$$\mathcal{X}^i_{N_{\rm ps},p} = \Big\{ tN_{\rm ps}/p + i \in \mathbb{N} \;\Big|\; 1 \le tN_{\rm ps}/p + i \le N_{\rm ps} \Big\}, \quad i = 1, \ldots, N_{\rm ps}/p. \tag{4.9}$$

Consequently, all members of $\Pi_{\ge\xi_{N_{\rm ps}}}\Big(\big[N_{\rm ps}\big]\Big)$ include at least one $\mathcal{X}_{N_{\rm ps},p_1}$, where $\xi_{N_{\rm ps}} = N_{\rm ps} - \frac{N_{\rm ps}}{p_1} + 1$. ■

□ **Lemma 3**: For an $N_{\rm ps}$ with prime factors p_1 and p_2, some members of $\Pi_{\ge p_1+p_2-1}\Big(\big[N_{\rm ps}\big]\Big)$ include both $\mathcal{X}_{N_{\rm ps},p_1}$ and $\mathcal{X}_{N_{\rm ps},p_2}$. ■

4.2.2 Subset of Zero-Summation Set

For an even $N_{\rm ps}$, consider two subsets $\mathcal{R}_{N_{\rm ps},p}$ and $\mathcal{B}_{N_{\rm ps},p}$ of $\mathcal{X}_{N_{\rm ps},p}$ such that $\mathcal{X}_{N_{\rm ps},p} = \mathcal{R}_{N_{\rm ps},p} \cup \mathcal{B}_{N_{\rm ps},p}$, so:

$$\sum_{m\in\mathcal{B}_{N_{\rm ps},p}} P_m + \sum_{m\in\mathcal{R}_{N_{\rm ps},p}} P_m = 0. \tag{4.10}$$

Also, consider $\bar{\mathcal{X}}_{N_{\rm ps},p}$ defined as:

$$\bar{\mathcal{X}}_{N_{\rm ps},p} = \left\{ \mathrm{mod}\left(x + \frac{N_{\rm ps}}{2}, N_{\rm ps}\right) \;\middle|\; x \in \mathcal{X}_{N_{\rm ps},p} \right\}. \tag{4.11}$$

Similarly, we have:

$$\sum_{m\in\bar{\mathcal{B}}_{N_{\rm ps},p}} P_m + \sum_{m\in\bar{\mathcal{R}}_{N_{\rm ps},p}} P_m = 0, \tag{4.12}$$

where $\bar{\mathcal{B}}_{N_{\rm ps},p}$ and $\bar{\mathcal{R}}_{N_{\rm ps},p}$ are subsets of $\bar{\mathcal{X}}_{N_{\rm ps},p}$, and their members correspond to members in $\mathcal{B}_{N_{\rm ps},p}$ and $\mathcal{R}_{N_{\rm ps},p}$ respectively. Since the difference between a member of $\bar{\mathcal{X}}_{N_{\rm ps},p}$ and its corresponding member in $\bar{\mathcal{X}}_{N_{\rm ps},p}$ is $N_{\rm ps}/2$, it results in $\pi/2$ phase difference between selected PSs. Therefore:

$$\sum_{m\in\mathcal{B}_{N_{\rm ps},p}} P_m + \sum_{m\in\bar{\mathcal{B}}_{N_{\rm ps},p}} P_m = 0. \tag{4.13}$$

From (4.10) and (4.13), there is a duality between $\mathcal{R}_{N_{\rm ps},p}$ and $\bar{\mathcal{B}}_{N_{\rm ps},p}$, i.e., $\sum_{m\in\mathcal{R}_{N_{\rm ps},p}} P_m = \sum_{m\in\bar{\mathcal{B}}_{N_{\rm ps},p}} P_m$. Therefore, we consider $|\mathcal{R}_{N_{\rm ps},p}| > |\bar{\mathcal{B}}_{N_{\rm ps},p}|$ and call $\mathcal{R}_{N_{\rm ps},p}$ as Subset of ZSSs (SZSS). For two sets $\mathcal{A}_i$ and $\mathcal{A}_j$ with common subset $\mathcal{A}_c = \mathcal{A}_i \bigcap \mathcal{A}_j$, if

$$\begin{cases} \mathcal{A}_i \bigcap \mathcal{X}_{N_{\rm ps},p} = \mathcal{R}_{N_{\rm ps},p} \\ \mathcal{A}_i \bigcap \bar{\mathcal{X}}_{N_{\rm ps},p} = \{\}, \end{cases} , \quad \begin{cases} \mathcal{A}_j \bigcap \mathcal{X}_{N_{\rm ps},p} = \{\} \\ \mathcal{A}_j \bigcap \bar{\mathcal{X}}_{N_{\rm ps},p} = \bar{\mathcal{B}}_{N_{\rm ps},p}, \end{cases} \tag{4.14}$$

$\mathcal{A}_i$ generates a duplicate point of $\mathcal{S}_{N_{\rm ps}}\Big(\mathcal{A}_j\Big)$, since:

$$\begin{aligned} \mathcal{S}_N(\mathcal{A}_i) &= \sum_{m\in\mathcal{A}_c} P_m + \sum_{m\in\mathcal{R}_{N_{\rm ps},p}} P_m \\ &= \sum_{m\in\mathcal{A}_c} P_m + \sum_{m\in\bar{\mathcal{B}}_{N_{\rm ps},p}} P_m \\ &= \mathcal{S}_{N_{\rm ps}}\Big(\mathcal{A}_j\Big) \end{aligned} \tag{4.15}$$

Figure 4.4 depicts an example of SZSS for $N_{\rm ps} = 10$. In order to determine the number of subsets including an SZSS, we define the following lemmas.

□ **Lemma 4**: For $p = 2$, there is no SZSS since $\mathcal{X}_{N_{\rm ps},2} = \bar{\mathcal{X}}_{N_{\rm ps},2}$. ■

□ **Lemma 5**: In each $\mathcal{X}_{N_{\rm ps},p}$ there are $\binom{p}{\kappa}$ SZSSs with cardinal κ where $p/2 < \kappa < p$. ■

Note that, if $\mathcal{A}_c$ contains a ZSS, we do not consider $\mathcal{A}_i$ as a set including a SZSS.

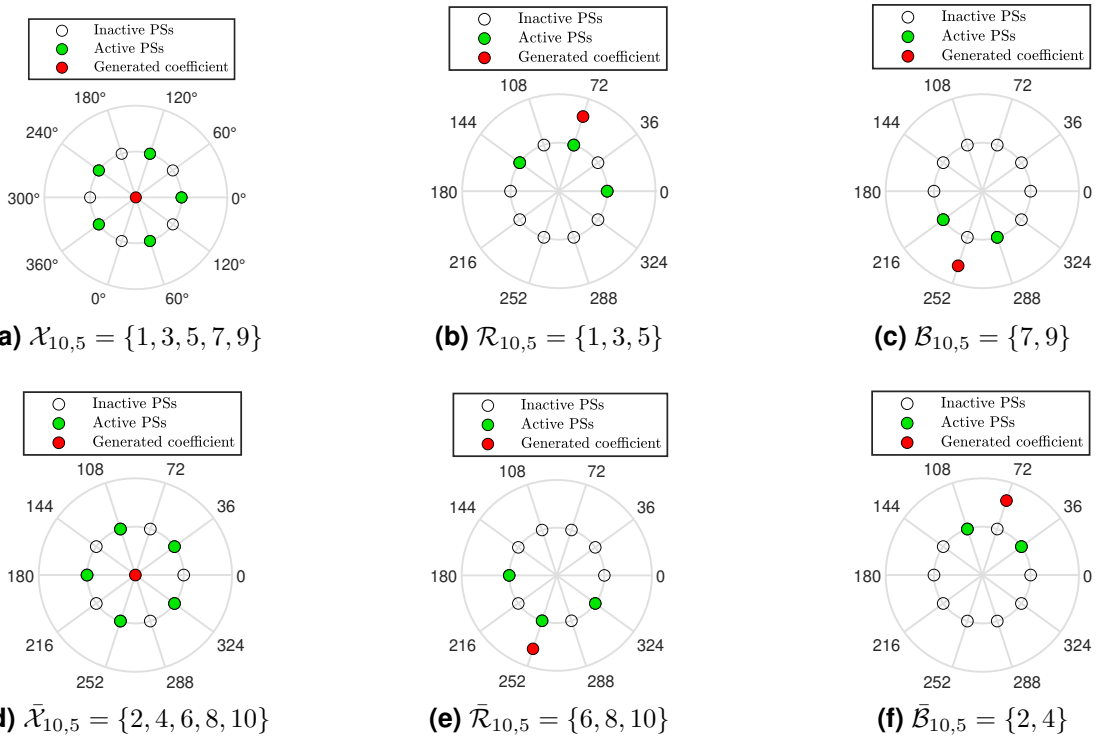

(a) $\mathcal{X}_{10,5} = \{1, 3, 5, 7, 9\}$ **(b)** $\mathcal{R}_{10,5} = \{1, 3, 5\}$ **(c)** $\mathcal{B}_{10,5} = \{7, 9\}$

(d) $\bar{\mathcal{X}}_{10,5} = \{2, 4, 6, 8, 10\}$ **(e)** $\bar{\mathcal{R}}_{10,5} = \{6, 8, 10\}$ **(f)** $\bar{\mathcal{B}}_{10,5} = \{2, 4\}$

Figure 4.4: An instance of superposed points generated by SZSSs for $N_{\mathrm{ps}} = 10$ [MATLAB code], [Source file].

4.2.3 Distinct Members of the Feasible Set

Regarding Lemma 2, all members of $\Pi_{\geq \xi_N}\Big(\big[N_{\mathrm{ps}}\big]\Big)$ generate repetitive points in $\mathcal{S}_{N_{\mathrm{ps}}}$. Therefore, we express the size of the feasible set $\big|\mathcal{F}_{N_{\mathrm{ps}}}\big|$ as:

$$\big|\mathcal{F}_{N_{\mathrm{ps}}}\big| = \sum_{n=0}^{\xi_{N_{\mathrm{ps}}}-1} \binom{N_{\mathrm{ps}}}{n} - \mathcal{Z}_{N_{\mathrm{ps}}}(n) - \mathcal{Q}_{N_{\mathrm{ps}}}(n), \tag{4.16}$$

where $\binom{N_{\mathrm{ps}}}{n}$ denotes the cardinal of $\Pi_n\Big(\big[N_{\mathrm{ps}}\big]\Big)$. Expressed in (4.17), $\mathcal{Z}_{N_{\mathrm{ps}}}(n)$ represents the number of members of $\Pi_n\Big(\big[N_{\mathrm{ps}}\big]\Big)$ containing at least one ZSS, and $\mathcal{Q}_{N_{\mathrm{ps}}}(n)$, expressed in (4.21), stands for the number of members of $\Pi_n\Big(\big[N_{\mathrm{ps}}\big]\Big)$ containing at least one SZSS. $\mathcal{Z}_{N_{\mathrm{ps}}}(n)$ can be written as:

$$\mathcal{Z}_{N_{\mathrm{ps}}}(n) = \begin{cases} \displaystyle\sum_{p \in \mathcal{P}_{N_{\mathrm{ps}}}} \mathcal{G}\big(N_{\mathrm{ps}}, p, n\big) - \mathcal{C}\big(N_{\mathrm{ps}}, n\big) & \text{for non-prime } N_{\mathrm{ps}} \\ 0 & \text{for prime } N_{\mathrm{ps}}, \end{cases} \tag{4.17}$$

where $\mathcal{G}\big(N_{\mathrm{ps}},p,n\big)$ computes the number of members of $\Pi_n\Big(\big[N_{\mathrm{ps}}\big]\Big)$ including at least one $\mathcal{X}_{N_{\mathrm{ps}},p}$ (see section A.3) :

$$\mathcal{G}\big(N_{\mathrm{ps}},p,n\big)=\begin{cases}0 & n<p\\ \displaystyle\sum_{m=1}^{\lfloor\frac{n}{p}\rfloor}\big(-1\big)^{m+1}\binom{\frac{N_{\mathrm{ps}}}{p}}{m}\binom{N_{\mathrm{ps}}-mp}{n-mp} & n\geq p,\end{cases}\tag{4.18}$$

and $\mathcal{C}\big(N_{\mathrm{ps}},n\big)$ represents the number of members of $\Pi_n\Big(\big[N_{\mathrm{ps}}\big]\Big)$ including both $\mathcal{X}_{N_{\mathrm{ps}},p_1}$ and $\mathcal{X}_{N_{\mathrm{ps}},p_2}$ simultaneously. For practical values of N_{ps}, for example $N_{\mathrm{ps}}\leq 17$, the condition in Lemma 3, $n\geq p_1+p_2-1$, only happens for $N_{\mathrm{ps}}=12$, and $N_{\mathrm{ps}}=15$. Therefore, in this interval, $\mathcal{C}\big(N_{\mathrm{ps}},n\big)=0$ except for $\mathcal{C}\big(12,n\big)$ and $\mathcal{C}\big(15,n\big)$, which are computed from (4.19) and (4.20) respectively (see section A.4 and section A.5):

$$\mathcal{C}\big(12,n\big)=\begin{cases}4\,\mathcal{G}\big(6,2,n-3\big)+\displaystyle\sum_{c=1}^{n-3}\binom{4}{(\lfloor\frac{c}{3}\rfloor+1)}\binom{3}{c}\binom{6}{n-c-3} & 4\leq n\leq 6\\ 0 & \text{Otherwise,}\end{cases}\tag{4.19}$$

and

$$\mathcal{C}\big(15,n\big)=\begin{cases}3\,\mathcal{G}\big(10,2,n-5\big) & 7\leq n\leq 10\\ 0 & \text{Otherwise.}\end{cases}\tag{4.20}$$

According to subsection 4.2.2 and Lemma 4, some combinations for $N_{\mathrm{ps}}=6,10,12,14$ include at least one SZSS. Therefore, $\mathcal{Q}_{N_{\mathrm{ps}}}\big(n\big)$ is expressed as:

$$\mathcal{Q}_{N_{\mathrm{ps}}}\big(n\big)=\begin{cases}\mathcal{Y}_{N_{\mathrm{ps}}}\big(n\big) & N_{\mathrm{ps}}=6,10,14\\ \mathcal{T}\big(n\big) & N_{\mathrm{ps}}=12\\ 0 & \text{Otherwise,}\end{cases}\tag{4.21}$$

where $\mathcal{Y}_{N_{\mathrm{ps}}}\big(n\big)$ is (see section A.6):

$$\mathcal{Y}_{N_{\mathrm{ps}}}\big(n\big)=\begin{cases}2\binom{\frac{N_{\mathrm{ps}}}{2}}{n} & \frac{N_{\mathrm{ps}}}{4}<n<\frac{N_{\mathrm{ps}}}{2}\\ 0 & \text{Otherwise,}\end{cases}\tag{4.22}$$

and $\mathcal{T}(n)$ is expressed as (see section A.7):

$$\mathcal{T}(n) = \begin{cases} 12\left[\binom{6}{n-2} - \mathcal{G}(6,3,n-2) + \mathcal{G}(6,2,n-2)\right] - 36\,\delta(n-4) & 2 \leq n \leq 5 \\ 0 & \text{Otherwise,} \end{cases} \tag{4.23}$$

4.3 System Analysis

This analysis provides a comprehensive view of the system from different perspectives: hardware complexity, computational complexity, and performance.

- **Hardware complexity**: is determined by the number of switches needed for a fixed number of users and BS antennas, which in turn depends on the number of deployed PSs. Therefore, N_{ps} can be interpreted as a *hardware complexity criterion.*

- **Computational complexity**: is determined by the size of the feasible set $\mathcal{F}_{N_{\mathrm{ps}}}$, which consists of N_{ps} shifted versions of a basic set $\mathcal{F}^b_{N_{\mathrm{ps}}}$ (as shown in Figure 4.5). This property reduces the search space in (4.4) to the basic set. Hence, the computational complexity increases by the size of $\mathcal{F}^b_{N_{\mathrm{ps}}}$ as $\mathcal{O}\left(N_{\mathrm{t}}K\left|\mathcal{F}^b_{N_{\mathrm{ps}}}\right|\right)$, where $\left|\mathcal{F}^b_{N_{\mathrm{ps}}}\right| = 1 + \frac{\left|\mathcal{F}_{N_{\mathrm{ps}}}\right|-1}{N_{\mathrm{ps}}}$.

- **Performance** is determined by the error between the desired BF coefficients and the implemented coefficients. Since the points of the feasible set are non-uniformly distributed on a circle with radius $\eta_{N_{\mathrm{ps}}}$, the cardinal of the feasible set, $\left|\mathcal{F}_{N_{\mathrm{ps}}}\right|$, cannot be considered an accurate performance criterion. Therefore, the Mean Square Error (MSE) of mapping is considered a performance criterion. To compute the MSE, a complex random variable υ uniformly distributed over the circle of radius $\eta_{N_{\mathrm{ps}}}$ is generated and then mapped to f, the nearest point of the feasible set. To be fair, the mapping error is normalized to the radius of the circle $\eta_{N_{\mathrm{ps}}}$. The

MSE is computed using:

$$\mathcal{E}_{N_{\mathrm{ps}}} = \frac{\mathbb{E}\left\{\left\|v - f\right\|^2\right\}}{\eta_{N_{\mathrm{ps}}}}. \tag{4.24}$$

The analysis presented in Table 4.1 examines the achieved results in relation to the number of PSs, where the values of N_{ps}, $\mathcal{F}^b_{N_{\mathrm{ps}}}$, and $\mathcal{E}_{N_{\mathrm{ps}}}$ serve as measures of hardware complexity, computational complexity, and performance, respectively. Additionally, the last column of the table displays the percentage of combinations that result in distinct points.

The findings from Table 4.1 reveal that when N_{ps} is an even value, the resulting feasible sets of $\mathcal{S}_{N_{\mathrm{ps}}}$ contain a small percentage of distinct points, leading to a sparse scattering diagram as depicted in Figure 4.5. This sparse distribution increases the mapping error $\mathcal{E}_{N_{\mathrm{ps}}}$ and ultimately degrades the system's performance. For example, the feasible sets generated by 9 and 12 PSs have sizes of 343 and 361, respectively, with almost identical performances ($\mathcal{E}_9 = 0.014$, $\mathcal{E}_{12} = 0.010$) and computational complexities $\left(\left|\mathcal{F}^b_9\right| = 39, \left|\mathcal{F}^b_{12}\right| = 31\right)$. However, selecting $N_{\mathrm{ps}} = 9$ reduces the number of PSs and corresponding switches by 25%. Therefore, it is preferable to use an odd number of PSs instead of an even number.

The comparison between $N_{\mathrm{ps}} = 11$ and odd $N_{\mathrm{ps}} > 11$ reveals that deploying $N_{\mathrm{ps}} > 11$ slightly reduces the MSE, but explodes the computational complexity. In addition, this requires more RF components, which is not interesting in practice. Therefore, it is expected that using $N_{\mathrm{ps}} = 9$ and $N_{\mathrm{ps}} = 11$ is able to handle the trade-off between hardware complexity, computational complexity and performance.

4.4 Simulation Results

The spectral efficiency is analyzed as the ultimate performance criterion for different values of phase resolutions N_{ps}. The Saleh-Valenzuela channel model, with the same parameters as chapter 3, is considered for these studies.

The system's spectral efficiency with respect to the number of PSs N_{ps} per RF chain

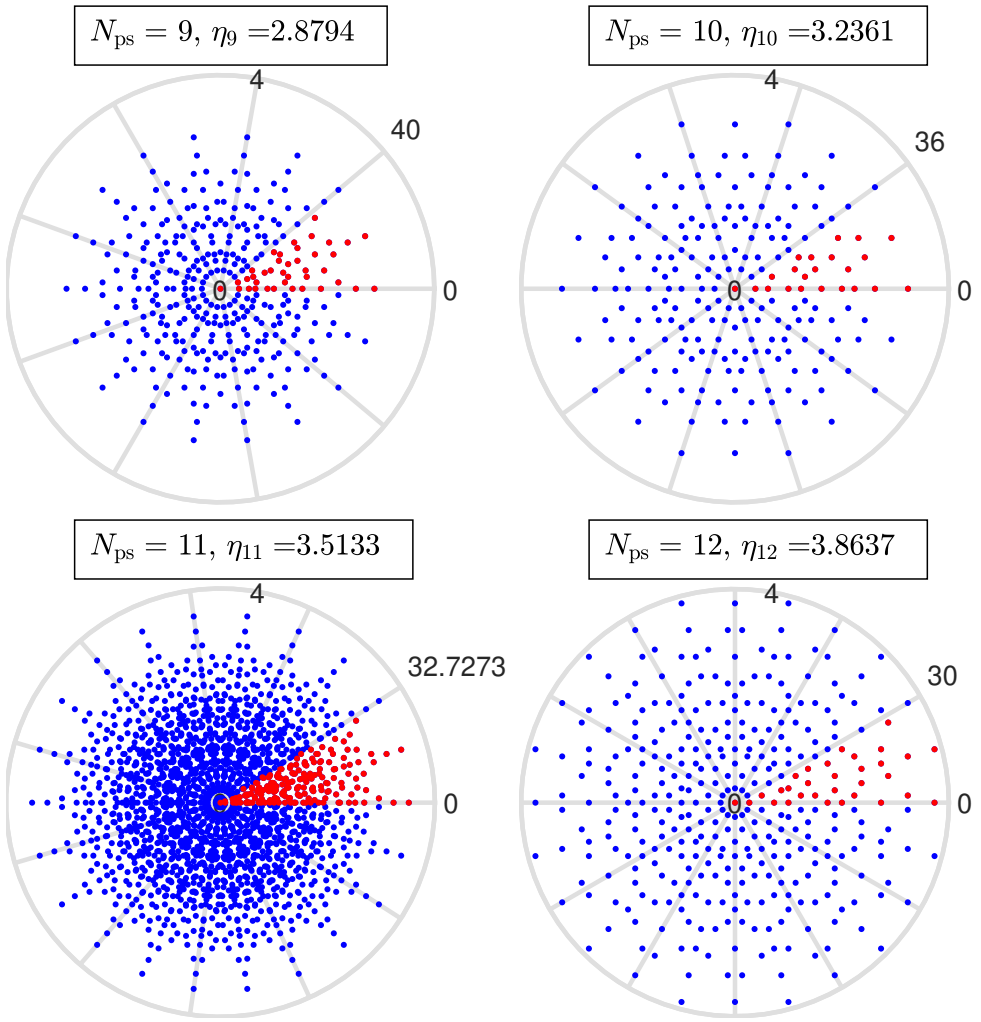

Figure 4.5: The feasible set (red and blue points) and the basic set (red points) for $N_{\text{ps}} = 9, 10, 11,$ and 12 [MATLAB code], [Source file].

is presented in Figure 4.6. The figure clearly illustrates that an odd number of PSs yields better performance compared to the next even number, despite having a higher phase resolution. Specifically, by employing an odd N_{ps} as small as 9, the system can approximately achieve the upper bound of performance. On the other hand, when using an even N_{ps}, the system requires 12 PSs to achieve a similar performance level. Therefore, it is more cost-effective to deploy an odd number of PSs rather than an even number.

The system's performance with N_{ps}=5, 7, 9, and 11 are depicted in Figure 4.7. The figure illustrates that deploying a small number of PSs, i.e., $N_{\text{ps}} = 5$ or 7, can achieve practically optimal performance in low SNR scenarios. Furthermore, with $N_{\text{ps}} = 11$, the

Table 4.1: Characteristics of the system as a function of N_{ps}

N_{ps}	$\xi_{N_{\mathrm{ps}}}$	$\eta_{N_{\mathrm{ps}}}$	$\lvert\mathcal{F}_{N_{\mathrm{ps}}}\rvert$	$\lvert\mathcal{F}^{b}_{N_{\mathrm{ps}}}\rvert$	$\mathcal{E}_{N_{\mathrm{ps}}} \times 10^2$	$\frac{\lvert\mathcal{F}_{N_{\mathrm{ps}}}\rvert}{\lvert\mathcal{S}_{N_{\mathrm{ps}}}\rvert}$
2	2	1	3	2	33.97	75.00%
3	3	1	7	3	13.48	87.50%
4	3	1.4142	9	3	10.87	56.25%
5	5	1.6180	31	7	4.34	96.88%
6	4	2	19	4	6.68	29.69%
7	7	2.2470	127	19	2.07	99.22%
8	5	2.6131	81	11	2.60	31.64%
9	7	2.8794	343	39	1.19	66.99%
10	6	3.2361	211	22	1.46	20.61%
11	11	3.5133	2047	187	0.69	99.95%
12	7	3.8637	361	31	1.05	08.81%
13	13	4.1481	8191	631	0.46	99.99%
14	8	4.4940	2059	148	0.58	12.57%
15	11	4.7834	16081	1073	0.34	49.08%
16	9	5.1258	6561	411	0.41	10.01%
17	17	5.4190	131071	7711	0.26	100.00%

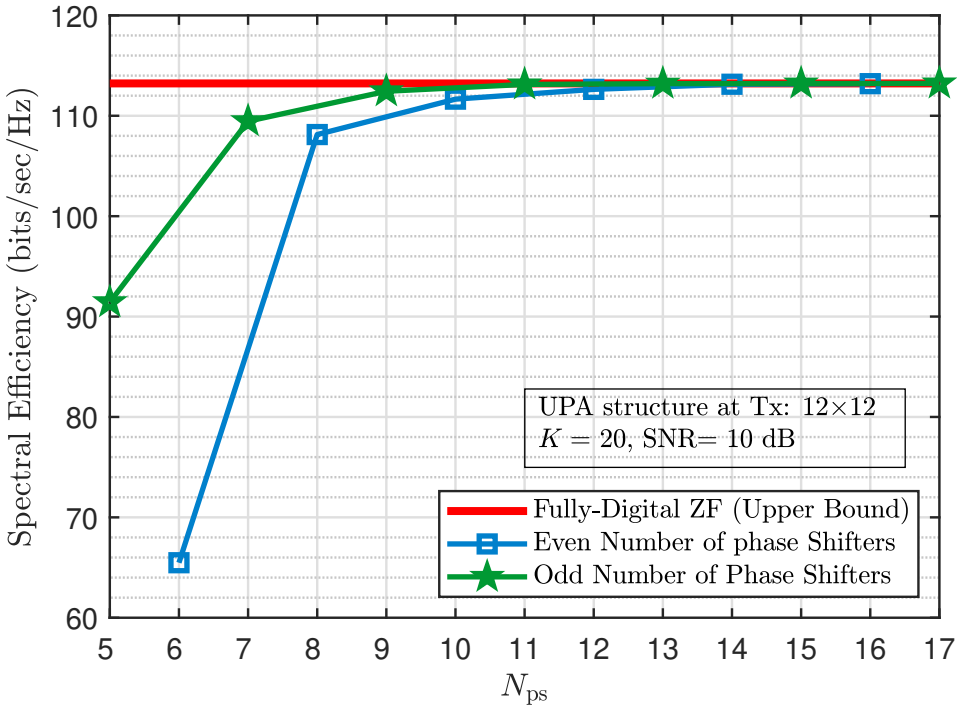

Figure 4.6: Performance comparison for different values of N_{ps} [MATLAB code], [Source file].

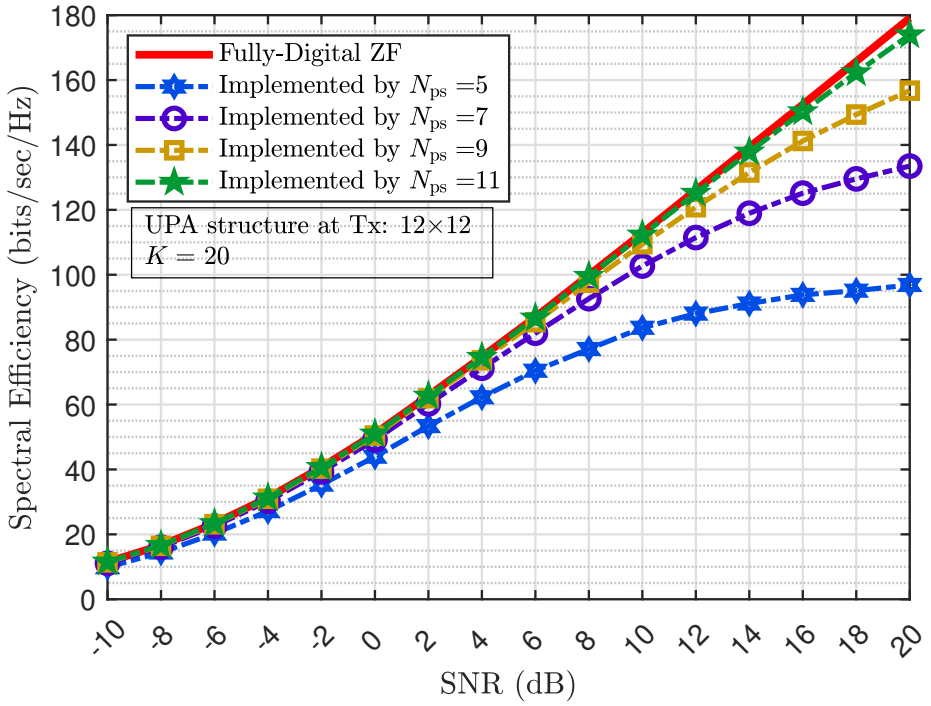

Figure 4.7: Performance comparison for different values of SNR [MATLAB code], [Source file].

system can achieve quasi-optimal performance in a practical SNR range. It is important to note that although a performance degradation is observed for $N_{\rm ps} = 9$ compared to $N_{\rm ps} = 11$, the hardware and computational complexity are reduced. Therefore, the appropriate choice of $N_{\rm ps}$ is a question of performance-complexity trade-off.

4.5 Summary

This chapter focuses on the hardware implementation of FPSs. The analytical results presented in the chapter show that the performance of the system depends on the number of distinct coefficients generated by the FPSs, rather than the total number of possible combinations. A closed-form formula is derived for calculating the number of distinct coefficients for practical values of $N_{\rm ps}$, which shows that using an even number of PSs is not ideal, while a prime number of PSs is the most efficient. Simulation results suggest that deploying only 11 PSs is a good trade-off between performance and hardware complexity.

5

Mapping Strategy: A Novel Machine Learning-Based Approach

Sommaire

THIS chapter presents an inquiry into mapping strategies used in the analog network, focusing specifically on how the number of RF paths impacts the trade-off between system performance and hardware complexity. The chapter puts forward a new mapping strategy and subsequently develops precoder algorithms for Multiple-Input and Single-Output (MISO) systems to address the performance-complexity dichotomy. This chapter makes two major contributions:

First, the Partially/Fully-Connected (PFC) strategy is introduced as a novel architecture that controls hardware complexity by considering the effects of RF paths. The architecture divides the antenna elements into two groups: the Fully-Connected Antennas (FCAs) and the Singly-Connected Antennas (SCAs). The FCAs scale up the number of RF paths by a factor proportional to the number of RF chains, while the SCAs need only one RF path. The number of FCAs is thus a crucial parameter that strongly influences system design, leading to systems with varying performance-complexity ratios. For this architecture, an algorithm is proposed to mitigate user interference. Specifically, the algorithm eliminates zero-entry elements (resulting from the fact that the total architecture is not fully connected) from the precoder matrix and reformulates the optimization problem, resulting in a significant reduction in the optimization complexity.

Second, to further enhance system performance, a dynamic architecture is introduced that adapts, dynamically, the RF paths to the CSI. This involves inserting a switch network between the RF chains and the antenna array, which raises the issue of

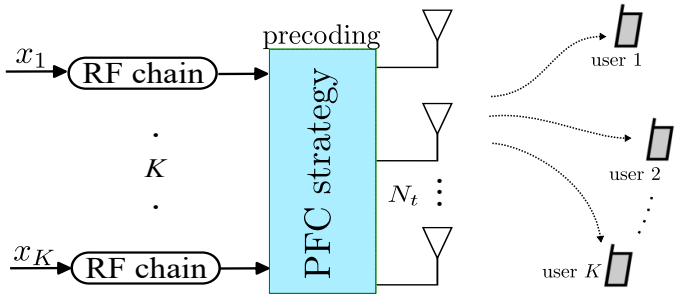

Figure 5.1: The BS designed by the proposed PFC architecture [Source file]

antenna selection: selecting the FCAs and allocating the SCAs to the RF chains. Since exhaustive search is infeasible, particularly for large arrays, a two-part approach is proposed. First, the FCAs are iteratively selected using a greedy algorithm. Then, a second algorithm assigns the remaining SCAs to the users. A Deep Neural Network (DNN) is trained, with the algorithm outputs and the simulated CSI, to enable real-time optimization.

5.1 System Model

Let us consider the downlink transmission of a multi-user massive MISO system, where a BS is equipped with an antenna array of size N_{t} to serve K single-antenna users as depicted in Figure 5.1. The BS is designed based on the PFC strategy, as explained in section 5.2, to perform the analog beamforming. It is shown that we can achieve the optimal performance of the fully digital BF for flat fading channels by using fully analog BF [30], [47], [48]. Accordingly, in this chapter, the digital BF part is not used and the number of RF chains, N_{RF}, is considered to be equal to the minimum, i.e., the number of data streams, K. The BS applies the precoder matrix $\mathbf{F} \in \mathbb{C}^{N_{\mathrm{t}} \times K}$ on data stream vector $\mathbf{x}$, where $\mathbb{E}\{\mathbf{x}\mathbf{x}^{\mathrm{H}}\} = \mathbf{I}_K$. Therefore, the received signals on the users' side are given by:

$$\mathbf{y} = \sqrt{\rho}\mathbf{H}\mathbf{F}\mathbf{x} + \mathbf{n}, \tag{5.1}$$

where $\mathbf{H} \in \mathbb{C}^{K \times N_{\mathrm{t}}}$ represents the channel matrix, $\mathbf{n} \in \mathbb{C}^{K \times 1}$ is the complex Gaussian noise vector with $\mathbf{n} \sim \mathcal{CN}\left(0, \mathbf{I}_K\right)$, and the normalization constant ρ is chosen to respect

the transmit power constraint P:

$$\rho = \frac{P}{\|\mathbf{F}\|_{\mathrm{F}}^2}. \tag{5.2}$$

In the following subsection, the proposed PFC architecture is presented, which is capable of handling the trade-off between hardware complexity and performance.

5.2 PFC architecture

Analog BF systems can be categorized, in general, based on the connection strategy in the analog part, as illustrated in Figure 2.4. As shown in Figure 2.4a, the FC strategy connects all the RF chains to all the antennas through $N_{\mathrm{RF}}N_{\mathrm{t}}$ RF paths. Although this architecture requires the most complex hardware, it puts no constraint on the precoder matrix, allowing the achievement of the optimal performance. Notice that each entry in the precoding matrix $\mathbf{F}$ represents an RF path connecting an RF chain to an antenna.

On the other hand, the PC architecture, the simplest one, has one RF path per antenna that drastically simplifies the hardware. It results in a block-diagonal precoder matrix with only N_{t} non-zero entries. In fact, a large number of zeros in the matrix represent the deleted connections compared with the FC strategy, which tumbles the performance.

The GC architecture, depicted in Figure 2.4c, divides RF chains and antennas into disjoint groups, which deploy the FC strategy for inside-group connections. The complexity of the architecture lies between the FC and PC. As a result, more RF paths exist in the system, which means there are more non-zero elements in the matrix. A certain flexibility is obtained because the number of groups can vary from 1 (equivalent to the FC architecture) to N_{RF} (equivalent to the PC). Therefore, the number of non-zero elements (or RF paths) to be optimized can be selected from the set $\{N_{\mathrm{t}}, 2N_{\mathrm{t}}, \ldots, N_{\mathrm{RF}}N_{\mathrm{t}}\}$.

As shown in Figure 2.4d, the OSA structure allows the groups to overlap to cope with the hardware complexity-performance challenge. Here, each RF chain is connected to a subarray of the size $M_{\mathrm{t}} = N_{\mathrm{t}} - (N_{\mathrm{RF}} - 1)\Delta M_{\mathrm{t}}$, where ΔM_{t} represents the number of overlapped elements. Therefore, $N_{\mathrm{t}}/N_{\mathrm{RF}} + 1$ different levels of performance can be designed by adjusting the number of overlapped elements ΔM_{t}. In fact, FC and PC

architectures are two special cases for $\Delta M_{\mathrm{t}} = 0$ and $\Delta M_{\mathrm{t}} = N_{\mathrm{t}}/N_{\mathrm{RF}}$, respectively. The GC and OSA, nevertheless, offer the view of adjusting the number of RF paths, and it seems that the development of this approach is essential for the effective management of the hardware performance trade-off.

This chapter proposes a novel mapping strategy, called partially/fully connected (PFC), that can adjust the number of RF paths in $N_{\mathrm{t}} + 1$ different levels while maintaining a simple precoder matrix suitable for analytical optimization. As shown in Figure 5.2, in this architecture, the antennas are divided into two groups. The first group, comprising N_{U} antennas, is implemented as PC, i.e., one RF path per antenna. The second group, comprising the remaining antennas, $N_{\mathrm{c}} = N_{\mathrm{t}} - N_{\mathrm{U}}$, is implemented via FC architecture, i.e., each antenna is connected to all RF chains. The antennas of the first group are called singly connected antennas (SCAs), and those of the second group are fully connected antennas (FCAs). Notably, $N_{\mathrm{c}} = 0$ converges to the PC strategy, while $N_{\mathrm{c}} = N_{\mathrm{t}}$ converges to the FC strategy. One advantage of this structure is the flexibility in controlling user priority by assigning more or fewer SCAs to a specific user. If the number of antennas assigned to the kth user is denoted by N_{u_k}, then the expression $\sum N_{\mathrm{u}_k} = N_{\mathrm{U}}$ should be satisfied.

Assuming the following ordering for antenna connections: the first N_{u_1} antennas are connected to the first RF chain, the next N_{u_2} antennas to the second RF chain, and so on. The last N_{c} antennas are the FCAs connected to all RF chains. Using this ordering, the analog precoding matrix $\mathbf{F}$ can be expressed as:

$$\mathbf{F} = \begin{bmatrix} \mathbf{f}_{\mathrm{u}_1} & \mathbf{0} & \dots & \mathbf{0} \\ \mathbf{0} & \mathbf{f}_{\mathrm{u}_2} & \dots & \mathbf{0} \\ \vdots & \vdots & \ddots & \vdots \\ \mathbf{0} & \mathbf{0} & \dots & \mathbf{f}_{\mathrm{u}_K} \\ \mathbf{f}_{\mathrm{c}_1} & \mathbf{f}_{\mathrm{c}_2} & \dots & \mathbf{f}_{\mathrm{c}_K} \end{bmatrix}, \tag{5.3}$$

where $\mathbf{f}_{\mathrm{u}_k} \in \mathbb{C}^{N_{\mathrm{u}_k} \times 1}$ and $\mathbf{f}_{\mathrm{c}_k} \in \mathbb{C}^{N_{\mathrm{c}} \times 1}$ contain the beamforming coefficients of the SCAs and FCAs related to the kth RF chain, respectively.

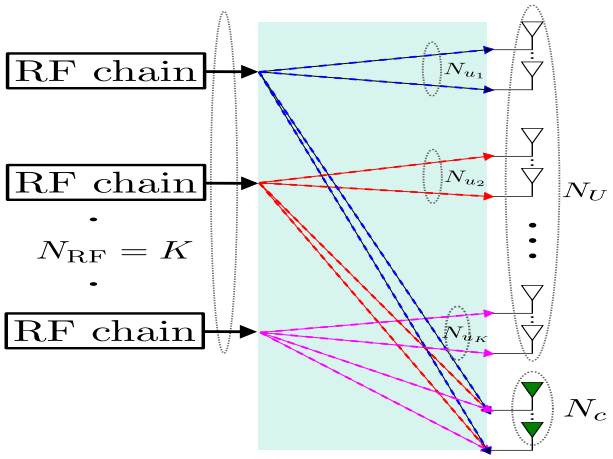

Figure 5.2: FPC Mapping strategies [Source file]

5.2.1 Precoder Optimization

This section aims to derive the precoding matrix $\mathbf{F}$ by solving an optimization problem based on the ZF precoder. The entries of $\mathbf{F}$ are not subject to any constraints, as the analog front-end design proposed in the previous chapter eliminates any such restrictions. However, the matrix structure undergoes simplification by eliminating certain RF paths, leading to the special form of $\mathbf{F}$ as presented in equation (5.3). Consequently, a considerable number of entries are forced to zero. Given that inter-user interference poses a severe challenge to the performance of multi-user systems, the design of $\mathbf{F}$ focuses on counteracting such interference. Specifically, the kth column of $\mathbf{F}$, denoted as $\mathbf{f}_k$, must satisfy the null space criterion. This ensures that the transmitted signal at each user's side remains free of any inter-user interference, leading to improved system performance.

$$\begin{cases} \mathbf{h}_k \mathbf{f}_{k'} = 1, & k = k' \\ \mathbf{h}_k \mathbf{f}_{k'} = 0, & k \neq k'. \end{cases} \tag{5.4}$$

where $\mathbf{h}_k$ is the kth row of the channel matrix $\mathbf{H}$. Based on this, the optimization problem is formulated as follows:

$$\mathbf{F} = \underset{\mathbf{F}}{\operatorname{argmin}} \quad \|\mathbf{F}\|_{\mathrm{F}}^2 \tag{5.5a}$$

$$\text{s.t.} \quad \mathbf{HF} = \mathbf{I}_K. \tag{5.5b}$$

The objective is to select the solution with the minimum transmit power from all feasible solutions. However, the sparsity of the precoder matrix $\mathbf{F}$, which contains $(K-1)N_{\mathrm{U}}$ zero elements, renders it challenging to solve problem (5.5) using conventional methods. To address this issue, the non-zero elements, N_{nz}, of $\mathbf{F}$ are collected and stored in the vector $\widehat{\mathbf{f}} \in \mathbb{C}^{N_{\mathrm{nz}}\times 1}$, as shown below:

$$\widehat{\mathbf{f}} = \left[\widehat{\mathbf{f}}_1, \ldots, \widehat{\mathbf{f}}_K\right]^{\mathrm{T}}, \tag{5.6}$$

where the kth element of $\widehat{\mathbf{f}}$ is defined as $\widehat{\mathbf{f}}_k = \left[\mathbf{f}_{\mathrm{u}_k}^{\mathrm{T}}, \mathbf{f}_{\mathrm{c}_k}^{\mathrm{T}}\right]$. Furthermore, the channel matrix can be expressed as:

$$\mathbf{H} = \left[\mathbf{H}_{\mathcal{U}_1}, \mathbf{H}_{\mathcal{U}_2}, \ldots, \mathbf{H}_{\mathcal{U}_K}, \mathbf{H}_{\mathcal{C}}\right]_{K\times N_{\mathrm{t}}}, \tag{5.7}$$

where the sub-matrix of the channel matrix corresponding to the FCAs is denoted by $\mathbf{H}_{\mathcal{C}} \in \mathbb{C}^{K\times N_{\mathrm{c}}}$, while $\mathbf{H}_{\mathcal{U}_k} \in \mathbb{C}^{K\times N u_k}$ is the channel sub-matrix that corresponds to the N_{u_k} SCAs allocated to the kth user. Substituting these definitions into (5.5), we can obtain the following equivalent expression:

$$\widehat{\mathbf{f}} = \underset{\widehat{\mathbf{f}}}{\operatorname{argmin}} \quad \left\|\widehat{\mathbf{f}}\right\|_{\mathrm{F}}^2 \tag{5.8a}$$

$$\text{s.t.} \quad \widehat{\mathbf{H}}\widehat{\mathbf{f}} = \widehat{\mathbf{i}}, \tag{5.8b}$$

where $\widehat{\mathbf{i}} = \mathrm{vec}\big(\mathbf{I}\big)$ and $\widehat{\mathbf{H}} \in \mathbb{C}^{K^2\times N_{\mathrm{nz}}}$ is defined as:

$$\widehat{\mathbf{H}} = \mathrm{Blckdg}\Big(\mathbf{H}_1, \ldots, \mathbf{H}_K\Big), \tag{5.9}$$

and $\mathbf{H}_k = \left[\mathbf{H}_{\mathcal{U}_k}\middle|\mathbf{H}_{\mathcal{C}}\right]$. The problem (5.8), under some conditions discussed below, has a straightforward solution as:

$$\widehat{\mathbf{f}} = \widehat{\mathbf{H}}^{\mathrm{H}}\left(\widehat{\mathbf{H}}\widehat{\mathbf{H}}^{\mathrm{H}}\right)^{-1}\widehat{\mathbf{i}}. \tag{5.10}$$

Once $\widehat{\mathbf{f}}$ is computed, we put its entries back to the matrix $\mathbf{F}$ by using (5.6).

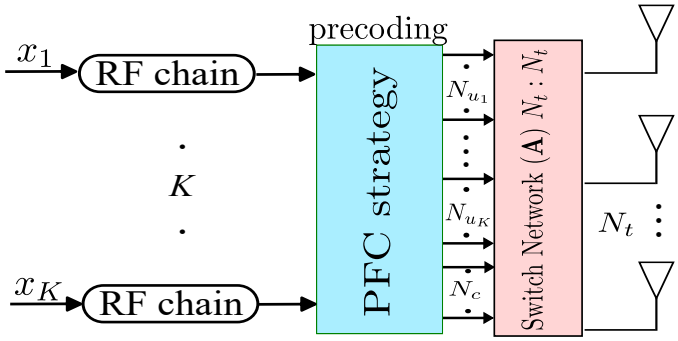

Figure 5.3: The BS architecture deploying the dynamic PFC strategy [Source file].

5.2.2 Discussions

1. Since the matrix $\widehat{\mathbf{H}}$ is a block diagonal matrix, the computation of $\widehat{\mathbf{f}}_k$ can be performed independently for each k. $\widehat{\mathbf{f}}_k$ can be obtained as follows:

$$\widehat{\mathbf{f}}_k = \mathbf{H}_k^{\mathrm{H}} \left(\mathbf{H}_k \mathbf{H}_k^{\mathrm{H}} \right)^{-1} \mathbf{i}_k, \tag{5.11}$$

   where $\mathbf{i}_k$ is the kth column of the identity matrix $\mathbf{I}_K$. This observation significantly reduces the computational complexity of the problem.

2. In order for $\mathbf{H}_k \mathbf{H}_k^{\mathrm{H}}$ to be an invertible matrix, the following constraint is required: $N_{\mathrm{u}_k} + N_{\mathrm{c}} \geq K, \forall k$.

3. In the FC case, where $N_{\mathrm{c}} = N_{\mathrm{t}}$, the submatrices $\mathbf{H}_{\mathcal{U}_k}$ are not present, and all users share the same channel matrix, i.e., $\mathbf{H}_k = \mathbf{H}$ for all $k = 1, \ldots, K$. Therefore, the precoding matrix $\mathbf{F}$ reduces to the conventional ZF precoder, which can be obtained as:

$$\mathbf{F} = \mathbf{H}^{\mathrm{H}} \left(\mathbf{H} \mathbf{H}^{\mathrm{H}} \right)^{-1}. \tag{5.12}$$

5.3 Dynamic PFC Architecture

In the previous section, the focus was on optimization problem formulation. However, the selection of FCAs and the assignment of SCAs to users were not discussed. It is evident that the optimal selection of antennas is dependent on the CSI to achieve SE improvement. In this regard, we propose a dynamic mapping that adapts the RF

paths to CSI through a switch network that controls the connection of the outputs to the antennas dynamically. The "dynamic PFC architecture" can be mathematically represented by multiplying the output signals by a permutation matrix $\mathbf{A}$ of size $N_{\mathrm{t}} \times N_{\mathrm{t}}$. The received signals at the users' side can then be expressed as:

$$\mathbf{y} = \sqrt{\rho}\mathbf{HAFx} + \mathbf{n}. \tag{5.13}$$

Let us define the set $\mathcal{C}$ containing the indexes of FCAs and the set $\mathcal{U}_k$ containing the indexes of SCAs assigned to the kth user. The switch matrix $\mathbf{A}$ can be written as:

$$\mathbf{A} = \Big[\mathbf{a}_{\mathcal{P}(1)}, \ldots, \mathbf{a}_{\mathcal{P}(N_{\mathrm{t}})}\Big], \tag{5.14}$$

where $\mathbf{a}_{\mathcal{P}(i)}$ denotes a column vector of length N_{t} with 1 in the $\mathcal{P}(i)$th position and 0 elsewhere, and the permutation $\mathcal{P}$ is defined as:

$$\mathcal{P} : \Big\{1, \ldots, N_{\mathrm{t}}\Big\} \rightarrow \Big\{\mathcal{U}_1, \ldots, \mathcal{U}_K, \mathcal{C}\Big\}. \tag{5.15}$$

By taking into account the permutation, a new channel matrix can be defined as:

$$\begin{aligned} \widetilde{\mathbf{H}} &= \mathbf{HA} \\ &= \Big[\mathbf{H}_{\mathcal{U}_1}, \mathbf{H}_{\mathcal{U}_2}, \ldots, \mathbf{H}_{\mathcal{U}_K}, \mathbf{H}_{\mathcal{C}}\Big]_{K \times N_{\mathrm{t}}}, \end{aligned} \tag{5.16}$$

where $\mathbf{H}_{\mathcal{U}_k} \in \mathbb{C}^{K \times N_{\mathrm{u}_k}}$ and $\mathbf{H}_{\mathcal{C}} \in \mathbb{C}^{K \times N_{\mathrm{c}}}$ consist of the columns indicated in $\mathcal{U}_k$ and $\mathcal{C}$, respectively. If the switch matrix $\mathbf{A}$ is known, the beamforming matrix $\mathbf{F}$ is derived as before from (5.5) by substituting $\mathbf{H}$ by $\widetilde{\mathbf{H}}$.

The equation $\mathbf{HAF} = \mathbf{I}_K$ implies that the minimization of $\|\mathbf{F}\|_{\mathrm{F}}^2$ is required for all possible combinations given by $\mathbf{A}$. Therefore, the optimal permutation can then be obtained from:

$$\Big(\mathcal{C}^{opt}, \mathcal{U}_1^{opt}, \ldots, \mathcal{U}_K^{opt}\Big) = \underset{\mathcal{C}, \mathcal{U}_1, \ldots, \mathcal{U}_K}{\operatorname{argmin}} \quad \|\mathbf{F}\|_{\mathrm{F}}^2 \tag{5.17a}$$

$$\text{s.t.} \quad \mathbf{HAF} = \mathbf{I}_K. \tag{5.17b}$$

Since $\left\|\mathbf{F}\right\|_{\mathrm{F}}^2 = \sum_{k=1}^{K} \left\|\widehat{\mathbf{f}}_k\right\|_{\mathrm{F}}^2$, we can simplify the argument of the summation as:

$$\begin{aligned}\left\|\widehat{\mathbf{f}}_k\right\|_{\mathrm{F}}^2 =& \widehat{\mathbf{f}}_k^{\mathrm{H}} \widehat{\mathbf{f}}_k \\ =& \mathbf{i}_k^{\mathrm{H}} \left(\left(\mathbf{H}_k \mathbf{H}_k^{\mathrm{H}}\right)^{-1}\right)^{\mathrm{H}} \mathbf{H}_k \mathbf{H}_k^{\mathrm{H}} \left(\mathbf{H}_k \mathbf{H}_k^{\mathrm{H}}\right)^{-1} \mathbf{i}_k \\ =& \mathbf{i}_k^{\mathrm{H}} \left(\left(\mathbf{H}_k \mathbf{H}_k^{\mathrm{H}}\right)^{-1}\right)^{\mathrm{H}} \mathbf{i}_k \\ =& \left[\left(\mathbf{H}_k \mathbf{H}_k^{\mathrm{H}}\right)^{-1}\right]_{k,k}. \end{aligned} \tag{5.18}$$

By substituting (5.18) in (5.17), we have:

$$\left(\mathcal{C}^{opt}, \mathcal{U}_1^{opt}, \ldots, \mathcal{U}_K^{opt}\right) = \underset{\mathcal{C}, \mathcal{U}_1, \ldots, \mathcal{U}_K}{\operatorname{argmin}} \quad \sum_{k=1}^{K} \left[\left(\mathbf{H}_k \mathbf{H}_k^{\mathrm{H}}\right)^{-1}\right]_{k,k}. \tag{5.19}$$

One significant advantage of this approach is that it does not require the computation of an optimized $\mathbf{F}$ for each permutation, as only $\|\mathbf{F}\|_{\mathrm{F}}^2$ is needed, using the last simplified expression. However, the number of permutations is prohibitively large for an exhaustive search. In the next section, we propose two relatively simple heuristic algorithms: the first selects the FCAs, and the second assigns the SCAs to users.

5.3.1 Algorithm 2: Selecting FCAs

As common antennas perform the majority of beamforming, selecting the FCAs is prioritized. To this end, we aim to select N_{c} columns of the matrix $\mathbf{H}$, representing the most informative part of $\mathbf{H}$. This is a combinatorial column selection problem that can be formulated as [69]:

$$\mathcal{C} = \underset{\mathcal{C}}{\operatorname{argmin}} \quad \operatorname{Tr}\left\{\left(\mathbf{H}_{\mathcal{C}} \mathbf{H}_{\mathcal{C}}^{\mathrm{H}}\right)^{-1}\right\}, \tag{5.20}$$

where the set $\mathcal{C}$ contains the indexes of the selected columns. To solve this problem, we adopt a greedy removal method [70], which iteratively identifies and removes the least informative column from the matrix until N_{c} columns are left. The algorithm starts with an initial set of selected columns $\mathcal{C}^{(0)} = [N_{\mathrm{t}}]$, which contains all columns of $\mathbf{H}$. In each

Algorithm 2 Selecting FCAs

Require: $\mathbf{H}$, N_{c};

$\mathcal{C}^{(0)} = \left\{\ell \in \mathbb{N} : \ell \leq N_{\mathrm{t}}\right\}$;

For $t = 1, \ldots, N_{\mathrm{t}} - N_{\mathrm{c}}$

$\ell = \mathrm{argmin}_{\ell} \quad \mathrm{Tr}\left\{\left(\mathbf{H}_{\mathcal{C}^{(t)}}\mathbf{H}_{\mathcal{C}^{(t)}}^{\mathrm{H}} - \mathbf{h}_{\ell}\mathbf{h}_{\ell}^{\mathrm{H}}\right)^{-1}\right\}$;

$\mathrm{s.t} \quad \ell \in \mathcal{C}^{(t)}$;

$\mathcal{C}^{(t+1)} = \mathcal{C}^{(t)} - \left\{\ell\right\}$;

end

Output: $\mathcal{C}$ and $\mathbf{H}_{\mathcal{C}}$.

iteration t, we find the least informative column $\ell \in \mathcal{C}^{(t)}$ as follows:

$$\ell = \underset{\ell}{\mathrm{argmin}} \quad \mathrm{Tr}\left\{\left(\mathbf{H}_{\mathcal{C}^{(t)}}\mathbf{H}_{\mathcal{C}^{(t)}}^{\mathrm{H}} - \mathbf{h}_{\ell}\mathbf{h}_{\ell}^{\mathrm{H}}\right)^{-1}\right\}, \tag{5.21a}$$

$$s.t. \ \ell \in \mathcal{C}^{(t)} \tag{5.21b}$$

then ℓ is removed for the next iteration, i.e, $\mathcal{C}^{(t+1)} = \mathcal{C}^{(t)} - \ell$, and the ℓth column of the matrix $\mathbf{H}_{\mathcal{C}}^{(t)}$ to give $\mathbf{H}_{\mathcal{C}}^{(t+1)}$. The algorithm proceeds by removing one element at a time until $|\mathcal{C}^{(t)}| = N_{\mathrm{c}}$. A complete pseudocode of the algorithm is given in Algorithm 2.

5.3.2 Algorithm 3: Allocating SCAs to Users

The second algorithm aims to assign the remaining antennas, in the set $\mathcal{N} = [N_{\mathrm{t}}] - \mathcal{C}$, to the users in such a way that the Frobenius norm of $\mathbf{F}$ is minimized. For a given $\mathcal{C}$, the problem (5.19) can be written as:

$$\left(\mathcal{U}_1, \ldots, \mathcal{U}_K\right) = \underset{\mathcal{U}_1, \ldots, \mathcal{U}_K}{\mathrm{argmin}} \quad \sum_{k=1}^{K}\left[\left(\mathbf{H}_k\mathbf{H}_k^{\mathrm{H}}\right)^{-1}\right]_{k,k}. \tag{5.22}$$

As shown in Algorithm 3, we start with the empty sets $\mathcal{U}_k$ $(k = 1, \ldots, K)$ and add iteratively selected antennas to them. We construct the corresponding $\mathbf{H}_k = \mathbf{H}_{\mathcal{C}}$, for all k, then we append the carefully-selected ith column of the channel matrix, $\mathbf{h}_i$, to $\mathbf{H}_k$ as:

$$\widehat{\mathbf{H}}_{ki} = \left[\mathbf{h}_i, \mathbf{H}_k\right] \qquad i \in \mathcal{N}. \tag{5.23}$$

To analyze the effect of adding the ith column to the set $\mathcal{U}_k$ on the $\|\mathbf{F}\|_{\mathrm{F}}^2$, we define the matrix $\mathbf{\Delta}$ as:

$$\mathbf{\Delta}\big(k,i\big) = p_k - p_{ki}, \tag{5.24}$$

where

$$p_k = \left[\left(\mathbf{H}_k\mathbf{H}_k^{\mathrm{H}}\right)^{-1}\right]_{k,k}, \tag{5.25}$$

and

$$p_{ki} = \left[\left(\widehat{\mathbf{H}}_{ki}\widehat{\mathbf{H}}_{ki}^{\mathrm{H}}\right)^{-1}\right]_{k,k}. \tag{5.26}$$

$\mathbf{\Delta}(k,i)$ is interpreted as the amount of decreased power when the ith column is assigned to $\mathcal{U}_k$. Therefore, we use $\mathbf{\Delta}$ as the metric for column selection at each iteration in such a way that the pair (ℓ,k), generating the maximum value in Δ, is selected:

$$\begin{aligned}\big(k,\ell\big) = \underset{k,\ell\in\mathcal{N}}{\operatorname{argmax}} \quad & \mathbf{\Delta}\big(k,\ell\big) \\ \text{s.t} \quad & |\mathcal{U}_k| < N_{\mathrm{u}_k}.\end{aligned} \tag{5.27a}$$

The selected column ℓ is added to $\mathcal{U}_k$, which changes $\mathbf{H}_k$ and p_k. Therefore, the kth column of $\mathbf{\Delta}$ is updated before allocating another antenna. Then, Algorithm 3 proceeds until all antennas are allocated.

5.3.3 Proposed DNN for the Dynamic PFC Architecture

In this section, a DNN is utilized to directly predict the results of algorithms 2 and 3 from the CSI. The architecture of the neural network used is illustrated in Table 5.1. The network consists of four layers, including an input layer, two dense layers, and an output layer. The hidden layers have KN_{t} units and utilize the rectified linear unit (ReLU) function as the activation function, while the output layer uses the sigmoid function.

The input layer of the neural network is fed by a 3D matrix denoted as $\mathbf{X} \in \mathbb{R}^{K\times N_{\mathrm{t}}\times 3}$, where each $(i,j,:)$-th entry is a vector of size 3 containing the absolute value, real part, and imaginary part of the (i,j)-th entry of the channel matrix. The training label matrix

Algorithm 3 Allocating SCAs to the users

Require: $\mathbf{H}, \mathcal{C}$;

Initialization

$\mathcal{N} = [N_{\mathrm{t}}] - \mathcal{C}$;

$\mathcal{U}_k = \{\}, \qquad \forall k = 1, \ldots, K$;

$\mathbf{H}_k = \mathbf{H}_{\mathcal{C}}, \qquad \forall k = 1, \ldots, K$;

For $k = 1 : K$

$\widehat{\mathbf{H}}_{ki} = \Big[\mathbf{h}_i, \mathbf{H}_k\Big] \qquad \forall i \in \mathcal{N}$;

$p_k = \left[\left(\mathbf{H}_k \mathbf{H}_k^{\mathrm{H}}\right)^{-1}\right]_{k,k}$;

$p_{ki} = \left[\left(\widehat{\mathbf{H}}_{ki} \widehat{\mathbf{H}}_{ki}^{\mathrm{H}}\right)^{-1}\right]_{k,k}$;

$\boldsymbol{\Delta}\big(k, i\big) = p_k - p_{ki}$;

end

Repeat

$\big(k, \ell\big) = \underset{k,\ell \in \mathcal{N}}{\operatorname{argmax}} \quad \boldsymbol{\Delta}\big(k, \ell\big)$

$\text{s.t.} \quad |\mathcal{U}_k| < N_{\mathrm{u}_k}$;

Allocate ℓth ant. to the kth user: $\mathcal{U}_k = \mathcal{U}_k \bigcup \big\{\ell\big\}$;

Remove ℓth ant. from remained ant. and set: $\mathcal{N} = \mathcal{N} - \big\{\ell\big\}$;

Update $\mathbf{H}_k = \big[\mathbf{H}_{\mathcal{U}_k}, \mathbf{H}_{\mathcal{C}}\big]$;

Update kth row of $\boldsymbol{\Delta}$ from steps 5 to 10;

Until $|\mathcal{N}| = 0$

Output: $\mathcal{U}_k, \qquad \forall k = 1, \ldots, K$;

Table 5.1: Implementation Details of the DNN

Layer Name	Output Dim.	Activation Func.
Input Layer	$K \times N_{\mathrm{t}} \times 3$	–
Dense Layer 1	$KN_{\mathrm{t}} \times 1$	ReLU
Dense Layer 2	$KN_{\mathrm{t}} \times 1$	ReLU
Output Layer	$K \times N_{\mathrm{t}}$	Sigmoid

$\mathbf{Y}$, with size $K \times N_{\mathrm{t}}$, shows the connection between RF chains and antennas. $\mathbf{Y}$ is

constructed in the simulation using the previously proposed algorithms as follows:

$$\mathbf{Y}(k,n) = \begin{cases} 1 & n \in \mathcal{U}_k \quad \text{or} \quad n \in \mathcal{C} \\ 0 & otherwise \end{cases} \tag{5.28}$$

During the training phase, the DNN is trained in a supervised manner using a dataset consisting of pairs of the channel matrix $\mathbf{X}$ and the corresponding connection matrix $\mathbf{Y}$. The goal of training is to teach the DNN to predict the optimal connections for a given input channel matrix. The training process involves feeding the input channel matrix into the DNN and comparing its predicted output with the ground-truth connection matrix. The difference between the predicted and ground-truth matrices is measured using a loss function, and the weights of the DNN are updated using backpropagation to minimize the loss function. The process is repeated for multiple epochs until the DNN converges to a state where its predictions are accurate.

The dataset used for training the DNN consists of L_p noiseless channel matrices $\mathbf{H}^{(l_\mathrm{p})}$ generated with different user locations, and for each of these matrices, L_n noisy channel matrices $\mathbf{H}^{(l_p,l_n)}$ are generated by adding complex Gaussian noise as:

$$\mathbf{H}^{(l_p,l_n)} = \mathbf{H}^{(l_n)} + \mathbf{z}, \tag{5.29}$$

where $\mathbf{z}$ is a complex Gaussian noise matrix, whose entries are i.i.d. and follow the distribution $\mathcal{CN}(0,\sigma_z^2)$. For each noiseless channel matrix $\mathbf{H}^{(l_p)}$, the sets $\mathcal{C}$ and $\mathcal{U}_k$ are constructed using Algorithm 2 and Algorithm 3, respectively. The training label, $\mathbf{Y}^{(l_p)}$, is calculated using (5.28), and this label is used for all noisy forms of the $\mathbf{H}^{(L_n)}$, resulting in the input-output pairs for the training data.

During the training phase, the DNN is trained using the training data generated for $L_\mathrm{n} = 1000$ channel realizations. To introduce variability in the training data, $L_n = 99$ noisy channels are generated for each noiseless channel matrix using (5.29) with different values of σ_z to obtain different levels of SNR. Specifically, three values of SNR are used, $\mathrm{SNR}_{\mathsf{TRAIN}} \in \{15, 20, 25\}$, where $\mathrm{SNR}_{\mathsf{TRAIN}} = 20\log_{10}\left(\frac{|\mathbf{H}^{(l_\mathrm{p})}(i,j)|^2}{\sigma_z^2}\right)$. For each noise level, 33 noisy channels are generated, resulting in 99 noisy channels per noiseless channel matrix.

In the training process, 70% of all generated data is randomly selected as the training set and the remaining 30% is used as the validation set. This split helps to evaluate the performance of the trained DNN on unseen data and prevents overfitting.

Post-processing phase The trained DNN accepts the input of size $K \times N_{\mathrm{t}} \times 3$, and predicts the matrix $\widehat{\mathbf{Y}}$, which contains the connection "probabilities". To satisfy the connectivity constraints, post-processing is required to obtain the sets $\mathcal{C}$ and $\mathcal{U}_k$. A straightforward solution is to assign the N_{c} columns of $\widehat{\mathbf{Y}}$ with the largest sum-value to set $\mathcal{C}$. This consists of selecting the antennas with the highest connectivity to all users. To assign the antennas to the users, a max-min approach is applied by adding the number ℓ to the set $\mathcal{U}_k$. First, the least significant antenna is selected, and it is connected to the user with the highest probability of connection. To do this, the columns of $\widehat{\mathbf{Y}}$ are summed up, and the minimum value is selected. Next, the user with the highest probability of connection in that column is selected. The detailed steps for this post-processing method are provided in Algorithm 4.

5.3.4 Computational Complexity

The computational complexity of the proposed algorithms is a crucial factor to consider in evaluating their practicality. The primary determinants of complexity in our algorithms are the matrix inversion and data sorting operations, which are of the order $\mathcal{O}(n^3)$ and $\mathcal{O}(n \log n)$, respectively.

In Algorithm 2, the complexity grows linearly with the number of iterations, N_{c}. It involves calculating $N_{\mathrm{t}} - i$ matrix inversions in the ith iteration, leading to a total of $N_{\mathrm{c}}\Big(N_{\mathrm{t}} - \big(N_{\mathrm{c}} - 1\big)/2\Big)$ matrix inversion computations. Additionally, in each iteration, the algorithm sorts trace values in step 3, with a maximum of N_{t} values. Consequently, the overall computational complexity of Algorithm 2 is $\mathcal{O}\Big(N_{\mathrm{c}}\Big(\big(N_{\mathrm{t}} - \left(N_{\mathrm{c}} - 1\right)/2\big)K^3 + N_{\mathrm{t}} \log N_{\mathrm{t}}\Big)\Big)$.

Algorithm 3 includes two loops, with the first loop's complexity dependent on calculating N_{U} matrix inversions. The second loop's complexity grows linearly with N_{U} and involves computing $N_{\mathrm{U}}^2/2$ matrix inversions. Additionally, the algorithm sorts the values of matrix Δ in each iteration. As such, the computational complexity of Algorithm 3 is $\mathcal{O}\Big(N_{\mathrm{U}}\Big(K^4 + N_{\mathrm{U}}/2K^3 + N_{\mathrm{U}}K \log\left(N_{\mathrm{U}}K\right)\Big)\Big)$.

Algorithm 4 Post-processing for the proposed DNN

Require: $\widehat{\mathbf{Y}}$;

$\mathcal{N} = \left[N_{\mathrm{t}}\right]$;

$\mathcal{U}_k = \{\}, \qquad \forall k = 1, \ldots, K$;

$\mathcal{C} = \{\}$;

Repeat

  $\ell = \operatorname{argmax}_{\ell \in \mathcal{N}} \quad \sum_{k=1}^{K} \widehat{\mathbf{Y}}(k, \ell)$

  $\mathcal{C} = \mathcal{C} \cup \{\ell\}$;

  $\mathcal{N} = \mathcal{N} - \{\ell\}$;

Until $|\mathcal{C}| = N_{\mathrm{c}}$

Repeat

  $\ell = \operatorname{argmin}_{\ell \in \mathcal{N}} \quad \displaystyle\sum_{k=1}^{K} \widehat{\mathbf{Y}}(k, \ell)$

  $k = \operatorname{argmax}_{k} \quad \widehat{\mathbf{Y}}(k, \ell)$
  s.t. $\quad |\mathcal{U}_k| < N_{\mathrm{u}_k}$;

  $\mathcal{U}_k = \mathcal{U}_k \cup \{\ell\}$;
  $\mathcal{N} = \mathcal{N} - \{\ell\}$;

Until $|\mathcal{N}| = 0$

Outputs: $\mathcal{C}$, and $\mathcal{U}_k, \qquad \forall k = 1, \ldots, K$.

Table 5.2: Computation times (in milliseconds)

No. FACs, N_{c}	10	25	50	100	113
Alg. 2 & 3	1317.9	1219.3	1183.2	822.4	792.2
Proposed DNN	8.5	8.3	8.1	7.4	7.3

Algorithm 4 sorts a vector of size N_{t} in each iteration, leading to the computational complexity of the order $\mathcal{O}\left(N_{\mathrm{t}}^2 \log N_{\mathrm{t}}\right)$. Overall, the computational complexities of the proposed algorithms are reasonable, making them practical for use in real-world applications.

Moreover, Table 5.2 presents the computation time of the proposed algorithms for varying numbers of FACs when a BS equipped with 256 antennas is serving 10 users. The results highlight the significant reduction in computation time achieved by the proposed DNN.

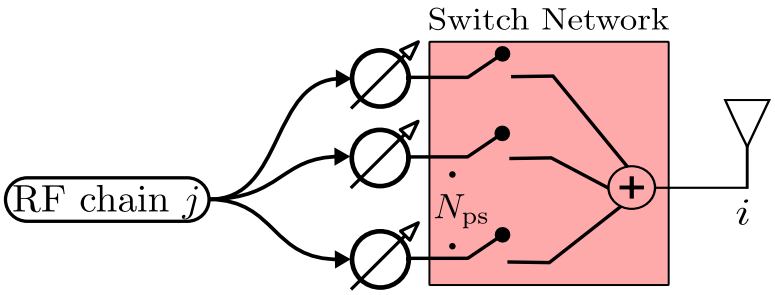

Figure 5.4: Signal flow from the RF chain j to the antenna i

5.4 Simulation Results

In this section, the simulation results are presented to show the relation between performance and hardware complexity in a multi-user massive MISO system, and to compare them with the FC and GC strategies. In the following simulations, the Saleh-Valenzuela channel model, with the same parameters as chapter 3, is considered. We consider hardware implementation architecture presented in Figure 5.4 which is able to obtain a quasi-optimal performance with only 11 FPSs per RF chain. In our simulations, the transmitter is equipped with a 16×16 UPA with half-wavelength spacing between elements, $N_{\text{ps}} = 11$, and $N_{\text{RF}} = K$. Furthermore, we assume that there is no priority between users, so the same number of antennas are assigned to them.

5.4.1 Spectral Efficiency

To analyze the performance of the proposed architecture, the sum-rate criterion is considered:

$$R_s = \sum_{k=1}^{K} \log_2 \left(1 + \frac{\rho \left| \mathbf{h}_k \mathbf{f}_k \right|^2}{\rho \sum_{k'=1, k' \neq k}^{K} \left| \mathbf{h}_k \mathbf{f}_{k'} \right|^2 + 1} \right). \tag{5.30}$$

Figure 5.5 illustrates the sum-rate as a function of N_{c}, going from PC to FC strategies. As it can be seen, for small values of N_{c}, the performance sharply increases by assigning more antennas to the set of FCAs, resulting in more complex hardware. The designer can select the desired trade-off between complexity and performance. As expected, the dynamic PFC significantly improves the SE for small values of N_{c}; the price to pay is the added switch matrix before the antennas.

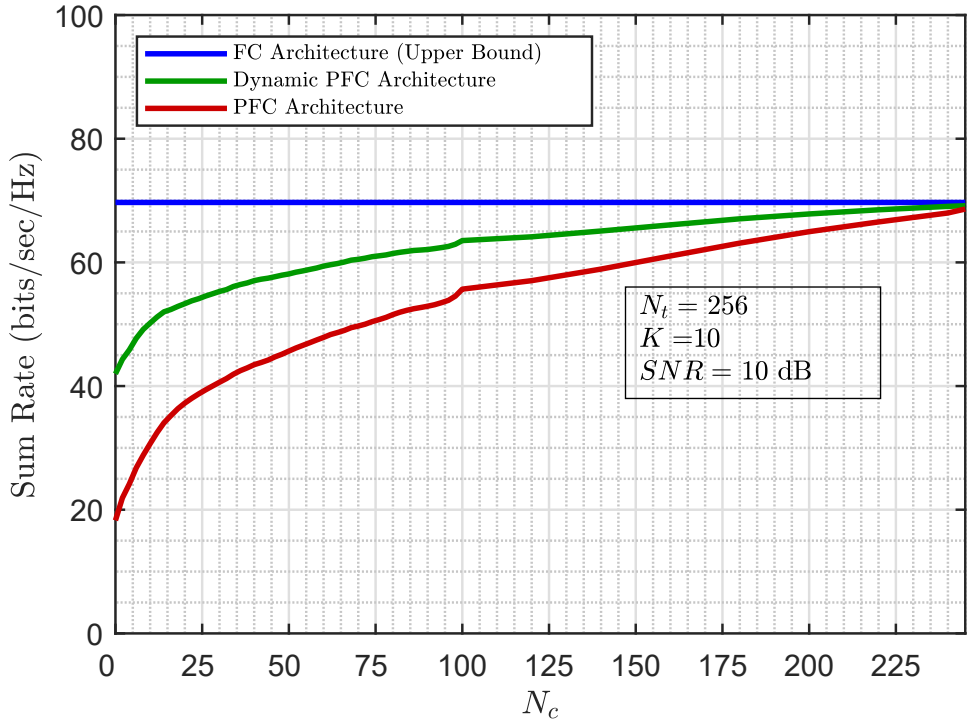

Figure 5.5: The sum-rate as a function of N_{c} for $N_{\mathrm{t}} = 256$, $K = 10$ and $\mathrm{SNR} = 10$ dB [MATLAB code], [Source file].

5.4.2 Energy Efficiency

To put the energy consumption into perspective, we define the EE as $\xi \triangleq \frac{R_s}{P_{\mathrm{tot}}}$, where P_{tot} is the total power consumption introduced as:

$$P_{\mathrm{tot}} = P + P_{\mathrm{BB}} + N_{\mathrm{RF}} P_{\mathrm{RF}} + N_{\mathrm{RF}} N_{\mathrm{ps}} P_{\mathrm{ps}}^{a} + N_{\mathrm{nz}} N_{\mathrm{ps}} P_{\mathrm{sw}} \tag{5.31}$$

In this equation, P is the transmit power; P_{ps}^{a}, P_{BB}, and L_{n} are, respectively, the powers consumed by a PS, by the baseband processor, and by an RF chain; P_{sw} represents the power consumed by a switch. In this simulation, their values are set to: $P_{\mathrm{ps}}^{F} = 10mW$, $P_{\mathrm{ps}}^{Q} = 30mW$,$P_{\mathrm{ps}}^{C} = 50mW$, $P_{\mathrm{BB}} = 200mW$, $P_{\mathrm{RF}} = 300mW$, and $P_{\mathrm{sw}} = 5mW$ [67]. Also, the number of switch networks N_{nz} in the FC, GC, PFC, and dynamic PFC architectures are KN_t, KN_t/G, $N_{\mathrm{U}} + KN_{\mathrm{c}}$, and $2N_{\mathrm{t}} + N_{\mathrm{c}}(K-1)$, respectively.

Figure 5.6 illustrates the EE as a function of the number of FCAs. This shows that the maximum EE is achieved by considering no antenna as FCA in dynamic PFC architecture, while the fixed PFC architecture requires a few FCAs.

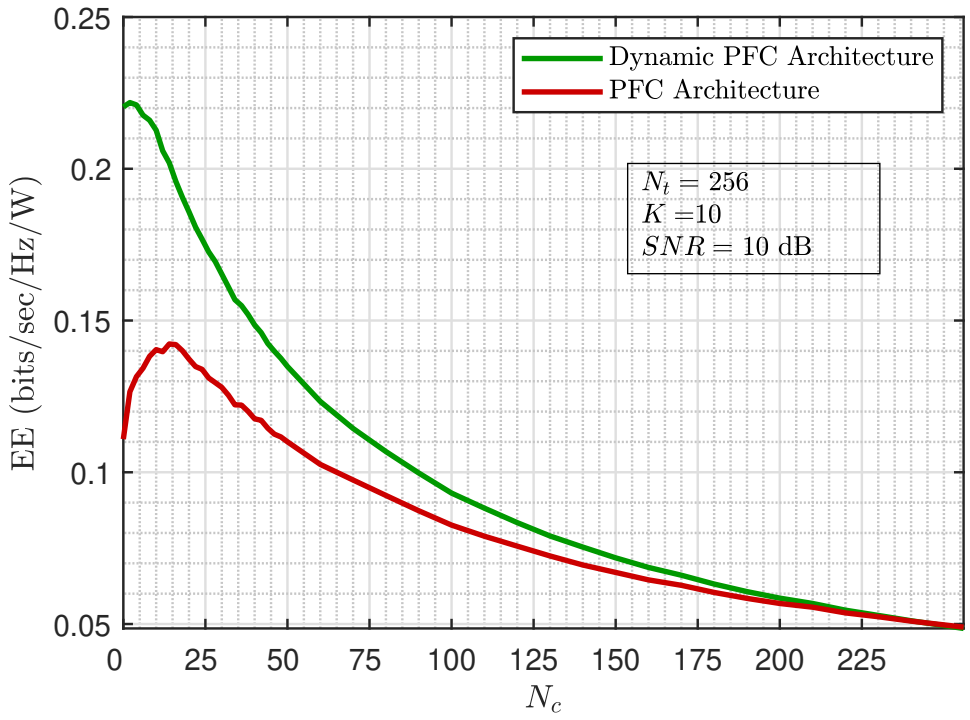

Figure 5.6: Energy efficiency achieved by different values of N_{c}, when $K = 10$, and $\mathrm{SNR} = 10$ dB [MATLAB code], [Source file].

5.4.3 DNN-Based Antenna Assignment

In Figure 5.7 and Figure 5.8, the trained DNN is used for antennas assignment in the dynamic PFC architecture. To have a fair comparison with the GC architecture [45], we consider approximately the same hardware complexity for both structures. Therefore, the number of shared antennas is determined by:

$$N_{\mathrm{c}} = \left\lfloor \frac{N_{\mathrm{t}}(K-G)}{G(K-1)} \right\rfloor, \tag{5.32}$$

where $\lfloor . \rfloor$ denotes the floor function. Since the performance of the GC strategy decreases by increasing G, to achieve comparable performance, the number of groups is set to the minimum, i.e., $G = 2$. Figure 5.7 reveals a non-negligible gain in the sum-rate for the dynamic PFC compared to the GC architecture. The performance of FC architecture deploying DPS and QPS is also illustrated. For instance, at 10 dB of SNR, the PFC and dynamic PFC architectures obtain 81.62% and 92.26% of the FC rate, respectively, while the GC strategy achieves 69% of that. Figure 5.8 presents the EE versus SNR. It indicates that the EE of the proposed architecture is significantly

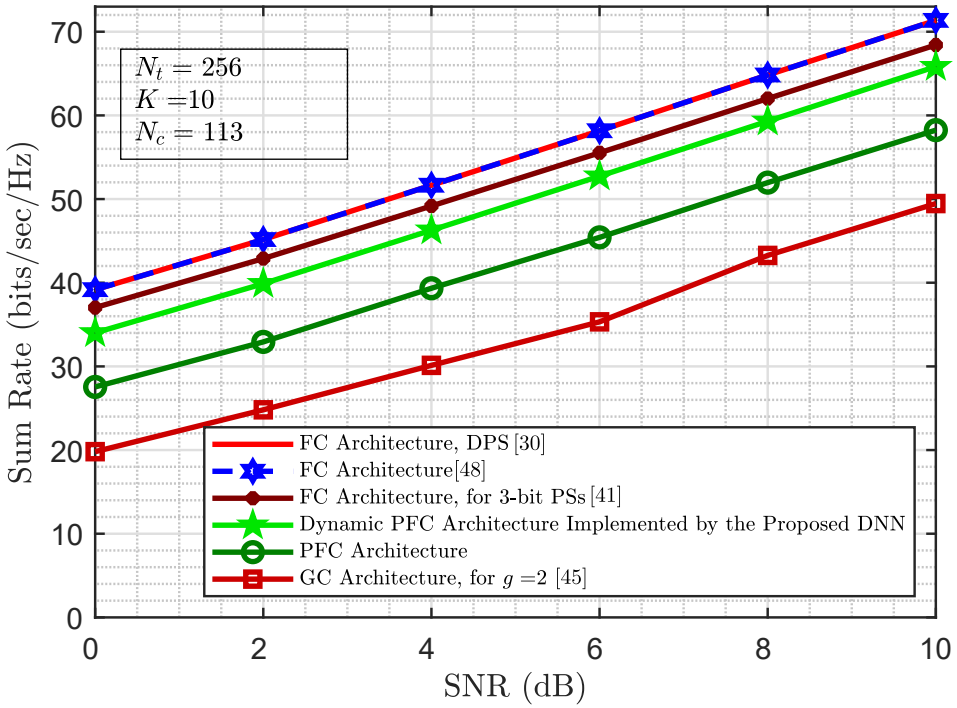

Figure 5.7: Sum-rate versus SNR, with $K = 10$, $N_{\mathrm{c}} = 113$ in the PFC, $G = 2$ in the GC [MATLAB code], [Source file].

better than that of the FC and the GC structures. It reveals that even though the FC structure has better SE , it has a lower EE because of the number of deployed switches.

5.5 Summary

The chapter focused on exploring mapping strategies for analog networks. A novel architecture was proposed that offered a cost-effective solution with $N_{\mathrm{t}} + 1$ distinct levels of complexity/performance trade-off. The proposed architecture divided the antenna elements into two distinct groups, with N_{c} antennas connected to all of the RF chains, while the remaining antennas were connected to only one RF chain.

To optimize the performance of this architecture, an analytic algorithm was introduced for optimizing the precoding matrix using the ZF approach. This algorithm had low complexity due to removing the zero entries in the precoding matrix.

Additionally, a dynamic mapping strategy was presented, which adjusted the RF paths

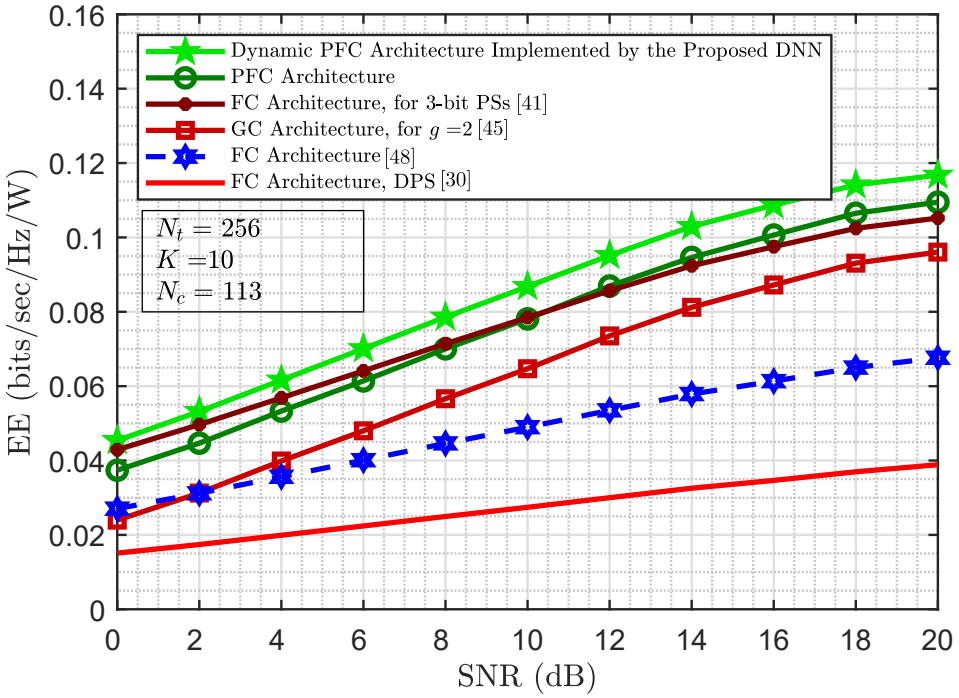

Figure 5.8: Energy efficiency achieved by different values of SNR, when $K = 10$, $N_{\mathrm{c}} = 113$ in the PFC, and $G = 2$ in the GC [MATLAB code], [Source file].

via a switch network. To find the switch states, a suboptimal greedy solution was provided. Moreover, to simplify the implementation of these strategies for real-time applications, a machine-learning approach was proposed to provide the antenna assignment matrix directly via a simple post-processing algorithm.

Finally, the chapter presented promising simulation results that demonstrated the efficacy of the proposed architectures and algorithms. These simulations showed that the proposed strategies provided better performance and more flexibility than other mapping strategies currently in use.

6

Hybrid Beamforming for Wideband Channels

Sommaire

THE design of HBF for wideband channels has received limited attention in previous research. To fill these research gaps, we explore a hybrid precoding design for a multiuser MISO system based on OFDM. Our design aims to maximize the downlink sum rate while satisfying the per-subcarrier power constraints by jointly optimizing the digital and analog precoder coefficients. To simplify the optimization problem, we make the assumption that the analog precoder coefficients can take any value within a specific circle on the complex plane, which eliminates the problem's combinatorial nature. To solve the resulting non-convex optimization problem, we propose using the alternating optimization approach. Specifically, we adopt a Fractional Programming (FP) technique called the Lagrangian dual transform to tackle the optimization problem. This approach involves reformulating the problem of maximizing the sum-of-ratios form by taking the ratio out of the logarithm. Then, we apply the quadratic transform to the sum-of-ratios term, which enables us to solve the problem iteratively. We evaluate our proposed approach using numerical simulations, which demonstrate how different parameters impact the achievable sum rate. Specifically, we investigate the effects of the number of antennas, the number of RF chains, and the size of the circle constraint on the achievable rate. Furthermore, we demonstrate the importance of a practical number of RF chains in achieving high rates, and we show that our proposed approach can outperform other benchmark schemes in terms of the achievable rate. Overall, our results show that the proposed approach can effectively optimize hybrid precoding for OFDM-based MISO systems.

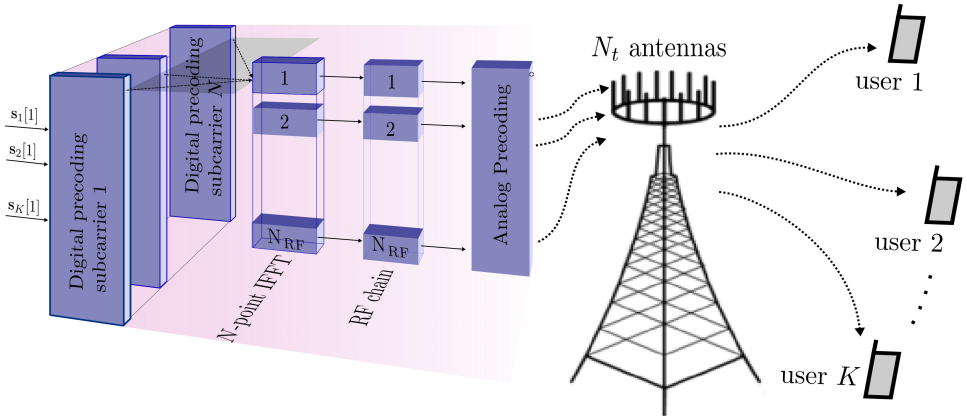

Figure 6.1: OFDM-based system model for multiuser MISO scenario [Source file].

6.1 OFDM-based System Model

We consider a multiuser MISO system that utilizes OFDM and an HBF architecture to address the challenges of frequency selective channels, as illustrated in Figure 6.1. The transmitting end consists of an antenna array with N_{t} elements, connected to N_{RF} RF chains, serving K users with single antennas. To transmit data, a low-dimensional digital precoder $\mathbf{F}_{\mathrm{BB}}[n] \in \mathbb{C}^{N_{\mathrm{RF}} \times N_s}$ is first applied to precode data symbols $\mathrm{s}[n]$ at each subcarrier $n = 1, \ldots, N$.

Subsequently, the transformed signals are converted to the time domain using N_{RF} N-point Inverse Fast Fourier Transformss (IFFTs). After upconverting the signals to the RF domain, the analog precoder $\mathbf{F}_{\mathrm{RF}} \in \mathbb{C}^{N_{\mathrm{t}} \times N_{\mathrm{RF}}}$ is applied. The received signal at the user's side is expressed as a function of the transmitted signal, channel conditions, and the effects of noise:

$$\mathbf{r}[n] = \mathbf{h}_k[n]\mathbf{F}_{\mathrm{RF}}\mathbf{F}_{\mathrm{BB}}[n]\mathbf{s}[n] + z[n], \tag{6.1}$$

where $\mathbf{h}_k[n] \in \mathbb{C}^{1 \times N_{\mathrm{t}}}$ is the channel of nth subcarrier from the transmitter to the kth user, and $z[n]$ is the complex Gaussian noise that follows $\mathcal{CN}(0, \sigma_z^2)$. The coefficients of the analog precoder are implemented using N_{ps} FPSs and a switch network, as illustrated in Figure 6.2. This design enables the selection of coefficients from a finite-size feasible set denoted as $\mathcal{F}_{N_{\mathrm{ps}}}$ [47], [48].

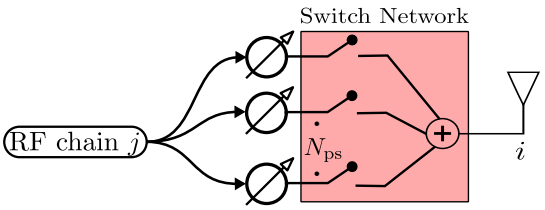

Figure 6.2: Signal flow from the RF chain j to the antenna i [Source file].

6.2 Problem Formulation

In the multiuser MISO scenario, our objective is to devise an optimal HBF strategy that maximizes the downlink sum rate of the system while satisfying a power constraint, denoted as P, for each subcarrier. We assume perfect CSI to be available, and then the problem can be mathematically formulated as follows:

$$\underset{\mathbf{F}_{\text{RF}},\{\mathbf{F}_{\text{BB}}[n]\}_{n=1}^{N}}{\text{maximize}} \quad \frac{1}{N}\sum_{n=1}^{N}\sum_{k=1}^{K}\log(1+\text{SINR}_{k,n}) \tag{6.2a}$$

$$\text{s.t} \quad \text{Tr}\left\{\mathbf{F}_{\text{RF}}\mathbf{F}_{\text{BB}}[n]\mathbf{F}_{\text{BB}}^{\text{H}}[n]\mathbf{F}_{\text{RF}}^{\text{H}}\right\} \leq P, \forall n, \tag{6.2b}$$

$$\mathbf{F}_{\text{RF}}(i,j) \in \mathcal{F}_{N_{\text{ps}}}, \tag{6.2c}$$

where $\text{SINR}_{k,n}$ is the signal-to-interference-plus-noise ratio (SINR) in the nth subcarrier for user k which is expressed as:

$$\text{SINR}_{k,n} = \frac{\mathbf{h}_k[n]\mathbf{F}_{\text{RF}}\mathbf{f}_{\text{BB}_k}[n]\mathbf{f}_{\text{BB}_k}^{\text{H}}[n]\mathbf{F}_{\text{RF}}^{\text{H}}\mathbf{h}_k^{\text{H}}[n]}{\sigma_z^2+\sum_{j\neq k}\mathbf{h}_k[n]\mathbf{F}_{\text{RF}}\mathbf{f}_{\text{BB}_j}[n]\mathbf{f}_{\text{BB}_j}^{\text{H}}[n]\mathbf{F}_{\text{RF}}^{\text{H}}\mathbf{h}_k^{\text{H}}[n]}, \tag{6.3}$$

where $\mathbf{f}_{\text{BB}_k}[n]$ is the kth column of $\mathbf{F}_{\text{BB}}[n]$. The optimization problem (6.2) is non-convex due to the non-convex functions in the objective and constraints (6.2b). In addition, this problem is more challenging than in single-carrier systems because of the identical analog precoder for all subcarriers. To tackle this problem, we propose an iterative algorithm and employ the technique of FP, which has demonstrated satisfactory performance.

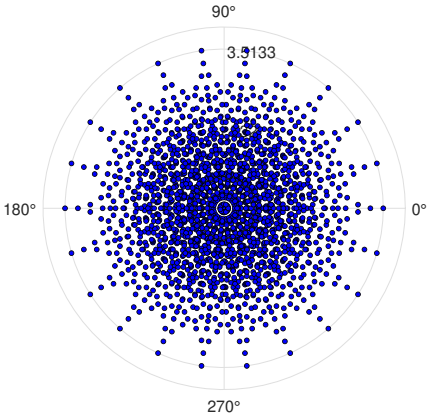

Figure 6.3: The feasible set $\mathcal{F}_{11}$ [Source file].

6.3 Hybrid Precoding Design for multiuser MISO

Designing hybrid analog and digital beamformers for the optimization problem (6.2) is challenging due to the combinatorial nature of the problem raised from the limited points in the feasible set. In [48], it has been shown that utilizing 11 phase shifters generates the feasible set, shown in Figure 6.3, that sufficiently covers the circular region with radius $r_0 = 3.51$. Therefore, the feasible set is assumed to encompass all the points inside the circular region with radius r_0. This assumption, while introducing negligible errors to the desired beamforming coefficients, eliminates the combinatorial nature of the optimization problem and makes it more tractable. Thus, considering $\mathbf{F}$ as the analog precoder which can have any value within the circle, the problem with a new constraint on the entries of $\mathbf{F}$ can be written as:

$$\underset{\mathbf{F},\{\mathbf{F}_{\mathrm{BB}}[n]\}_{n=1}^{N}}{\text{maximize}} \quad \frac{1}{N}\sum_{n=1}^{N}\sum_{k=1}^{K}\log(1+\mathrm{SINR}_{k,n}) \tag{6.4a}$$

$$\text{s.t} \quad \mathrm{Tr}\left\{\mathbf{F}\mathbf{F}_{\mathrm{BB}}[n]\mathbf{F}_{\mathrm{BB}}^{\mathrm{H}}[n]\mathbf{F}^{\mathrm{H}}\right\} \leq P, \forall n, \tag{6.4b}$$

$$|\mathbf{F}(i,j)| \leq r_0. \tag{6.4c}$$

It is noteworthy that the new constraint (6.4c) on $\mathbf{F}$ can be temporarily removed. This is because once the analog precoder has been designed, it can be normalized, and the digital beamforming part can satisfy the transmit power constraint. Therefore, we

attempt to solve the following problem:

$$\underset{\mathbf{F},\{\mathbf{F}_{\mathrm{BB}}[n]\}_{n=1}^{N}}{\text{maximize}} \quad \frac{1}{N}\sum_{n=1}^{N}\sum_{k=1}^{K}\log(1+\mathrm{SINR}_{k,n}) \tag{6.5a}$$

$$\text{s.t} \quad \mathrm{Tr}\left\{\mathbf{F}\mathbf{F}_{\mathrm{BB}}[n]\mathbf{F}_{\mathrm{BB}}^{\mathrm{H}}[n]\mathbf{F}^{\mathrm{H}}\right\} \leq P, \forall n. \tag{6.5b}$$

To optimize the problem at hand, we employ the Lagrangian dual transformation technique using FP method. This technique involves moving the SINR term outside the logarithm to simplify the problem. We then use the quadratic transform to decouple the numerator and denominator of each ratio term. This conversion enables us to express the problem as a sequence of convex optimization problems, which can be solved iteratively. For a more detailed explanation of this technique, please refer to [71].

We propose a **three-step algorithm** to solve the underlying optimization problem in the following sections. In Step 1, we employ the theory of Lagrangian dual transformation to transform the problem into an equivalent dual problem. This step enables us to simplify and express the problem in terms of Lagrange multipliers. In Step 2, we utilize the technique of Quadratic transformation to reformulate the problem further. This step involves decoupling the numerator and denominator of each ratio term and expressing the problem as a sequence of convex optimization problems. Finally, in Step 3, we analyze the problem and use a convex optimization solver to solve it efficiently. This step involves iteratively solving the sequence of convex optimization problems until we reach a solution that satisfies the desired accuracy and convergence criteria. By using this algorithm, we can efficiently solve the underlying optimization problem and obtain a solution that satisfies the given constraints.

6.3.1 Step 1 - Lagrangian Dual Transformation

Theorem 1 *Lagrangian Dual Transform*

Given a sequence of vector-valued functions $\mathbf{a}_i \in \mathbb{C}^{d\times 1}$, and matrix-valued function $\mathbf{B}_i \in \mathbb{C}^{d\times d}$, for $i = 1, ..., n$, along with a nonempty and compact constraint set $\mathcal{X}$, where

$d \in \mathbb{N}$, a sum logarithm FP problem:

$$\underset{\mathbf{x}}{\text{maximize}} \quad \sum_{i=1}^{M} \log\left(1 + \mathbf{a}_i^{\mathrm{H}}(\mathbf{x})\mathbf{B}_i^{-1}(\mathbf{x})\mathbf{a}_i(\mathbf{x})\right) \tag{6.6a}$$

$$\text{s.t} \quad \mathbf{x} \in \mathcal{X} \tag{6.6b}$$

is equivalent to

$$\underset{\mathbf{x},\boldsymbol{\gamma}}{\text{maximize}} \quad \mathcal{P}_r\left(\mathbf{x}, \boldsymbol{\gamma}\right) \tag{6.7a}$$

$$\text{s.t} \quad \mathbf{x} \in \mathcal{X}, \tag{6.7b}$$

where the new objective function $\mathcal{P}_r$ is

$$\mathcal{P}_r\left(\mathbf{x}, \boldsymbol{\gamma}\right) = \sum_{i=1}^{M} \log_2\left(1+\gamma_i\right) - \sum_{i=1}^{M} \gamma_i + \sum_{i=1}^{M} \left(1+\gamma_i\right) \mathbf{a}_i^{\mathrm{H}}(\mathbf{x}) \Big(\mathbf{a}_i(\mathbf{x})\mathbf{a}_i^{\mathrm{H}}(\mathbf{x}) + \mathbf{B}_i(\mathbf{x})\Big)^{-1} \mathbf{a}_i(\mathbf{x}). \tag{6.8}$$

In can be seen that $\mathcal{P}_r$ is a concave differentiable function over $\boldsymbol{\gamma}$ when $\mathbf{x}$ is held fixed, so $\boldsymbol{\gamma}$ can be optimally determined by setting each $\frac{\partial \mathcal{P}_r}{\partial \gamma_i}$ to zero; the optimal γ_i^* is $\mathbf{a}_i^{\mathrm{H}}(\mathbf{x})\mathbf{B}_i^{-1}\mathbf{a}_i(\mathbf{x})$. ■

By applying Theorem 1 on the problem (6.5), the objective function can be expressed as:

$$\begin{aligned} \mathcal{G}_r\left(\mathbf{F}, \mathbf{F}_{\mathrm{BB}}[n], \boldsymbol{\gamma}[n]\right) = & \sum_{k=1}^{K} \log_2\left(1+\gamma_k[n]\right) - \sum_{k=1}^{K} \gamma_k[n] \\ & + \sum_{k=1}^{K} \left(1+\gamma_k[n]\right) \left(\mathbf{h}_k[n]\mathbf{F}\mathbf{f}_{\mathrm{BB}_k}[n]\right)^{\mathrm{H}} \\ & \times \Big(\sigma_z^2 + \sum_{j=1}^{K} \mathbf{h}_k[n]\mathbf{F}\mathbf{f}_{\mathrm{BB}_j}[n]\mathbf{f}_{\mathrm{BB}_j}^{\mathrm{H}}[n]\mathbf{F}^{\mathrm{H}}\mathbf{h}_k[n]^{\mathrm{H}}\Big)\mathbf{h}_k[n]\mathbf{F}\mathbf{f}_{\mathrm{BB}_k}[n], \end{aligned} \tag{6.9}$$

where $\boldsymbol{\gamma}[n]$ refers to $(\gamma_1[n], \ldots, \gamma_K[n])$ and $\gamma_k[n]$ is introduced as an auxiliary variable.

With $\mathbf{F}$, $\mathbf{F}_{\mathrm{BB}}[n]$ fixed, the optimal $\gamma_k[n]$ can be obtained by setting $\frac{\partial \mathcal{G}_r}{\partial \gamma_k[n]} = 0$:

$$\gamma_k^{\star}[n] \quad = \quad \mathbf{f}_{\mathrm{BB}_k}^{\mathrm{H}}[n]\mathbf{F}^{\mathrm{H}}\mathbf{h}_k^{\mathrm{H}}[n]\left(\sigma_z^2 + \sum_{j\neq k}^{K}\mathbf{h}_k[n]\mathbf{F}\mathbf{f}_{\mathrm{BB}_j}[n]\mathbf{f}_{\mathrm{BB}_j}^{\mathrm{H}}[n]\mathbf{F}^{\mathrm{H}}\mathbf{h}_k^{\mathrm{H}}[n]\right)^{-1}\mathbf{h}_k[n]\mathbf{F}\mathbf{f}_{\mathrm{BB}_k}[n]. \tag{6.10}$$

6.3.2 Step 2 - Quadratic Transformation

Theorem 2 *Quadratic Transform*

A multidimensional single-ratio FP problem is defined to be

$$\underset{\mathbf{x}}{\text{maximize}} \qquad \sum_{i=1}^{M}\mathbf{a}_i^{\mathrm{H}}(\mathbf{x})\,\mathbf{B}_i^{-1}(\mathbf{x})\,\mathbf{a}_i(\mathbf{x}) \tag{6.11a}$$

$$\text{s.t} \qquad \mathbf{x}\in\mathcal{X}. \tag{6.11b}$$

The quadratic transform in the multidimensional and complex FP is equivalent to:

$$\underset{\mathbf{x},\mathbf{y}}{\text{maximize}} \qquad \sum_{i=1}^{M}2\mathfrak{Re}\left\{\mathbf{y}_i^{\mathrm{H}}\mathbf{a}_i(\mathbf{x})\right\} - \mathbf{y}_i^{\mathrm{H}}\mathbf{B}_i(\mathbf{x})\,\mathbf{y}_i \tag{6.12a}$$

$$\text{s.t} \qquad \mathbf{x}\in\mathcal{X}, \quad \mathbf{y}_i\in\mathbb{C}^d, \tag{6.12b}$$

where $\mathbf{y}$ refers to a collection of auxiliary variables $\{\mathbf{y}_1,...,\mathbf{y}_M\}$ and $\mathfrak{Re}\{.\}$ denotes the real part of the complex value. The optimal solution $\mathbf{y}_i^{*} = \mathbf{B}_i^{-1}(\mathbf{x})\,\mathbf{a}_i(\mathbf{x})$. ■

The multidimensional quadratic transform presented in Theorem 2 can be applied to recast the objective function $\mathcal{G}_r$ into a new form $\mathcal{G}_q$ as follows:

$$\begin{aligned}\mathcal{G}_q\left(\mathbf{F}, \mathbf{F}_{\mathrm{BB}}[n], \mathbf{Y}[n], \boldsymbol{\gamma}[n]\right) = & \sum_{k=1}^{K} \log_2\left(1+\gamma_k[n]\right) \\ & - \sum_{k=1}^{K} \gamma_k[n] + \sum_{k=1}^{K} 2\sqrt{1+\gamma_k[n]}\mathfrak{Re}\left(y_k[n]^{\mathrm{H}}\mathbf{h}_k[n]\mathbf{F}\mathbf{f}_{\mathrm{BB}_k}[n]\right) \\ & - y_k[n]^{\mathrm{H}}\left(\sigma_z^2 + \sum_{j=1}^{K} \mathbf{h}_k[n]\mathbf{F}\mathbf{f}_{\mathrm{BB}_j}[n]\mathbf{f}_{\mathrm{BB}_j}^{\mathrm{H}}[n]\mathbf{F}^{\mathrm{H}}\mathbf{h}_k^{\mathrm{H}}[n]\right) y_k[n],\end{aligned} \tag{6.13}$$

where $\mathbf{Y}[n]$ is the collection $(y_1[n], \ldots, y_K[n])$. The above $\mathcal{G}_q$ reformulation is obtained by treating $\sqrt{(1+\gamma_k[n])}\left(\mathbf{h}_k[n]\mathbf{F}\mathbf{f}_{\mathrm{BB}_k}[n]\right)$ as the numerator vector and also treating $\sigma_z^2 + \sum_{j=1}^{K} \mathbf{h}_k[n]\mathbf{F}\mathbf{f}_{\mathrm{BB}_j}[n]\mathbf{f}_{\mathrm{BB}_j}^{\mathrm{H}}[n]\mathbf{F}^{\mathrm{H}}\mathbf{h}_k^{\mathrm{H}}[n]$ as the denominator matrix in Theorem 2. The optimization problem is reformulated as follows:

$$\underset{\mathbf{F}, \{\mathbf{F}_{\mathrm{BB}}[n], \mathbf{Y}[n], \boldsymbol{\gamma}[n]\}_{n=1}^{N}}{\text{maximize}} \quad \frac{1}{N}\sum_{n=1}^{N} \mathcal{G}_q\left(\mathbf{F}, \mathbf{F}_{\mathrm{BB}}[n], \mathbf{Y}[n], \boldsymbol{\gamma}[n]\right) \tag{6.14a}$$

$$\text{s.t} \quad \mathrm{Tr}\left\{\mathbf{F}\mathbf{F}_{\mathrm{BB}}[n]\mathbf{F}_{\mathrm{BB}}^{\mathrm{H}}[n]\mathbf{F}^{\mathrm{H}}\right\} \leq P, \forall n. \tag{6.14b}$$

6.3.3 Step 3 - Solving Optimization Problem

In (6.14), the application of the quadratic transform decouples the numerator and denominator of each ratio term, making the problem amenable to iterative optimization over $\mathbf{F}_{\mathrm{BB}}[n]$. With the other variables fixed, the optimal $y_k[n]$ can be obtained by solving $\frac{\partial \mathcal{G}_q}{\partial y_k[n]} = 0$:

$$y_k^{\star}[n] = \left(\sigma_z^2 + \sum_{j=1}^{K} \mathbf{h}_k[n]\mathbf{F}\mathbf{f}_{\mathrm{BB}_j}[n]\mathbf{f}_{\mathrm{BB}_j}^{\mathrm{H}}[n]\mathbf{F}^{\mathrm{H}}\mathbf{h}_k^{\mathrm{H}}[n]\right)^{-1} \sqrt{1+\gamma_k[n]}\mathbf{h}_k[n]\mathbf{F}\mathbf{f}_{\mathrm{BB}_k}[n]. \tag{6.15}$$

Likewise, the optimal $\mathbf{f}_{\mathrm{BB}_k}[n]$ is

$$\mathbf{f}_{\mathrm{BB}_k}^{\star}[n] = \left(\eta\mathbf{F}^{\mathrm{H}}\mathbf{F} + \sum_{j=1}^{K} \mathbf{F}^{\mathrm{H}}\mathbf{h}_k^{\mathrm{H}}[n]y_j[n]y_j^{\mathrm{H}}[n]\mathbf{h}_k[n]\right)^{-1} \sqrt{1+\gamma_k[n]}\mathbf{F}^{\mathrm{H}}\mathbf{h}_k^{\mathrm{H}}[n]y_k, \tag{6.16}$$

where η is a dual variable introduced for the power constraint, optimally determined by

$$\eta^{\star} = \min \left\{ \eta \geq 0; \mathrm{Tr} \left\{ \mathbf{F}\mathbf{F}_{\mathrm{BB}}[n]\mathbf{F}_{\mathrm{BB}}^{\mathrm{H}}[n]\mathbf{F}^{\mathrm{H}} \right\} \leq P \right\}. \tag{6.17}$$

It is noteworthy that the optimal value of $\eta^{\star}$ can be obtained by bisection search. Since the analog precoder is identical for all subcarriers, the problem is quite complex to find $\mathbf{F}$. For given other variables, the optimization problem of $\mathbf{F}$ can be formulated as follows:

$$\underset{\mathbf{F}}{\text{maximize}} \quad \delta\big(\mathbf{F}\big) \tag{6.18a}$$

$$\text{s.t} \quad \mathrm{Tr}\left\{ \left| \mathbf{F}\mathbf{F}_{\mathrm{BB}}[n] \right|^2 \right\} \leq P, \forall n, \tag{6.18b}$$

where

$$\delta\big(\mathbf{F}\big) = \sum_{n=1}^{N} \sum_{k=1}^{K} \sqrt{1+\gamma_k[n]} 2\mathfrak{Re}\left(y_k[n]^{\mathrm{H}} \mathbf{h}_k[n]\mathbf{F}\mathbf{f}_{\mathrm{BB}_k}[n] \right) - \left| y_k[n] \right|^2 \sum_{j=1}^{K} \left| \mathbf{h}_k[n]\mathbf{F}\mathbf{f}_{\mathrm{BB}_j}[n] \right|^2. \tag{6.19}$$

It can be realized that $\left| \mathbf{F}\mathbf{F}_{\mathrm{BB}}[n] \right|^2$ is a convex function with respect to $\mathbf{F}$. Hence, the function $\mathrm{Tr}\left\{ \left| \mathbf{F}\mathbf{F}_{\mathrm{BB}}[n] \right|^2 \right\}$ is convex. Moreover, it can be seen that $\left| \mathbf{h}_k[n]\mathbf{F}\mathbf{f}_{\mathrm{BB}_j}[n] \right|^2$ is a convex function with respect to $\mathbf{F}$, then $-\sum_{j=1}^{K} \left| \mathbf{h}_k[n]\mathbf{F}\mathbf{f}_{\mathrm{BB}_j}[n] \right|^2$ is a concave function with respect to $\mathbf{F}$. Hence, $\delta\big(\mathbf{F}\big)$ is a concave function with respect to $\mathbf{F}$. Therefore, problem (6.18) is a convex problem, which can be solved effectively by any convex optimization solver such as CVX-Mosek [72]. As outlined in Algorithm 5, the aforementioned step can be iteratively executed until the desired level of performance coverage is achieved. Since CVX solver invokes the interior-point method to solve the underlying problem (6.18), the involved complexity is $\mathcal{O}(m_1^{1/2}(m_1+m_2)m_2^2)$, where m_1 is the number of inequality constraints, m_2 denotes the number of variables [73], and $\mathcal{O}$ denotes the big-O notation. Hence, the complexity of this step is $\mathcal{O}(L_1 N K^{\frac{7}{2}})$, where L_1 is the number of iterations required to achieve the convergence of Algorithm 5.

Algorithm 5 Hybrid beamforming for wideband channels

Require: K users, N subcarriers, N_{t}, N_{RF} RF chains;
1: **Initialization:** $\mathbf{F}$, $\mathbf{F}_{\mathrm{BB}}[n]$ for all n;
Ensure: Max sum rate;
2: **repeat**
3: Update $\gamma[n]$ for all n;
4: Update $\mathbf{y}[n]$ for all n;
5: Update $\mathbf{F}$;
6: Update $\mathbf{F}_{\mathrm{BB}}[n]$ for all n;
7: **until** Convergence
8: Obtain $\mathbf{F}_{\mathrm{RF}}$ via mapping $\mathbf{F}$ into $\mathcal{F}_{N_{\mathrm{ps}}}$.

6.4 A low-complex approach to obtain the analog precoder

The proposed algorithm can handle the constraints directly, but the number of constraints can become very large due to the challenge of finding the analog precoder. This results in high computational complexity that makes practical implementation difficult. Hence, this motivates us to develop a hybrid precoding algorithm with lower computational complexity and slight performance loss.

Since the analog precoder is identical for all subcarriers, the optimal solution for the matrix $\mathbf{F}_{\mathrm{RF}}$ is designed to include the most significant principal components from the fully digital precoder matrix $\widetilde{\mathbf{F}}_{\mathrm{opt}}$, which is defined as:

$$\widetilde{\mathbf{F}}_{\mathrm{opt}} = \left[\mathbf{F}_{\mathrm{opt}_1}, \mathbf{F}_{\mathrm{opt}_2}, \ldots, \mathbf{F}_{\mathrm{opt}_N}\right], \tag{6.20}$$

where $\mathbf{F}_{\mathrm{opt}_n}$ represents the optimal fully digital beamformer for the nth subcarrier. To obtain a compact and informative representation of $\widetilde{\mathbf{F}}_{\mathrm{opt}}$ using sorted columns, SVD can be used. SVD of $\widetilde{\mathbf{F}}_{\mathrm{opt}}$ can be performed as $\widetilde{\mathbf{F}}_{\mathrm{opt}} = \mathbf{U}\mathbf{S}\mathbf{V}^{\mathrm{H}}$, where $\mathbf{U}$ and $\mathbf{V}$ are unitary matrices and $\mathbf{S}$ is a diagonal matrix containing singular values. By selecting the first N_{RF} columns of $\mathbf{U}$, denoted as $\mathbf{U}_{N_{\mathrm{RF}}}$, we can extract the most important principal information of $\widetilde{\mathbf{F}}_{\mathrm{opt}}$ based on the sorted columns.

Therefore, it is possible to obtain the matrix $\mathbf{F}_{\mathrm{RF}}$ by scaling the coefficients of $\mathbf{U}_{N_{\mathrm{RF}}}$ within the circular region and finding the closest points in $\mathcal{F}_{N_{\mathrm{ps}}}$ [48]. As outlined in Algorithm 6, the analog precoder is moved from the iteration, and the rest of the steps

Algorithm 6 Low-complex precoder design for wideband channels

Require: K users, N subcarriers, N_{t}, N_{RF} RF chains;
Initialization:
  Obtain $\mathbf{U}_{N_{\mathrm{RF}}}$ via calculating SVD of $\widetilde{\mathbf{F}}_{\mathrm{opt}}$;
  Obtain $\mathbf{F}_{\mathrm{RF}}$ via mapping $\mathbf{U}_{N_{\mathrm{RF}}}$ into $\mathcal{F}_{N_{\mathrm{ps}}}$;
Ensure: Max sum rate;
repeat
  Update $\gamma[n]$ for all n;
  Update $\mathbf{y}[n]$ for all n;
  Update $\mathbf{F}_{\mathrm{BB}}[n]$ for all n;
until Convergence

can be iteratively executed until the desired level of performance coverage is achieved.

6.5 Numerical results

We consider a multiuser MISO system with $K = 10$ users and $N = 64$ subcarriers. The transmitter is equipped with an 8×8 uniform planar array, wherein the antenna elements are spaced half a wavelength. Additionally, we adopt the Saleh-Valenzuela channel model, which is established for mmWave transmission [74]. The channel characteristics for each user channel consist of 3 clusters and 5 rays in each cluster. The departure angles follow a Laplacian distribution with uniformly distributed mean angles in the $[0 \quad 2\pi)$ range and an angular spread of 10 degrees.

To investigate the effectiveness of the proposed design, we present a numerical assessment of the proposed algorithm's efficacy compared to the OFDM-based beamforming designs presented in [29] and [30], as well as the performance of optimal fully-digital beamforming. Notably, [29] and [30] employ double phase shifters and quantized phase shifters, respectively, to implement analog precoder coefficients.

Figure 6.4 presents the sum rate of the proposed HBF algorithms in comparison to the algorithms presented in [29] and [30], as well as the optimal fully digital algorithm in the scenario of $K = 10$ users and $N_{\mathrm{RF}} = 11$ RF chains. It can be seen that the proposed algorithm achieves higher spectral efficiency than the other algorithms across all signal-to-noise ratios (SNRs). Moreover, our results show that Algorithm 6 has negligible performance degradation.

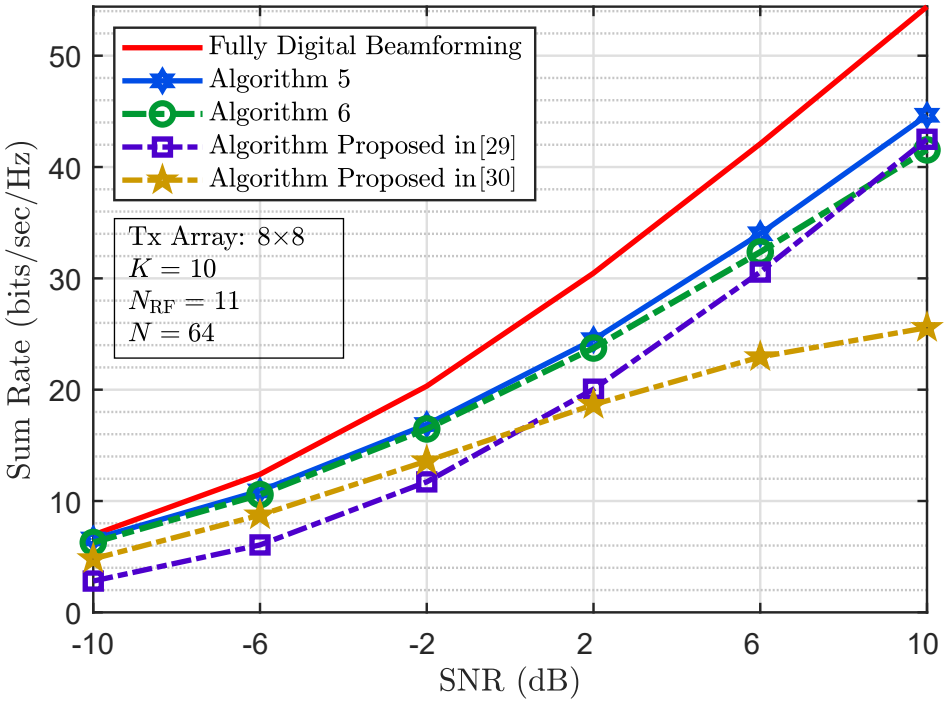

Figure 6.4: Sum rate for different values of SNR [Source file].

The performance comparison of different HBF methods and a fully digital technique in terms of the sum rate versus the number of RF chains is presented in Figure 6.5 with $K = 10$ users and $\mathrm{SNR} = 0$ dB. The plot shows that HBF methods can achieve similar performance to fully digital techniques by utilizing a sufficient number of RF chains, specifically $N_{\mathrm{RF}} = 3K$ in this case. Moreover, the results demonstrate the superiority of our proposed algorithms over the other two approaches, especially when the number of RF chains is equal to the minimum required for serving all users.

Furthermore, Figure 6.6 illustrates the sum rate with the different numbers of users, and the number of RF chains is equal to the number of users, i.e., $N_{\mathrm{RF}} = K$, and $\mathrm{SNR} = 0$ dB. One can see the ability of the proposed approach to maintain performance even with high interuser interference. The results demonstrate the effectiveness of our approach in maximizing the sum rate while satisfying a per-subcarrier power constraint.

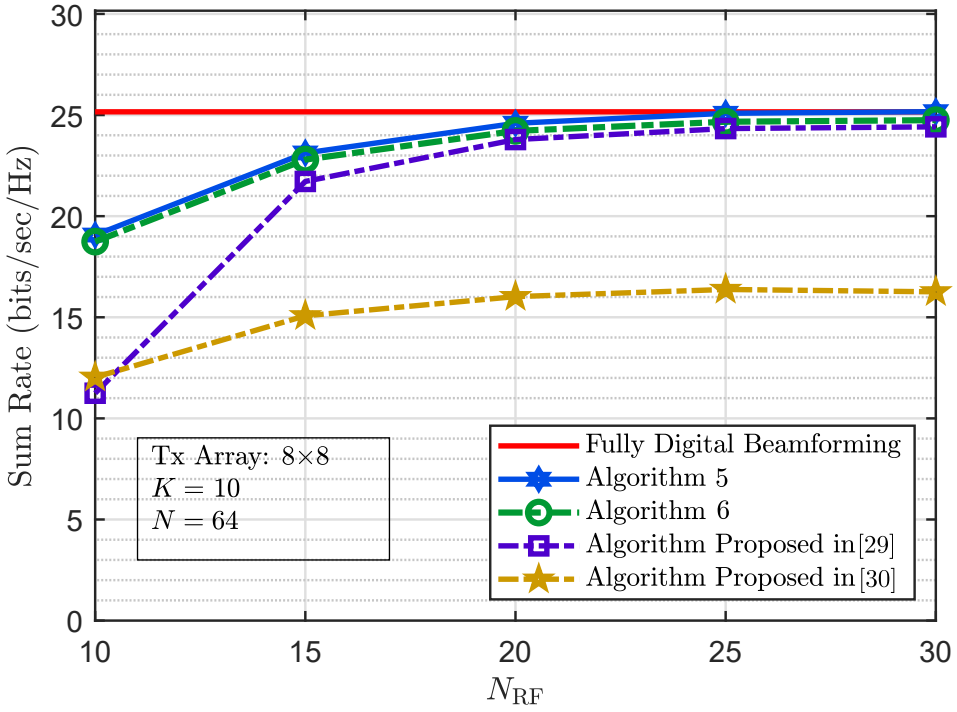

Figure 6.5: Sum rate for different numbers of RF chains [Source file].

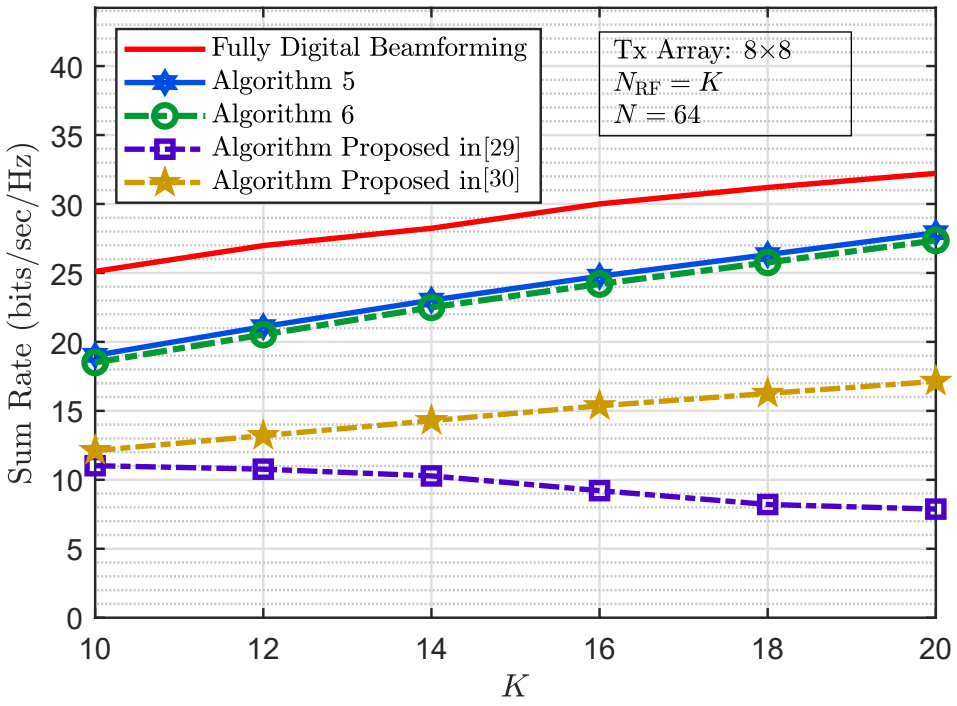

Figure 6.6: Sum rate for different numbers of users [Source file].

6.6 Summary

This chapter presents a novel approach for designing hybrid precoding in an OFDM-based multiuser MISO system using FPS to perform the analog precoder. The primary objective of this approach is to maximize the downlink sum rate while satisfying a per-subcarrier power constraint. To address the combinatorial nature of the optimization problem, our proposed method employs a small number of fixed phase shifters. Additionally, using Lagrangian dual transformation and Quadratic transformation techniques, a low complex iterative optimization method has been proposed. We developed all the required formulations to derive the HBF matrices. We then validate the approach's efficacy in achieving the stated objective using simulation. Overall, our proposed method offers a promising solution to the challenge of designing hybrid precoding in OFDM-based multiuser MISO systems using FPS.

7

Conclusion and Future Works

THIS thesis has extensively investigated the potential of HBF in mmWave massive MIMO systems, with the goal of proposing cost-efficient architecture and low-complexity algorithms for various transmission scenarios. Specifically, the analog network architecture utilizing a combination of fixed phase shifters and switches to generate analog precoder coefficients in each RF path connecting an RF chain to an antenna element has been analyzed. This hardware implementation scheme offers a significant advantage in massive MIMO systems by decoupling the number of phase shifters from the number of antennas. Despite this advantage, the architecture still faces significant challenges related to computational and hardware complexity. One of the major computational complexity issues is obtaining the optimal switch states for the hybrid design problem due to its combinatorial nature. This requires an exhaustive search over all possible switch states, making it impractical for real-world applications. Additionally, the hardware challenges arise from the large number of switches present in the analog network, which is proportional to the number of antennas and data streams. This can result in increased complexity and cost of the architecture, making it less attractive for practical settings.

This thesis proposes an algorithm to address the combinatorial complexity issue. The algorithm offers an efficient and low-complexity solution to obtain optimal switch states for various transmission scenarios. The proposed algorithm comprises several steps aimed at facilitating the optimization process. Initially, the problem is decomposed into independent and tractable sub-problems, which reduces the search space to a

manageable size. Subsequently, further reduction in the search space is achieved by identifying superimposed points in the feasible set. Additionally, the utilization of the basic set, which is a subset of the feasible set, leads to a reduction in the search space by a factor proportional to the number of phase shifters.

This thesis has addressed the hardware complexity issue associated with hardware implementation and mapping strategy in the analog network.

Regarding hardware implementation, the study has focused on determining the optimal number of phase shifters required to generate analog precoder coefficients with negligible error. The investigation has shown that the system's performance primarily depends on the number of distinct coefficients that fixed phase shifters can generate, rather than the total number of feasible combinations. Consequently, a closed-form formula has been derived to calculate the number of distinct coefficients for practical values of the phase shifters, up to a limit of 17. The results indicate that even with a modest number of phase shifters, the upper bound performance can be approached closely. The study has also highlighted the importance of selecting a prime number of phase shifters as the most efficient strategy for generating distinct elements within the feasible set and the suboptimal nature of an even number of phase shifters. Based on the simulation results, the thesis recommends the use of 11 phase shifters as a judicious trade-off between performance and hardware complexity.

In terms of mapping strategy, this thesis has proposed a novel mapping strategy. The proposed strategy offers $N_{\mathrm{t}}+1$ distinct levels of complexity and performance trade-off, with each level having a specific number of RF paths selected from a set comprising $\{N_{\mathrm{t}}, N_{\mathrm{t}}+(N_{\mathrm{RF}}-1), \ldots, N_{\mathrm{t}}+N_{\mathrm{c}}(N_{\mathrm{RF}}-1), \ldots, N_{\mathrm{t}}N_{\mathrm{RF}}\}$. Specifically, the antenna elements are partitioned into two groups: N_{c} antennas are connected to all RF chains, each requiring $N_{\mathrm{c}}N_{\mathrm{RF}}$ RF paths, while the remaining $N_{\mathrm{t}}-N_{\mathrm{c}}$ antennas are connected to only one RF chain. To further enhance spectral and energy efficiency, a dynamic version of the mapping strategy has also been developed. In this dynamic version, fully connected antennas can be selected, and the single connected antenna can be assigned to different RF chains. A switch network has been incorporated behind the antenna array to enable the adjustment of RF path connections based on the channel state information.

The study has presented innovative methodologies for obtaining the analog precoder matrix for both fixed and dynamic mapping strategies, exploiting two fundamental insights; firstly, precoding coefficients can be implemented with minimal error using a mere 11 phase shifters, and secondly, the analog precoding matrix pattern is significantly influenced by RF paths, resulting in zero elements when an RF path is absent.

In terms of the fixed mapping strategy, the proposed approach involves reshaping the matrix by eliminating zero entries, resulting in a lower-dimensional equivalent matrix that simplifies matrix inversion and facilitates the implementation of the zero forcing precoder via non-zero elements, thereby mitigating interference.

Regarding the dynamic mapping strategy, the study proposed a novel approach based on a greedy solution to address the challenge of determining switch states which adjust RF paths in the analog network. This approach offers a practical and feasible solution, given the massive search space and computational complexity associated with the large-dimensional switch network, making a global solution intractable. The proposed approach comprises two parts for the dynamic mapping strategy. Firstly, the approach selects fully connected antennas, which involves initially selecting all antennas and then removing one antenna in each iteration until the desired number of N_{c} antennas remains. This selection process reduces the search space, making the optimization problem more feasible. Secondly, the remaining antennas are allocated to RF chains, which involves creating empty sets initially and assigning an antenna to an RF chain in each iteration.

Additionally, to simplify the proposed approach's implementation in real-time applications, a DNN is introduced. The DNN is trained based on the two-part approach's results and CSI. After the training phase, the DNN directly provides the antenna assignment matrix with the given CSI, eliminating the need for additional post-processing steps.

Finally, The thesis has presented a novel approach for designing hybrid precoding in an OFDM-based multiuser MISO system. The primary objective of this approach is to maximize the downlink sum rate while satisfying a per-subcarrier power constraint. To address the combinatorial nature of the optimization problem, the proposed method employs a small number of fixed phase shifters. Moreover, an iterative optimization

method with low complexity is proposed using Lagrangian dual transformation and Quadratic transformation techniques. The required formulations to derive the HBF matrices are developed, and the effectiveness of the approach is verified through simulations.

It should be mentioned that all the aforementioned proposed algorithms for HBF architecture are based on the assumption of the perfect and instantaneous CSI. However, obtaining accurate CSI is very challenging in practice, especially for systems with large scale antenna arrays. One of the possible directions for the future work is to device a scheme to efficiently estimate the channel of a large-scale MIMO system with HBF architecture. It would also be desirable to characterize the CSI error of that scheme and to design the hybrid beamformers that are robust to that CSI error.

The proposed mapping strategy is analyzed with the assumption that the analog precoder coefficients in each RF path can be implemented perfectly, which is valid for the two hardware implementations: DPS and FPS. However, future research could explore the application of this mapping strategy to the SPS and QPS hardware implementations to develop algorithms for the corresponding HBF design problem. Examining the performance of the proposed mapping strategy under different hardware configurations may require further optimize the design of HBF architectures. Therefore, it is an important direction for future work to investigate the extension of the proposed mapping strategy to other hardware implementations beyond DPS and FPS.

The proposed mapping strategy has been investigated for single-carrier multiuser (SC-MU) systems. However, there is a need to investigate the extension of this mapping strategy to multicarrier scenarios. Future research could focus on developing algorithms for the corresponding HBF design problem for multicarrier systems.

The thesis acknowledges that the issue of user scheduling remains unresolved and suggests further investigation in future works. Specifically, the use of random scheduling may result in the scheduling of users from the same or different clusters within each time slot. Although scheduling users from the same cluster may increase signal power due to the similarity of channel response vectors, it may also lead to higher inter-user interference. Hence, it is not immediately evident whether scheduling users from the

same cluster is advantageous for rate maximization. Further research is needed to clarify the impact of user clustering on scheduling and to identify optimal scheduling strategies that balance competing factors such as signal power and interference.

In summary, this thesis presents a comprehensive study of HBF for mmWave massive MIMO systems using fixed phase shifters and switches. The primary objective of this study is to handle the trade-off between computational and hardware complexity. Towards this end, the thesis proposes various algorithms and system architectures for different transmission scenarios. The proposed approaches achieve a significant reduction in hardware complexity compared to full-digital beamforming, while still achieving near-optimal performance. The contributions of this thesis extend to both theoretical and practical aspects of mmWave massive MIMO systems and provide valuable insights into the design and implementation of HBF architectures.

A

Annexes

Sommaire

A.1 Channel Model

A.1.1 MIMO Channel

A widely-used channel model for millimeter electromagnetic waves is that of Saleh-Valenzuela [74]. Because the attenuation is more important at higher frequencies, the number of effective scatters decreases. Suppose that the channel consists of N_{cl} independent clusters, with N_{ray} paths inside each of them. Therefore, the channel matrix $\mathbf{H}$ can be expressed as

$$\mathbf{H} = \sqrt{\frac{N_t N_r}{N_{cl} N_{ray}}} \sum_{i=1}^{N_{cl}} \sum_{\ell=1}^{N_{ray}} \alpha_{i\ell} \mathbf{a}_r \left(\phi_{i\ell}^r, \theta_{i\ell}^r\right) \mathbf{a}_t \left(\phi_{i\ell}^t, \theta_{i\ell}^t\right)^{\mathsf{H}} \tag{A.1}$$

where α_{il} represents the gain of the l^{th} ray in the i^{th} cluster. We assume also that all clusters have the same average power, $\alpha_{il} \sim \mathcal{CN}(0,1)$. Although in practice this assumption may not be valid, but the principle of all the following discussions remain valid. Under this assumption $\mathbb{E}\left\{\|\mathbf{H}\|_{\mathsf{F}}^2\right\} = N_t N_r$. The $\phi_{i\ell}^r(\theta_{i\ell}^r)$ and $\phi_{i\ell}^t(\theta_{i\ell}^t)$ respectively are Angles of Arrival (AoA) and Angles of Departure (AoD). The distribution of the N_{ray} rays in each cluster can be model as Laplacian distribution [75]:

$$\begin{aligned} \phi_{i\ell}^r &\sim \mathcal{L}\left(\Phi_i^t, \frac{\sigma_{\phi^t}}{\sqrt{2}}\right) \\ \theta_{i\ell}^r &\sim \mathcal{L}\left(\Theta_i^t, \frac{\sigma_{\theta^t}}{\sqrt{2}}\right) \end{aligned} \tag{A.2}$$

where σ_{ϕ^t} and σ_{θ^t} are the angular spread at transmitter, and Φ_i^t and Θ_i^t are the mean angles of the ith cluster and have uniform distribution

$$\begin{aligned} \Phi_i^t &\sim \mathcal{U}(0, 2\pi) \\ \Theta_i^t &\sim \mathcal{U}(0, 2\pi). \end{aligned} \tag{A.3}$$

$\mathbf{a}_r\left(\phi_{i\ell}^r, \theta_{i\ell}^r\right)$ and $\mathbf{a}_t\left(\phi_{i\ell}^t, \theta_{i\ell}^t\right)$ represent the array response vectors of transmitter and receiver antenna arrays. For a Uniform Planar Array (UPA) structure, deployed in yz-axis with N and M elements on the y and z axes respectively, $\mathbf{a}_r\left(\phi_{i\ell}^r, \theta_{i\ell}^r\right) \in \mathbb{C}^{N_r \times 1}$ and

$\mathbf{a}_t\left(\phi_{i\ell}^t, \theta_{i\ell}^t\right) \in \mathbb{C}^{N_t \times 1}$ are given by [76]

$$\begin{aligned}\mathbf{a}\left(\phi_{i\ell}, \theta_{i\ell}\right) =& \frac{1}{\sqrt{NM}}[1, \ldots, e^{\jmath \frac{2\pi}{\lambda_c} d(n \sin(\phi_{i\ell}) \sin(\theta_{i\ell}) + m \cos(\theta_{i\ell}))}, \\ & \ldots, e^{\jmath \frac{2\pi}{\lambda_c} d((N-1) \sin(\phi_{i\ell}) \sin(\theta_{i\ell}) + (M-1) \cos(\theta_{i\ell}))}]^{\mathsf{T}}\end{aligned} \tag{A.4}$$

where d and λ_c denote inter-element spacing and the wavelength, and $0 \leq n < N$ and $0 \leq m < M$ are the y and z indices of an antenna element respectively.

A.1.2 MISO Channel

which models the propagation environment as a geometric channel with N_{cl} paths [74]. The channel vector between user k and the BS , $\mathbf{h}_k$, is expressed as:

$$\mathbf{h}_k = \sqrt{\frac{N_{\mathrm{t}}}{N_{cl}}} \sum_{i=1}^{N_{cl}} \alpha_i \mathbf{a}_t\left(\phi_i, \theta_i\right)^H, \tag{A.5}$$

where α_i represents the channel gain of the ith path. We assume that all the paths have the same average power, $\alpha_i \sim \mathcal{CN}\left(0, 1\right)$. The ϕ_i and θ_i are angles of departure uniformly distributed across 60 degrees in the azimuth domain and 20 degrees in elevation [39]. The $\mathbf{a}\left(\phi_i, \theta_i\right)$ represents the array response vector of transmitter antenna array. For a $N \times M$ UPA, $\mathbf{a}\left(\phi_i, \theta_i\right)$ is given by [76]

$$\begin{aligned}\mathbf{a}\left(\phi_i, \theta_i\right) =& \frac{1}{\sqrt{NM}} \Big[1, \ldots, e^{\jmath \frac{2\pi}{\lambda_c} d(n \sin(\phi_i) \sin(\theta_i) + m \cos(\theta_i))}, \\ & \ldots, e^{\jmath \frac{2\pi}{\lambda_c} d((N-1) \sin(\phi_i) \sin(\theta_i) + (M-1) \cos(\theta_i))}\Big]^{\mathrm{T}},\end{aligned} \tag{A.6}$$

where λ_c is the the wavelength, d is the inter-element spacing, and $0 \leq n < N$ and $0 \leq m < M$ are the y and z indexes of antenna elements, respectively.

A.2 The Proof of the Maximum Amplitude in the Feasible Set

Consider that the nth phase shifter is placed on $P_n = e^{\jmath \frac{2\pi}{N_{\mathrm{ps}}}(n-1)}, \quad \forall n = 1, \ldots, N_{\mathrm{ps}}$. Therefore, $N_{\mathrm{ps}}/2$ active phase shifters, which are next to each other, generate the point with an amplitude below:

□ When $\lceil \frac{N_{\rm ps}}{2} \rceil$ is an even number:

$$\begin{aligned}\eta_{N_{\rm ps}} &= \left| \sum_{n=1}^{\lfloor \frac{N_{\rm ps}}{4} \rfloor} e^{\jmath \frac{2\pi}{N_{\rm ps}}(n-1)} \right| \\ &= \left| \sum_{n=1}^{\lfloor \frac{N_{\rm ps}}{4} \rfloor} P_n + P_{\frac{N_{\rm ps}}{2}-n+1} \right| \end{aligned} \tag{A.7}$$

where $P_n + P_{\frac{N_{\rm ps}}{2}-n+1}$ can be computed as:

$$\begin{aligned} P_n + P_{\frac{N_{\rm ps}}{2}-n+1} &= e^{\jmath \frac{2\pi}{N_{\rm ps}}(n-1)} + e^{\jmath \frac{2\pi}{N_{\rm ps}}\left(\frac{N_{\rm ps}}{2}-n\right)} \\ &= 2e^{\jmath \frac{\pi}{N_{\rm ps}}(\frac{N_{\rm ps}}{2}-1)} \cos\left(\pi \frac{2n-1}{N_{\rm ps}}\right). \end{aligned} \tag{A.8}$$

By substituting (A.8) in (A.7), we have:

$$\begin{aligned}\eta_{N_{\rm ps}} &= \left| \sum_{n=1}^{\lfloor \frac{N_{\rm ps}}{4} \rfloor} 2e^{\jmath \frac{\pi}{N_{\rm ps}}(\frac{N_{\rm ps}}{2}-1)} \cos\left(\pi \frac{2n-1}{N_{\rm ps}}\right) \right| \\ &= 2 \sum_{n=1}^{\lfloor \frac{N_{\rm ps}}{4} \rfloor} \cos\left(\pi \frac{2n-1}{N_{\rm ps}}\right). \end{aligned} \tag{A.9}$$

□ When $\lceil \frac{N_{\rm ps}}{2} \rceil$ is an odd number:

$$\begin{aligned}\eta_{N_{\rm ps}} &= \left| \sum_{n=-\lfloor \frac{N_{\rm ps}}{4} \rfloor}^{\lfloor \frac{N_{\rm ps}}{4} \rfloor} e^{\jmath \frac{2\pi}{N_{\rm ps}}(n-1)} \right| \\ &= \left| 1 + \sum_{n=2}^{\lfloor \frac{N_{\rm ps}}{4} \rfloor} P_n + P_{-n} \right| \\ &= \left| 1 + \sum_{n=1}^{\lfloor \frac{N_{\rm ps}}{4} \rfloor} P_{n+1} + P_{-n-1} \right| \end{aligned} \tag{A.10}$$

where $P_{n+1} + P_{-n-1}$ can be computed as:

$$\begin{aligned} P_{n+1} + P_{-n-1} &= e^{\jmath \frac{2\pi}{N_{\rm ps}}(n+1-1)} + e^{\jmath \frac{2\pi}{N_{\rm ps}}(-n-1+1)} \\ &= e^{\jmath \frac{2\pi}{N_{\rm ps}}(n)} + e^{\jmath \frac{2\pi}{N_{\rm ps}}(-n)} \\ &= 2\cos\left(\pi \frac{2n}{N_{\rm ps}}\right) \\ &= \cos\left(\pi \frac{-2n}{N_{\rm ps}}\right) + \cos\left(\pi \frac{2n}{N_{\rm ps}}\right) \end{aligned} \tag{A.11}$$

By substituting (A.11) in (A.10), we have:

$$\begin{aligned} \eta_{N_{\rm ps}} &= \left| 1 + \sum_{n=1}^{\lfloor \frac{N_{\rm ps}}{4} \rfloor} \cos\left(\pi \frac{-2n}{N_{\rm ps}}\right) + \cos\left(\pi \frac{2n}{N_{\rm ps}}\right) \right| \\ &= \sum_{n=-\lfloor \frac{N_{\rm ps}}{4} \rfloor}^{\lfloor \frac{N_{\rm ps}}{4} \rfloor} \cos\left(\pi \frac{2n}{N_{\rm ps}}\right) \end{aligned} \tag{A.12}$$

A.3 The Proof of Equation (4.18)

According to Lemma 2, for a given pair $(N_{\rm ps}, p)$, there are $N_{\rm ps}/p$ disjoint ZSSs, i.e., $\mathcal{X}^i_{N_{\rm ps},p}$ where $i \in [1, N_{\rm ps}/p]$. It is explicit that the members of $\Pi_n\Big([N_{\rm ps}]\Big)$ cannot form any $\mathcal{X}_{N_{\rm ps},p}$ if $n < p$. For $p \leq n < 2p$, some members of $\Pi_n\Big([N_{\rm ps}]\Big)$ form one $\mathcal{X}_{N_{\rm ps},p}$. In this case, the number of ways create a subset of $[N_{\rm ps}]$ of size n including $\mathcal{X}_{N_{\rm ps},p}$ is:

$$\mathcal{G}\Big(N_{\rm ps}, p, n\Big) = \binom{\frac{N_{\rm ps}}{p}}{1} \binom{N_{\rm ps}-p}{n-p} \qquad p \leq n < 2p. \tag{A.13}$$

For the case $2p \leq n < 3p$, the members of $\Pi_n\Big([N_{\rm ps}]\Big)$ can include one or two $\mathcal{X}_{N_{\rm ps},p}$. Similarly, there are $\binom{N_{\rm ps}/p}{1}\binom{N_{\rm ps}-p}{n-p}$ way to create a subset of $[N_{\rm ps}]$ including $\mathcal{X}_{N_{\rm ps},p}$. Note that the number of subsets including two $\mathcal{X}_{N_{\rm ps},p}$ is $\binom{N_{\rm ps}/p}{2}\binom{N_{\rm ps}-2p}{n-2p}$. Therefore, the number of subsets including at least one $\mathcal{X}_{N_{\rm ps},p}$ is:

$$\mathcal{G}\Big(N_{\rm ps}, p, n\Big) = \binom{\frac{N_{\rm ps}}{p}}{1} \binom{N_{\rm ps}-p}{n-p} - \binom{\frac{N_{\rm ps}}{p}}{2} \binom{N_{\rm ps}-2p}{n-2p} \quad 2p \leq n < 3p. \tag{A.14}$$

By deductive reasoning, the general formulation can be reached as (4.18).

A.4 The Proof of Equation (4.19)

According to Lemma 3, some member of $\Pi_{\geq 4}\Big(\big[12\big]\Big)$ can contain two ZSSs ($\mathcal{X}_{12,2}$ and $\mathcal{X}_{12,3}$) simultaneously. Consider $\mathcal{A}_j \in \Pi_{\geq 4}\Big(\big[12\big]\Big)$ containing $\mathcal{X}^i_{12,3}$ where $i \in \big[1,4\big]$ (see Lemma 2), so there are $\binom{4}{1}$ ways to choose a $\mathcal{X}_{12,3}$. To $\mathcal{A}_j$ forms at least one $\mathcal{X}_{12,2}$, it must include one of three members of $\bar{\mathcal{X}}^i_{12,3}$ (defined in (4.11)) or two of six members of the set $\Gamma = \big[12\big] - \Big(\mathcal{X}^i_{12,3} \bigcup \bar{\mathcal{X}}^i_{N_{\mathrm{ps}},p}\Big)$ in such way they form a $\mathcal{X}_{12,2}$.

1. For $\mathcal{A}_j \in \Pi_4\Big(\big[12\big]\Big)$:
   It must Include $\mathcal{X}^i_{12,3}$ and one member of $\bar{\mathcal{X}}^i_{12,3}$ i.e., $\binom{4}{1}\binom{3}{1}$ ways.

2. For $\mathcal{A}_j \in \Pi_5\Big(\big[12\big]\Big)$:
   It must Include $\mathcal{X}^i_{12,3}$ and one of these cases:
   - Two members of $\bar{\mathcal{X}}^i_{12,3}$ i.e., $\binom{4}{1}\binom{3}{2}$ ways.
   - One member of $\bar{\mathcal{X}}^i_{12,3}$ and one member of Γ i.e., $\binom{4}{1}\binom{3}{1}\binom{6}{1}$ ways.
   - Two members of set Γ including $\mathcal{X}_{12,2}$. Since $\big|\Gamma\big| = 6$, it leads to $\mathcal{G}\big(6,2,2\big)$, i.e., $\binom{4}{1}\mathcal{G}\big(6,2,2\big)$ ways.

3. For $\mathcal{A}_j \in \Pi_6\Big(\big[12\big]\Big)$:
   It must Include $\mathcal{X}^i_{12,3}$ and one of these cases:
   - One member of $\bar{\mathcal{X}}^i_{12,3}$ and two members from Γ, i.e., $\binom{4}{1}\binom{3}{1}\binom{6}{2}$ ways.
   - Two members of $\bar{\mathcal{X}}^i_{12,3}$ and one member of Γ, i.e., $\binom{4}{1}\binom{3}{2}\binom{6}{1}$ ways.
   - Whole set $\bar{\mathcal{X}}^i_{12,3}$. It is equivalent to choose one of two 6-members subsets so there are $\binom{2}{1}$ ways.

- Three members of Γ generating one $\mathcal{X}_{12,2}$., it leads to $\mathcal{G}\big(6,2,3\big)$, i.e., $\binom{4}{1}\mathcal{G}\big(6,2,3\big)$ ways.

Therefore, we express the general formula as (4.19).

A.5 The Proof of Equation (4.20)

According to Lemma 3, some member of $\Pi_{\geq 7}\Big(\big[15\big]\Big)$ can contain two ZSSs ($\mathcal{X}_{15,3}$ and $\mathcal{X}_{15,5}$) simultaneously. Consider $\mathcal{A}_j \in \Pi_{\geq 7}\Big(\big[15\big]\Big)$ such that five members of that form $\mathcal{X}^i_{15,5}$ where $i \in \big[1,3\big]$ (Lemma 2), so there are three ways to choose a $\mathcal{X}_{15,5}$. In this case, $\mathcal{A}_j$ also includes one member of each $\mathcal{X}^m_{15,3}$ ($m = 1,\ldots,5$). Therefore, to $\mathcal{A}_j$ generate at least one $\mathcal{X}_{15,3}$, two of $n-5$ remained members of $\mathcal{A}_j$ must be from the same $\mathcal{X}_{15,3}$. It leads to $\mathcal{G}\big(10,2,n-5\big)$. Therefore, the number of members of $\Pi_{\geq 7}\Big(\big[15\big]\Big)$, which include $\mathcal{X}_{15,3}$ and $\mathcal{X}_{15,5}$, is expressed as (4.20).

A.6 The Proof of Equation (4.22)

For $N_{\rm ps} = 6, 10, 14$, $p_1 = 2$ and $p_2 = N_{\rm ps}/2$. From Lemma 4, $p_1 = 2$ cannot form any Subset of Zero-Summation Set (SZSS). Also, according to Lemma 5 in each $\mathcal{X}_{N_{\rm ps},p_2}$ there are $\binom{N_{\rm ps}/2}{n}$ SZSSs. Furthermore, since $\mathcal{A}_c$ (see subsection 4.2.2) is an empty set, all $\binom{N_{\rm ps}/2}{n}$ sets are considered as SZSSs. Therefore:

$$\mathcal{Y}_{N_{\rm ps}}(n) = \binom{2}{1}\binom{N_{\rm ps}/2}{n} \qquad p/2 \leq n \leq p/4. \tag{A.15}$$

A.7 The Proof of Equation (4.23)

In this case, $p_1 = 2$ and $p_2 = 3$. From Lemma 4, $p_1 = 2$ cannot generate any SZSS. Also, according to Lemma 2 and Lemma 5, there are four $\mathcal{X}^i_{12,3}$ that in each $\mathcal{X}_{N_{\rm ps},3}$ there are $\binom{3}{2}$ SZSSs ($\mathcal{R}_{12,3}$). Consider $\mathcal{A}_j \in \Pi_n\Big(\big[12\big]\Big)$ such that

$$\begin{cases} \mathcal{A}_j \bigcap \mathcal{X}_{12,3} = \mathcal{R}_{12,3} \\ \mathcal{A}_j \bigcap \bar{\mathcal{X}}_{12,3} = \{\}\,, \end{cases} \tag{A.16}$$

where $\mathcal{R}_{12,3}$ is of size two (see subsection 4.2.2). Therefore, $n-2$ members $\mathcal{A}_c = \mathcal{A}_j - \mathcal{R}_{12,3}$ are selected from six members of Γ, which is defined as:

$$\Gamma = \big[12\big] - \Big(\mathcal{X}^i_{12,3} \bigcup \bar{\mathcal{X}}^i_{N_{\mathrm{ps}},p}\Big). \tag{A.17}$$

1. For $n=2$, $\mathcal{A}_c$ is empty. Therefore, the number of members of $\Pi_2\Big(\big[12\big]\Big)$, which satisfies (A.16), is:

$$\mathcal{Y}_{12}(2) = \binom{4}{1}\binom{3}{2}. \tag{A.18}$$

2. For $n=3$, $\mathcal{A}_c$ includes one member of Γ, so it cannot include any ZSS. Therefore, the number of members in $\Pi_3\Big(\big[12\big]\Big)$, which satisfies (A.16), is:

$$\mathcal{Y}_{12}(3) = \binom{4}{1}\binom{3}{2}\binom{6}{1}. \tag{A.19}$$

3. For $\mathcal{A}_j \in \Pi_4\Big(\big[12\big]\Big)$, $\mathcal{A}_c$ has two members from Γ. In this case, $\mathcal{A}_c$ may include a $\mathcal{X}_{12,2}$ $\left(\binom{4}{1}\binom{3}{2}\mathcal{G}(6,2,2)\text{cases}\right)$ or a subset of $\mathcal{X}_{12,3}$ $\left(\binom{4}{1}\binom{3}{2}\binom{2}{1}\binom{3}{2}\right)$ cases. Therefore:

$$\mathcal{Y}_{12}(4) = \tbinom{4}{1}\binom{3}{2}\left[\binom{6}{2} - \mathcal{G}(6,2,2)\right] - \frac{1}{2}\binom{4}{1}\binom{3}{2}\binom{2}{1}\binom{3}{2} \tag{A.20}$$

4. For $n=5$, $\mathcal{A}_c$ includes three members of Γ. The number of members in $\Pi_5\Big(\big[12\big]\Big)$, which satisfies (A.16), is $\binom{4}{1}\binom{3}{2}\binom{6}{3}$. Note that $\mathcal{A}_c$ may include a ZSS ($\mathcal{X}_{12,2}$ or $\mathcal{X}_{12,3}$). Therefore, the number of members in $\Pi_5\Big(\big[12\big]\Big)$ is:

$$\mathcal{Y}_{12}(5) = \binom{4}{1}\binom{3}{2}\left[\binom{6}{3} - \mathcal{G}(6,2,3) - \mathcal{G}(6,3,3)\right]. \tag{A.21}$$

B

Bibliography

Sommaire

References

[1] "Ericsson mobility report," in *https://www.ericsson.com/en/reports-and-papers/mobility-report/reports/november-2022*, Ericsson, 2022.

[2] Z. Pi and F. Khan, "An introduction to millimeter-wave mobile broadband systems," *IEEE communications magazine*, vol. 49, no. 6, pp. 101–107, 2011.

[3] D. M. Pozar, *Microwave engineering*. John wiley & sons, 2011.

[4] T. L. Marzetta, "Noncooperative cellular wireless with unlimited numbers of base station antennas," *IEEE transactions on wireless communications*, vol. 9, no. 11, pp. 3590–3600, 2010.

[5] R. W. Heath, N. Gonzalez-Prelcic, S. Rangan, W. Roh, and A. M. Sayeed, "An overview of signal processing techniques for millimeter wave mimo systems," *IEEE journal of selected topics in signal processing*, vol. 10, no. 3, pp. 436–453, 2016.

[6] T. L. Marzetta and H. Q. Ngo, *Fundamentals of massive MIMO*. Cambridge University Press, 2016.

[7] J. Beiranvand and H. Meghdadi, "Analytical performance evaluation of mrc receivers in massive mimo systems," *IEEE Access*, vol. 6, pp. 53 226–53 234, 2018.

[8] H. Q. Ngo, E. G. Larsson, and T. L. Marzetta, "Energy and spectral efficiency of very large multiuser mimo systems," *IEEE Transactions on Communications*, vol. 61, no. 4, pp. 1436–1449, 2013.

[9] B. D. Van Veen and K. M. Buckley, "Beamforming: a versatile approach to spatial filtering," *IEEE assp magazine*, vol. 5, no. 2, pp. 4–24, 1988.

[10] T. E. Bogale and L. B. Le, "Beamforming for multiuser massive mimo systems: digital versus hybrid analog-digital," in *2014 IEEE Global Communications Conference*, IEEE, 2014, pp. 4066–4071.

[11] S. Hur, T. Kim, D. J. Love, J. V. Krogmeier, T. A. Thomas, and A. Ghosh, “Millimeter wave beamforming for wireless backhaul and access in small cell networks,” *IEEE transactions on communications*, vol. 61, no. 10, pp. 4391–4403, 2013.

[12] J. Via, I. Santamaria, V. Elvira, and R. Eickhoff, “A general criterion for analog tx-rx beamforming under ofdm transmissions,” *IEEE Transactions on Signal Processing*, vol. 58, no. 4, pp. 2155–2167, 2010.

[13] S. Sanayei and A. Nosratinia, “Antenna selection in mimo systems,” *IEEE Communications magazine*, vol. 42, no. 10, pp. 68–73, 2004.

[14] J. Wang, Z. Lan, C.-w. Pyo, *et al.*, “Beam codebook based beamforming protocol for multi-gbps millimeter-wave wpan systems,” *IEEE Journal on Selected Areas in Communications*, vol. 27, no. 8, pp. 1390–1399, 2009.

[15] F. Gholam, J. Via, and I. Santamaria, “Beamforming design for simplified analog antenna combining architectures,” *IEEE Transactions on Vehicular Technology*, vol. 60, no. 5, pp. 2373–2378, 2011.

[16] X. Yang, M. Matthaiou, J. Yang, C.-K. Wen, F. Gao, and S. Jin, “Hardware-constrained millimeter-wave systems for 5g: challenges, opportunities, and solutions,” *IEEE Communications Magazine*, vol. 57, no. 1, pp. 44–50, 2019.

[17] I. Ahmed, H. Khammari, A. Shahid, *et al.*, “A survey on hybrid beamforming techniques in 5g: architecture and system model perspectives,” *IEEE Communications Surveys & Tutorials*, vol. 20, no. 4, pp. 3060–3097, 2018.

[18] A. F. Molisch, V. V. Ratnam, S. Han, *et al.*, “Hybrid beamforming for massive mimo: a survey,” *IEEE Communications magazine*, vol. 55, no. 9, pp. 134–141, 2017.

[19] A. B. Gershman, N. D. Sidiropoulos, S. Shahbazpanahi, M. Bengtsson, and B. Ottersten, “Convex optimization-based beamforming,” *IEEE Signal Processing Magazine*, vol. 27, no. 3, pp. 62–75, 2010.

[20] S. Han, I. Chih-Lin, Z. Xu, and C. Rowell, “Large-scale antenna systems with hybrid analog and digital beamforming for millimeter wave 5g,” *IEEE Communications Magazine*, vol. 53, no. 1, pp. 186–194, 2015.

[21] “Selection table for digital phase shifter, parametric search, analog devices,” 2023. [Online]. Available: https://www.analog.com/en/parametricsearch/10700#/.

[22] R. Méndez-Rial, C. Rusu, N. González-Prelcic, A. Alkhateeb, and R. W. Heath, “Hybrid mimo architectures for millimeter wave communications: phase shifters or switches?” *IEEE access*, vol. 4, pp. 247–267, 2016.

[23] A. M. Abbosh, “Broadband fixed phase shifters,” *IEEE microwave and wireless components letters*, vol. 21, no. 1, pp. 22–24, 2010.

[24] A. Alkhateeb and R. W. Heath, “Frequency selective hybrid precoding for limited feedback millimeter wave systems,” *IEEE Transactions on Communications*, vol. 64, no. 5, pp. 1801–1818, 2016.

[25] X. Yu, J.-C. Shen, J. Zhang, and K. B. Letaief, “Alternating minimization algorithms for hybrid precoding in millimeter wave mimo systems,” *IEEE Journal of Selected Topics in Signal Processing*, vol. 10, no. 3, pp. 485–500, 2016.

[26] J. Lee and Y. H. Lee, “Af relaying for millimeter wave communication systems with hybrid rf/baseband mimo processing,” in *2014 IEEE International Conference on Communications (ICC)*, IEEE, 2014, pp. 5838–5842.

[27] W. Ni and X. Dong, “Hybrid block diagonalization for massive multiuser mimo systems,” *IEEE transactions on communications*, vol. 64, no. 1, pp. 201–211, 2015.

[28] L. Liang, W. Xu, and X. Dong, “Low-complexity hybrid precoding in massive multiuser mimo systems,” *IEEE Wireless Communications Letters*, vol. 3, no. 6, pp. 653–656, 2014.

[29] F. Sohrabi and W. Yu, “Hybrid analog and digital beamforming for mmwave ofdm large-scale antenna arrays,” *IEEE Journal on Selected Areas in Communications*, vol. 35, no. 7, pp. 1432–1443, 2017.

[30] X. Yu, J. Zhang, and K. B. Letaief, “Doubling phase shifters for efficient hybrid precoder design in millimeter-wave communication systems,” *Journal of Communications and Information Networks*, vol. 4, no. 2, pp. 51–67, 2019.

[31] J. Zhang, X. Yu, and K. B. Letaief, “Hybrid beamforming for 5g and beyond millimeter-wave systems: a holistic view,” *IEEE Open Journal of the Communications Society*, vol. 1, pp. 77–91, 2019.

[32] S. A. Busari, K. M. S. Huq, S. Mumtaz, L. Dai, and J. Rodriguez, “Millimeter-wave massive mimo communication for future wireless systems: a survey,” *IEEE Communications Surveys & Tutorials*, vol. 20, no. 2, pp. 836–869, 2017.

[33] M. Rihan, T. A. Soliman, C. Xu, L. Huang, and M. I. Dessouky, “Taxonomy and performance evaluation of hybrid beamforming for 5g and beyond systems,” *IEEE Access*, vol. 8, pp. 74 605–74 626, 2020.

[34] X. Zhang, A. F. Molisch, and S.-Y. Kung, “Variable-phase-shift-based rf-baseband codesign for mimo antenna selection,” *IEEE Transactions on Signal Processing*, vol. 53, no. 11, pp. 4091–4103, 2005.

[35] V. Venkateswaran and A.-J. van der Veen, “Analog beamforming in mimo communications with phase shift networks and online channel estimation,” *IEEE Transactions on Signal Processing*, vol. 58, no. 8, pp. 4131–4143, 2010.

[36] O. El Ayach, R. W. Heath, S. Abu-Surra, S. Rajagopal, and Z. Pi, “Low complexity precoding for large millimeter wave mimo systems,” in *2012 IEEE international conference on communications (ICC)*, IEEE, 2012, pp. 3724–3729.

[37] A. Alkhateeb, O. El Ayach, G. Leus, and R. W. Heath, “Hybrid precoding for millimeter wave cellular systems with partial channel knowledge,” in *2013 Information Theory and Applications Workshop (ITA)*, IEEE, 2013, pp. 1–5.

[38] O. El Ayach, R. W. Heath, S. Rajagopal, and Z. Pi, “Multimode precoding in millimeter wave mimo transmitters with multiple antenna sub-arrays,” in *2013 IEEE Global Communications Conference (GLOBECOM)*, IEEE, 2013, pp. 3476–3480.

[39] O. El Ayach, S. Rajagopal, S. Abu-Surra, Z. Pi, and R. W. Heath, “Spatially sparse precoding in millimeter wave mimo systems,” *IEEE transactions on wireless communications*, vol. 13, no. 3, pp. 1499–1513, 2014.

[40] C. Kim, T. Kim, and J.-Y. Seol, “Multi-beam transmission diversity with hybrid beamforming for mimo-ofdm systems,” in *2013 IEEE Globecom Workshops (GC Wkshps)*, IEEE, 2013, pp. 61–65.

[41] F. Sohrabi and W. Yu, “Hybrid digital and analog beamforming design for large-scale antenna arrays,” *IEEE Journal of Selected Topics in Signal Processing*, vol. 10, no. 3, pp. 501–513, 2016.

[42] F. Sohrabi and W. Yu, “Hybrid digital and analog beamforming design for large-scale mimo systems,” in *2015 IEEE International Conference on Acoustics, Speech and Signal Processing (ICASSP)*, IEEE, 2015, pp. 2929–2933.

[43] F. Sohrabi, “Hybrid beamforming and one-bit precoding for large-scale antenna arrays,” Ph.D. dissertation, 2018.

[44] T. E. Bogale, L. B. Le, A. Haghighat, and L. Vandendorpe, “On the number of rf chains and phase shifters, and scheduling design with hybrid analog–digital beamforming,” *IEEE Transactions on Wireless Communications*, vol. 15, no. 5, pp. 3311–3326, 2016.

[45] X. Yu, J. Zhang, and K. B. Letaief, “A hardware-efficient analog network structure for hybrid precoding in millimeter wave systems,” *IEEE Journal of Selected Topics in Signal Processing*, vol. 12, no. 2, pp. 282–297, 2018.

[46] X. Yu, J. Zhang, and K. B. Letaief, “Hybrid precoding in millimeter wave systems: how many phase shifters are needed?” In *GLOBECOM 2017-2017 IEEE Global Communications Conference*, IEEE, 2017, pp. 1–6.

[47] J. Beiranvand, V. Meghdadi, C. Menudier, and J. P. Cances, “An efficient low-complexity method to calculate hybrid beamforming matrices for mmwave mas-

sive mimo systems," *IEEE Open Journal of the Communications Society*, vol. 2, pp. 1239–1248, 2021.

[48] J. Beiranvand, V. Meghdadi, C. Menudier, and J.-P. Cances, "How many fixed phase shifters are needed in a hybrid bf structure?" In *ICC 2022-IEEE International Conference on Communications*, IEEE, 2022, pp. 444–449.

[49] J. Beiranvand, V. Meghdadi, C. Menudier, and J. P. Cances, "An efficient beamforming architecture to handle the trade-off between performance and hardware complexity in multiuser massive miso systems," *IEEE Access*, vol. 10, pp. 132 853–132 862, 2022.

[50] J. Du, W. Xu, H. Shen, X. Dong, and C. Zhao, "Hybrid precoding architecture for massive multiuser mimo with dissipation: sub-connected or fully connected structures?" *IEEE Transactions on Wireless Communications*, vol. 17, no. 8, pp. 5465–5479, 2018.

[51] X. Gao, L. Dai, S. Han, I. Chih-Lin, and R. W. Heath, "Energy-efficient hybrid analog and digital precoding for mmwave mimo systems with large antenna arrays," *IEEE Journal on Selected Areas in Communications*, vol. 34, no. 4, pp. 998–1009, 2016.

[52] S. Park, A. Alkhateeb, and R. W. Heath, "Dynamic subarrays for hybrid precoding in wideband mmwave mimo systems," *IEEE Transactions on Wireless Communications*, vol. 16, no. 5, pp. 2907–2920, 2017.

[53] S. He, C. Qi, Y. Wu, and Y. Huang, "Energy-efficient transceiver design for hybrid sub-array architecture mimo systems," *IEEE Access*, vol. 4, pp. 9895–9905, 2016.

[54] A. Li and C. Masouros, "Hybrid precoding and combining design for millimeter-wave multi-user mimo based on svd," in *2017 IEEE International Conference on Communications (ICC)*, IEEE, 2017, pp. 1–6.

[55] X. Zhu, Z. Wang, L. Dai, and Q. Wang, "Adaptive hybrid precoding for multiuser massive mimo," *IEEE Communications Letters*, vol. 20, no. 4, pp. 776–779, 2016.

[56] N. T. Nguyen and K. Lee, "Unequally sub-connected architecture for hybrid beamforming in massive mimo systems," *IEEE Transactions on Wireless Communications*, vol. 19, no. 2, pp. 1127–1140, 2019.

[57] X. Yu, J. Zhang, and K. B. Letaief, "Partially-connected hybrid precoding in mm-wave systems with dynamic phase shifter networks," in *2017 IEEE 18th International Workshop on Signal Processing Advances in Wireless Communications (SPAWC)*, IEEE, 2017, pp. 1–5.

[58] R. Chen, J. G. Andrews, and R. W. Heath, “Efficient transmit antenna selection for multiuser mimo systems with block diagonalization,” in *IEEE GLOBECOM 2007-IEEE Global Telecommunications Conference*, IEEE, 2007, pp. 3499–3503.

[59] D. Zhang, Y. Wang, X. Li, and W. Xiang, “Hybridly connected structure for hybrid beamforming in mmwave massive mimo systems,” *IEEE Transactions on Communications*, vol. 66, no. 2, pp. 662–674, 2017.

[60] N. Song, T. Yang, and H. Sun, “Overlapped subarray based hybrid beamforming for millimeter wave multiuser massive mimo,” *IEEE Signal Processing Letters*, vol. 24, no. 5, pp. 550–554, 2017.

[61] S. Payami, M. Ghoraishi, and M. Dianati, “Hybrid beamforming for large antenna arrays with phase shifter selection,” *IEEE Transactions on Wireless Communications*, vol. 15, no. 11, pp. 7258–7271, 2016.

[62] J.-C. Guo, Q.-Y. Yu, W.-X. Meng, and W. Xiang, “Energy-efficient hybrid precoder with adaptive overlapped subarrays for large-array mmwave systems,” *IEEE Transactions on Wireless Communications*, vol. 19, no. 3, pp. 1484–1502, 2019.

[63] L. Yan, C. Han, and J. Yuan, “A dynamic array-of-subarrays architecture and hybrid precoding algorithms for terahertz wireless communications,” *IEEE Journal on Selected Areas in Communications*, vol. 38, no. 9, pp. 2041–2056, 2020.

[64] X. Xue, Y. Wang, L. Yang, J. Shi, and Z. Li, “Energy-efficient hybrid precoding for massive mimo mmwave systems with a fully-adaptive-connected structure,” *IEEE Transactions on Communications*, vol. 68, no. 6, pp. 3521–3535, 2020.

[65] H. Li, M. Li, Q. Liu, and A. L. Swindlehurst, “Dynamic hybrid beamforming with low-resolution pss for wideband mmwave mimo-ofdm systems,” *IEEE Journal on Selected Areas in Communications*, vol. 38, no. 9, pp. 2168–2181, 2020.

[66] D. P. Palomar, J. M. Cioffi, and M. A. Lagunas, “Joint tx-rx beamforming design for multicarrier mimo channels: a unified framework for convex optimization,” *IEEE Transactions on Signal Processing*, vol. 51, no. 9, pp. 2381–2401, 2003.

[67] H. Li, M. Li, and Q. Liu, “Hybrid beamforming with dynamic subarrays and low-resolution pss for mmwave mu-miso systems,” *IEEE Transactions on Communications*, vol. 68, no. 1, pp. 602–614, 2019.

[68] H. Q. Ngo, *Massive MIMO: Fundamentals and system designs*. Linköping University Electronic Press, 2015, vol. 1642.

[69] H. Avron and C. Boutsidis, “Faster subset selection for matrices and applications,” *SIAM Journal on Matrix Analysis and Applications*, vol. 34, no. 4, pp. 1464–1499, 2013.

[70] F. De Hoog and R. Mattheij, “Subset selection for matrices,” *Linear Algebra and its Applications*, vol. 422, no. 2-3, pp. 349–359, 2007.

[71] K. Shen and W. Yu, “Fractional programming for communication systems—part i: power control and beamforming,” *IEEE Transactions on Signal Processing*, vol. 66, no. 10, pp. 2616–2630, 2018.

[72] M. Grant and S. Boyd, *CVX: MATLAB software for disciplined convex programming, version 2.1*, Dec. 2018. [Online]. Available: http://cvxr.com/cvx/.

[73] M. D. Nguyen, L. B. Le, and A. Girard, “Integrated uav trajectory control and resource allocation for uav-based wireless networks with co-channel interference management,” *IEEE Internet of Things Journal*, vol. 9, no. 14, pp. 12 754–12 769, 2021.

[74] T. S. Rappaport, R. W. Heath Jr, R. C. Daniels, and J. N. Murdock, *Millimeter wave wireless communications*. Pearson Education, 2015.

[75] S. Singh, R. Mudumbai, and U. Madhow, “Interference analysis for highly directional 60-ghz mesh networks: the case for rethinking medium access control,” *IEEE/ACM Transactions on networking*, vol. 19, no. 5, pp. 1513–1527, 2011.

[76] C. A. Balanis, “Antenna theory: design and analysis,” *The 3rd Edition, John Wiley and Sons, NJ*, pp. 978–979, 1997.

List of Publications

Conférences internationales à comité de lecture

- J. Beiranvand, V. Meghdadi, C. Menudier, and J. P. Cances, “How many fixed phase shifters are needed in a hybrid bf structure?” *IEEE International Conference on Communications (ICC)*, May 2022. [Online]. Available: https://ieeexplore.ieee.org/document/9838503.
- J. Beiranvand, M. D. Nguyen, V. Meghdadi, C. Menudier, and J. P. Cances, “Hybrid beamforming with fixed phase shifters in ofdm-based multiuser miso systems,” *IEEE Global Communications Conference (GLOBECOM)*, 2023.

Journaux internationales à comité de lecture

- J. Beiranvand, V. Meghdadi, C. Menudier, and J. P. Cances, “An Efficient Low-Complexity Method to Calculate Hybrid Beamforming Matrices for mmWave Massive MIMO Systems,” *IEEE Open Journal of the Communications Society*, vol. 2, pp. 1239–1248, May 2021. [Online]. Available: https://ieeexplore.ieee.org/document/9442813.
- J. Beiranvand, V. Meghdadi, C. Menudier, and J. P. Cances, “An efficient beamforming architecture to handle the trade-off between performance and hardware complexity in multiuser massive miso systems,” *IEEE ACCESS*, 2022. [Online]. Available: https://ieeexplore.ieee.org/document/9991158.

Formation de faisceaux hybride par l'utilisation massive d'antennes pour les réseaux de capteurs fixes

Résumé : Cette thèse présente une étude complète du beamforming hybride pour les systèmes massive MIMO à ondes millimétriques utilisant des déphaseurs fixes et des commutateurs. L'objectif principal de cette étude est de gérer le compromis entre la complexité de calcul et de matériel. À cette fin, la thèse propose divers algorithmes et architectures de système pour différents scénarios de transmission. Les approches proposées permettent une réduction significative de la complexité matérielle par rapport au beamforming entièrement numérique, tout en atteignant une performance proche de l'optimal. Les contributions de cette thèse s'étendent aux aspects théoriques et pratiques des systèmes massive MIMO à ondes millimétriques et fournissent des connaissances précieuses sur la conception et la mise en œuvre d'architectures de beamforming hybrides.

Mots clés : Systèmes Massive MIMO, beamforming hybride, déphaseurs fixes, commutateurs.

Hybrid beamforming using massive antenna arrays for fixed sensor networks

Abstract: This thesis presents a comprehensive study of hybrid beamforming for mmWave massive MIMO systems using fixed phase shifters and switches. The primary objective of this study is to handle the trade-off between computational and hardware complexity. Towards this end, the thesis proposes various algorithms and system architectures for different transmission scenarios. The proposed approaches achieve a significant reduction in hardware complexity compared to full-digital beamforming, while still achieving near-optimal performance. The contributions of this thesis extend to both theoretical and practical aspects of mmWave massive MIMO systems and provide valuable insights into the design and implementation of hybrid beamforming architectures.

Keywords: Massive MIMO systems, hybrid beamforming, fixed phase shifter, switch.

Univ. de Limoges, CNRS, XLIM, UMR 7252, F-87000 Limoges, France